DYNAMIC RESPONSE CHARACTERISTICS OF THE SAPPHIRE BUILDING IN ISTANBUL ESTIMATED FROM EARTHQUAKE AND WIND DATA

by

Hakan Doğukan Savaş

B.S., Civil Engineering, Istanbul University, 2014

Submitted to the Kandilli Observatory and Earthquake Research Institute
in partial fulfillment of the requirements for the degree of
Master of Science

Graduate Program in Earthquake Engineering

Boğaziçi University

2019

ACKNOWLEDGEMENTS

This thesis has been possible with the help and support of many people. Firstly, I would like to thank my family for their unconditional love and support during this study. I also would like to send my deepest thanks to Dilan for her patience and support during my study.

I would like to thank Mahir, Mahmut, Mustafa, Selman, Yusuf, Erhan, and Fatih who constantly motivated me when I encountered a problem, and also Yavuz, Ümit and Hanefi for their help.

I also would like to express my appreciation to the Department of Earthquake Engineering during my graduate education.

Finally, I would like to express my sincere thanks to my thesis supervisor Prof. Dr. Eser Çaktı for her guidance in the study and her assistance in preparing my thesis.

ABSTRACT

DYNAMIC RESPONSE CHARACTERISTICS OF THE SAPPHIRE BUILDING IN ISTANBUL ESTIMATED FROM EARTHQUAKE AND WIND DATA

The number of tall buildings has been increasing all around the world due to the current population growth and limited space in city centers. After major earthquakes, countries located in earthquake-prone areas face catastrophic conditions. In addition to building damages, deaths, and injuries, financial losses due to business interruption are also an important part of overall earthquake losses. Therefore, buildings home to organizations such as financial institutions, health care facilities, governmental buildings need to remain functional following an earthquake to constrain financial losses and secure public services. The condition of structures can be estimated by evaluating the change in the in-situ dynamic characteristics of the structures in real time day by day. In this study, the dynamic parameters of the Sapphire Building during strong wind and earthquake records are estimated in the time and frequency domain.

Earthquake and wind events were selected from catalogs derived from Bogazici University Kandilli Observatory and Earthquake Research Institute Regional Earthquake-Tsunami Monitoring Center and Bogazici University Kandilli Observatory and Earthquake Research Institute Meteorology Laboratory.

In time domain analyses, correlations between peak accelerations, velocities, displacements; and magnitude and distance are estimated. The effects of faraway earthquakes on displacement time histories and damping are also investigated. Average drift ratios, computed from both wind and earthquake records, are compared with the limitations provided in the codes. In the frequency domain, natural frequencies, damping and mode shapes are identified by means of spectral analysis for wind and earthquake data. The result of wind and earthquake events on the Sapphire building are compared.

ÖZET

İSTANBUL SAPPHIRE BİNASININ DİNAMİK DAVRANIŞ ÖZELLİKLERİNİN DEPREM VE RÜZGAR VERİLERİ İLE BELİRLENMESİ

Yüksek binaların oranı, nüfus artışı ve şehir merkezlerindeki alanların kısıtlı olması nedeniyle tüm dünyada artmaktadır. Büyük depremlerden sonra ülkeler kaotik koşullarla karşı karşıya kalmaktadır. Bina hasarlarına, ölümlere ve yaralanmalara ek olarak, iş kesintilerine bağlı finansal zararlar da genel deprem zararlarının önemli bir parçasıdır. Bu nedenle, finansal kurumlar, sağlık tesisleri ve hükümet binaları gibi kurumlara ev sahipliği yapan binaların, maddi kayıplarını sınırlamak ve kamu hizmetlerini güvenceye almak için deprem sonrasında işlevsel kalması gerekmektedir. Depremlerden sonra yapıların mevcut durumları, yapıların dinamik özelliklerinde meydana gelen değişimlerin günden güne değerlendirilmesiyle tahmin edilebilmektedir. Bu nedenle, bu çalışmada, Sapphire binasının rüzgar ve deprem olayları sırasındaki dinamik parametreleri zaman tanım alanı ve frekans tanım alanında belirlenmiştir.

Analizlerde kullanılan deprem ve rüzgâr olaylarının bilgileri, Boğaziçi Üniversitesi Kandilli Rasathanesi ve Deprem Araştırma Enstitüsü Bölgesel Deprem-Tsunami İzleme Merkezi ve Boğaziçi Üniversitesi Kandilli Rasathanesi ve Deprem Araştırma Enstitüsü Meteoroloji Laboratuvarı'ndan edinilen kataloglardan seçilmiştir.

Zaman tanım alanı analizlerinde, 51 deprem olayı için belirlenen tepe ivmeleri, hızları ve yer değiştirmelerle, deprem büyüklüklüleri ve depremin merkez üssüne olan mesafeleri arasındaki korelasyonlar belirlendi. Uzak depremlerin yer değiştirme zamanları ve sönümleme üzerindeki etkileri de incelendi. Ortalama göreli ötelenme oranları yapısal yönetmeliklerde izin verilen sınırlamalarla karşılaştırılmıştır. Frekans tanım alanında yapılan analizler neticesinde ise doğal frekanslar, sönüm oranları ve mod şekilleri rüzgar ve deprem verileri için yapılan spektral analizler neticesinde belirlenmiştir.

TABLE OF CONTENTS

LIST OF FIGURES

LIST OF TABLES

LIST OF ACRONYMS

SHM	: Structural Health Monitoring
KOERI	: Kandilli Observatory and Earthquake Research Institude
PA	: Peak Acceleration
PV	: Peak Velocity
PD	: Peak Displacement
GPS	: Global Positioning System
FAS	: Fourier Amplitude Spectrum
EW	: East-West direction
NS	: North-South direction
UD	: Up-Down direction
B1	: Basement 1 level of the building
B9	: Basement 9 level of the building

1. INTRODUCTION

Local governors and contractors prefer tall buildings considering current population growth and limited space in city centers. These tall buildings are built not only for the purpose of accommodation but also to be functioned as business and shopping centers. Some of these are also used by tourism agencies to promote some cities and they are introduced as the landmark of these cities such as the cases of Empire State, Taipei 101, Burj Khalifa, and Petronas Towers. Therefore, recently, the rate of tall buildings has been increasing all around the world.

After major earthquakes, countries located in earthquake-prone areas face catastrophic conditions. In addition to building damages, deaths, and injuries, financial losses due to business interruption are also an important part of overall earthquake losses. For instance, many tall buildings were not functional for weeks because of the strong shaking in the M9.0 Tohoku, Japan earthquake of March 11, 2011 (Çelebi, 2014). Buildings home to organizations such as financial institutions, health care facilities, governmental buildings need to remain functional following an earthquake to constrain financial losses and secure public services.

Continued serviceability of operations, in such structures, is necessary. However, after the construction process, it is not possible to observe that a building designed carefully and detailed have the same dynamic characteristics assumed in the design process. In addition, dynamic properties of structures can change in time due to earthquakes, strong winds, corrosion etc. (Uchida *et al.*, 2004). The effects of these excitations on structures can be estimated by following the changes in the in-situ dynamic properties of structures.

In Turkey, a number of structures, such as tunnels, bridges, museums, and tall buildings are being monitored in real-time. For example, Hagia Sophia Museum, Suleymaniye Mosque, Fatih Mosque, Sultanahmet Mosque, Mihrimah Sultan Mosque, Fatih Sultan Mehmet Bridge, Marmaray tube tunnel and Sapphire Building have dedicated

Structural Health Monitoring (SHM) systems conducted by Kandilli Observatory and Earthquake Research Institute (KOERİ) (Çaktı & Şafak, 2014).

1.1. Objectives

The main objective of this thesis is the estimation of the dynamic characteristics of the Sapphire building, which is the 4th tallest building in Turkey as of 2019 and has an SHM system.

Numerous excitations ranging from winds to earthquakes have been recorded in Sapphire by means of the real-time monitoring system. In this study, wind and earthquake records are analyzed in the time domain and frequency domain in order to identify the dynamic parameters of the Sapphire Building.

In time domain analyses, correlations between peak accelerations (PAs), corresponding peak velocities (PVs), peak displacements (PDs); and magnitude and distance are estimated. The effects of faraway earthquakes on displacement time histories and damping are also estimated. Average drift ratios, computed from both wind and earthquake records, and are compared with the limitations provided in the codes. Thanks to the real-time monitoring system, recordings of several strong wind excitations are available. Both of them are analyzed and compared with those derived from earthquake data.

In the frequency domain, natural frequencies, damping, and mode shapes are estimated by means of spectral analysis for wind and earthquake data.

1.2. Scope and Organizations

In chapter 1, after the brief summary about why SHM is important and necessary, the structural properties of the building which are analyzed in this study are explained and then the SHM system in this building is explained.

In chapter 2, both wind and earthquake data used in the analysis are detailed as to how these are chosen and then signal processing methods applied to the data are presented. After that, the methods and calculations used in the analysis are explained in detail.

In chapter 3, the findings and results of time domain and frequency domain analysis due to wind and earthquake are presented and discussed. Drift ratios and damping computations are also detailed in this chapter.

In chapter 4, the conclusion of the study is summarized.

1.3. Structural Health Monitoring

The construction industry provides great benefit from developing technologies as much as all business sectors do (Constructconnect, 2018). From the first ages to today, numerous structures were designed and constructed with the help of experiences and design codes. Up until today, it was not easy to estimate whether in-situ dynamic characteristics of structures are the same, assumed in the design process. Nowadays, in-situ dynamic characteristics of the structures can be identified by means of software and electronic devices such as accelerometers, displacement meters, Global Positioning System (GPS) sensors, data communication tools (Çelebi & Şanlı, 2002). By this means, design and analysis methods can be checked, and structural design codes can be improved.

If structures are observed in long-term, damage can be detected by means of evaluation of data inventory after an extreme event, losses resulting from power, natural gas and water can be prevented by the prediction of the behavior for future extreme loads.

1.4. The Sapphire Building

Sapphire, located in the central business district of Levent at coordinate 41°5′6.28″N, 29°0′21.96″E on Büyükdere Street in Istanbul, was the tallest building in Istanbul, and the 4th tallest building in Europe when completed in 2011 (Wikipedia). Today, it is the 4th tallest building in Turkey, the 12th tallest building in Europe and 315th tallest building in the World. The general location of the Sapphire is shown in Figure 1.1.

Sapphire is a 65-storey reinforced concrete building supported by steel elements. 55 of the 65 floors are above the ground and 10 floors are below ground where the street level entrance from the main street is to the shopping area after a small plaza. The two top floors are reserved for the café and simulation hall. In different levels of the building, there are residences of different sizes with a private terrace or garden; the building is planned as 4 separate housing zones, and in the 4 common areas between the sections; there are various social areas and indoor gardens for the residents of the building: these buffer zones also house the maintenance and support facilities and the mechanical systems of the building (Tabanlıoğlu Architects). Architectural features of the Sapphire Building are shown in Figure 1.3.

Structural height is 235 m whereas, with the antenna, construction is 261-meter high. The thin building form is supported by the two cores with an 80 cm width at the narrow ends. In addition, there are 16 shear walls with 60 cm width placed symmetrically through the short direction of the building that would add lateral stiffness to the building. The foundation pit excavation for the project – 42.5 meters deep – is the deepest foundation pit excavation for any structure in Turkey (Wikipedia).

A plan view of stories above the shopping area placed above ground is typical rectangular as shown in Figure 1.4, and floor dimensions of 32.3 m x 52.2 m.

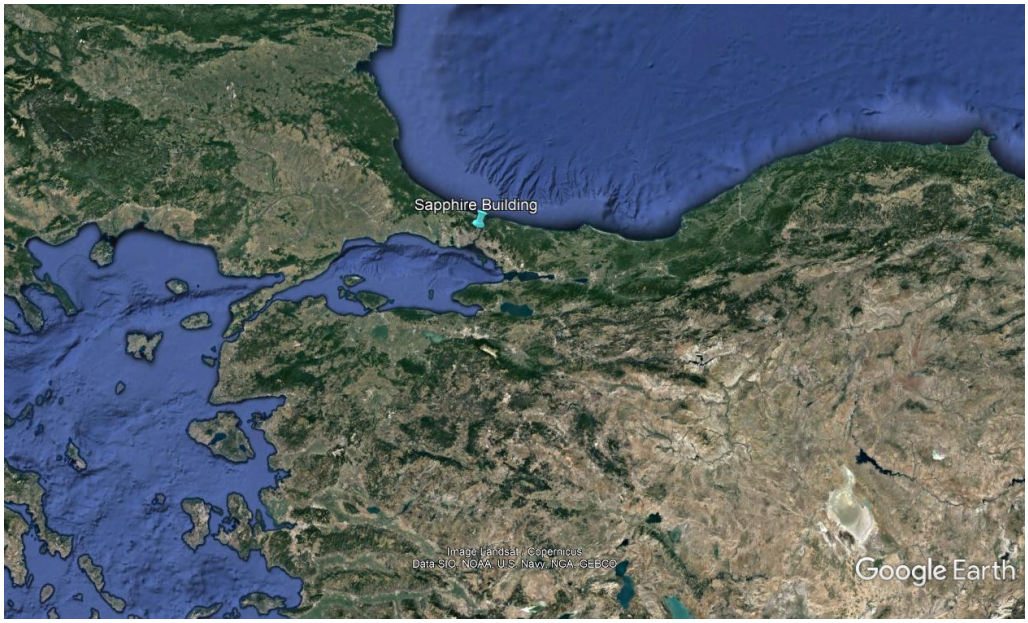

Figure 1.1. General location of the Sapphire Building (Google Earth).

Figure 1.2. The Sapphire Building (Murat Germen, CTBUH).

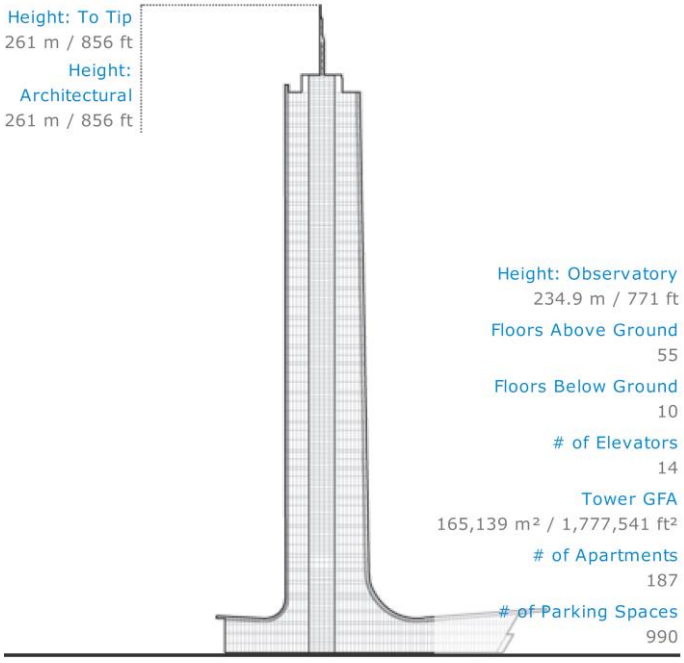

Figure 1.3. Architectural features of Sapphire Building (The Skyscraper Center).

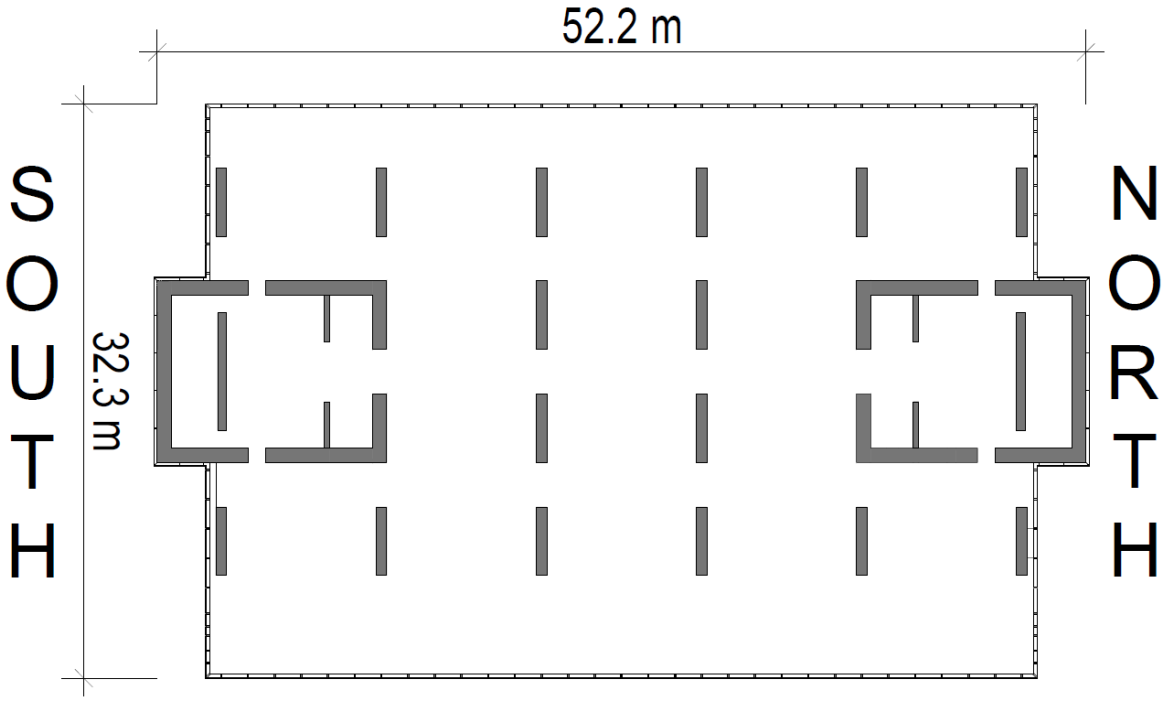

Figure 1.4. Typical plan view (the figure shows the 9th floor).

1.5. Sapphire Structural Vibration Monitoring System

Many earthquakes and strong winds have been recorded in Sapphire since 2012 when the SHM system was installed. The real-time system consists of 13 accelerometers installed on two vertical lines as the northern side and the southern side.

Accelerometers are placed at 7 different floor levels on both the northern and southern sides of the building. They are located at basement 9 (called as B9 hereafter), basement 1 (called as B1 hereafter), 9^{th}, 14^{th}, 25^{th}, 36^{th}, 52^{nd} floor levels. Three-component accelerometers are placed at 9^{th}, 14^{th}, 25^{th}, 36^{th}, 52^{nd} floors and they record vibrations in the East-West direction (called as EW hereafter), in the North-South direction (called as NS hereafter), and Up-Down direction (called as UD hereafter). On level B1, there is only one accelerometer with 3 channels installed on the southern side of the building. However, those located on level B9 on both the northern and southern sides of the building have 2 channels (EW and NS). Instrument layout in 9^{th}, 14^{th}, 25^{th}, 36^{th}, 52^{nd} are identical with each other. The instrument layout placed at floor levels is shown in Figure 1.6.

In Sapphire, there are totally 37 channels and by this means, the vibration monitoring system in the Sapphire Building was satisfied following the minimum instrumentation criteria in “An Alternative Procedure for Seismic Analysis and Design of Tall Buildings Located in The Los Angeles Region” (2017). The criteria are given in Table 1.1. In Sapphire, the number of stories above ground is higher than 50, and thus at least there should be a minimum of 30 channels. In addition, each additional channel allows more realistic results.

The Güralp CMG-5T, which is a three-axis strong motion force feedback accelerometer is chosen in the Sapphire SHM System. The system was operated at 200 Hz level.

Table 1.1. Minimum number of channels of instrumentations (An Alternative Procedure for Seismic Analysis and Design of Tall Buildings Located in the Los Angeles Region, 2017).

Number of Stories Above Ground	Minimum Number of Channels
10-20	15
20-30	21
30-50	24
>50	30

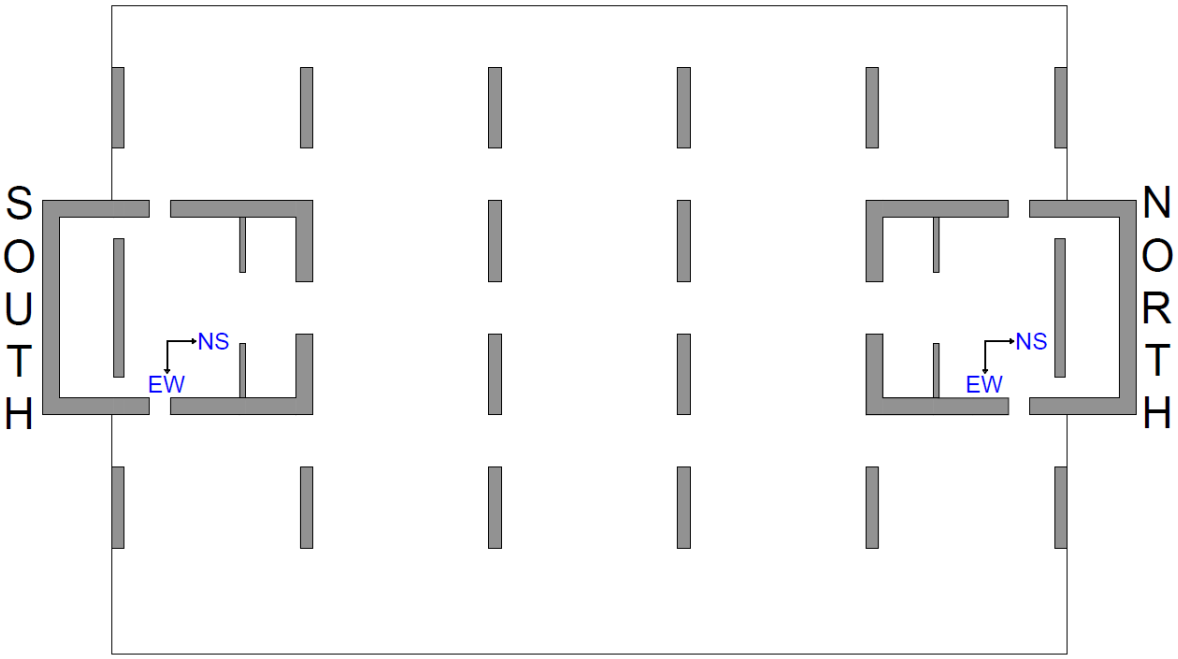

Figure 1.5. Instrument layout in plan view.

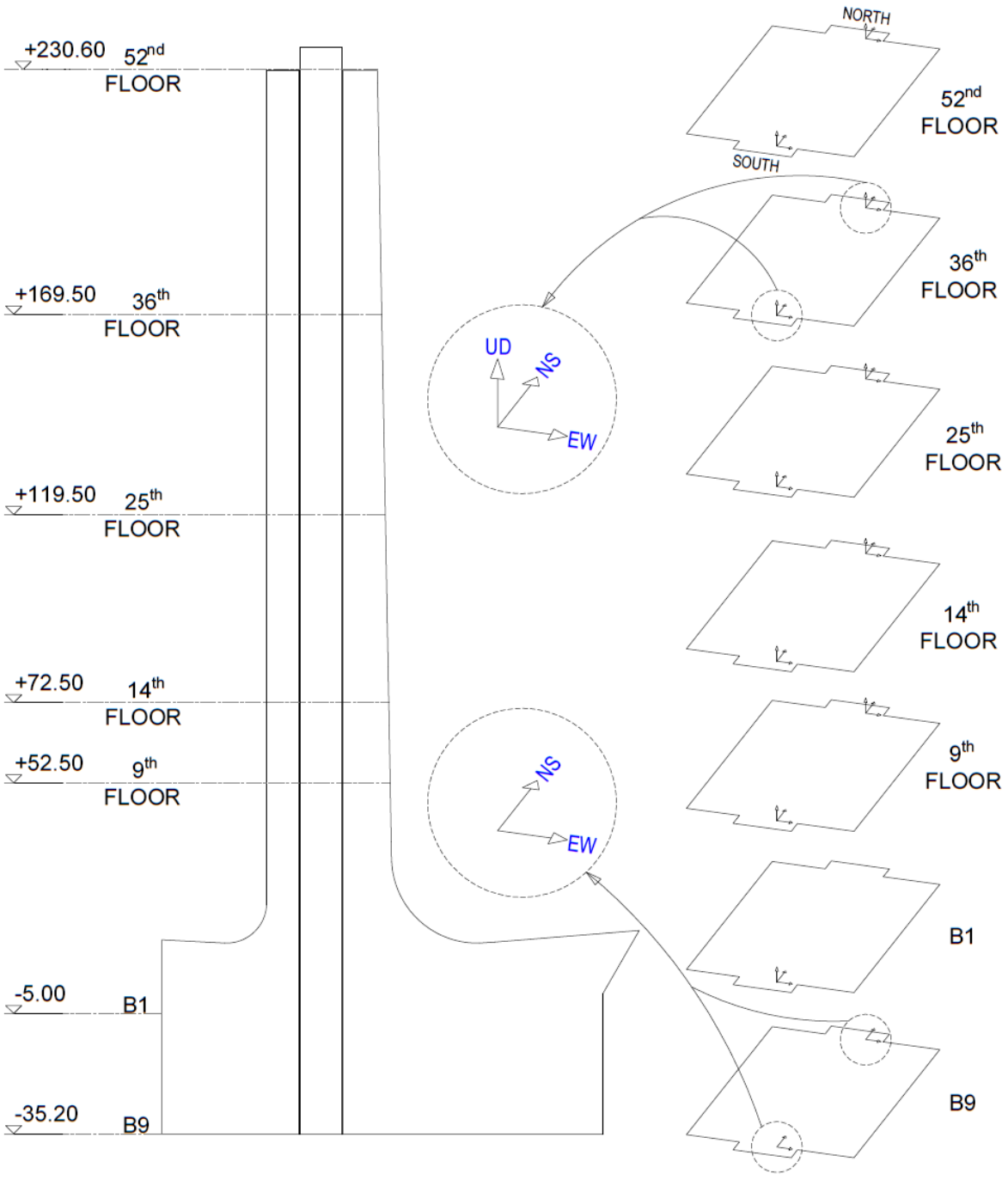

Figure 1.6. Instrument layout in the vertical section for the Sapphire Building (37 channels).

2. DATA REDUCTION AND SIGNAL PROCESSING

Thanks to the real time monitoring system there is a big data set in Sapphire Building. Earthquake and wind events are selected from catalogs derived by Bogazici University KOERI Regional Earthquake-Tsunami Monitoring Center and Bogazici University KOERI Meteorology Laboratory in order to use in the analyses. However, it is not possible to evaluate all records due to both huge amount of data set and errors in records. Therefore, records are eliminated by considering some criteria. In this chapter, these criteria and signal processing methods are explained. In addition, analysis methods and calculation techniques are detailed in chapter 2.4.

2.1. Earthquake Data

In this study, firstly 171 earthquake events are selected and then some of which are eliminated. Firstly, earthquakes which their epicentral distances are far away from 700 km are not included to analyze. Secondly, earthquakes with a magnitude greater than 4 on the Richter scale are selected. Finally, 51 earthquakes occurred in the years between 2013 and 2017 were selected to observe how to affect the dynamic behaviors of Sapphire. The epicenters of selected earthquakes are shown in Figure 2.1. 4 earthquake events, which have the strongest effects, were selected to detailed analyses carried in the time and frequency domain. These events, shown from Figure 3.21 to Figure 3.26 were selected after the analyses of 51 earthquake events.

As seen in Figure 2.2, most of the earthquakes are in the range of M_w=4 and M_w=4.5. And with the increase in the magnitude of the earthquake, the number of earthquakes is decreased. However, there are 3 earthquakes which their moment magnitude greater than 6.0 considered in the analysis.

The distance histogram is seen in Figure 2.3. The closest earthquake occurred in Çınarcık/Yalova which 45 km away from Istanbul. However, the farthest earthquake occurred in Great Island which is 685 km away from Istanbul.

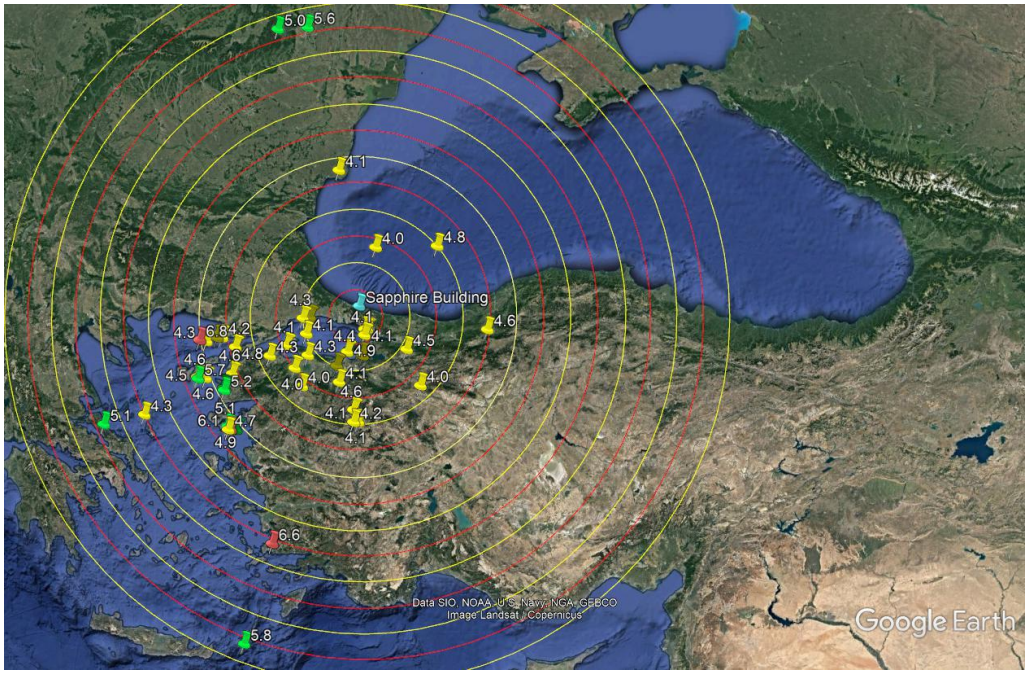

Figure 2.1. Epicenters of earthquakes (Google Earth), the radius of the first circle is 50km and consecutively each radius of circles increases 50km.

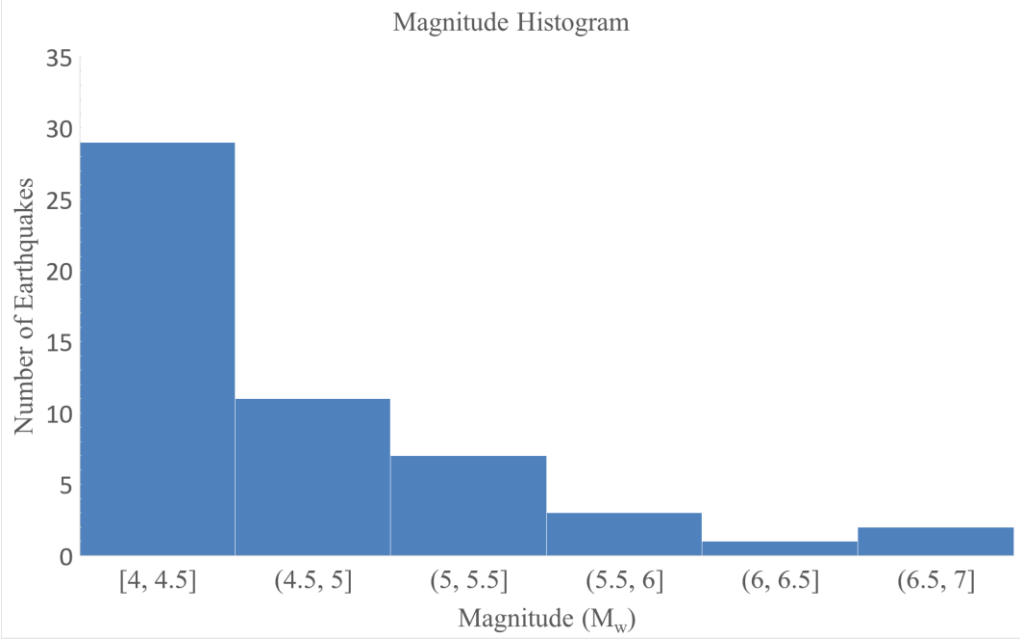

Figure 2.2. Magnitude histogram.

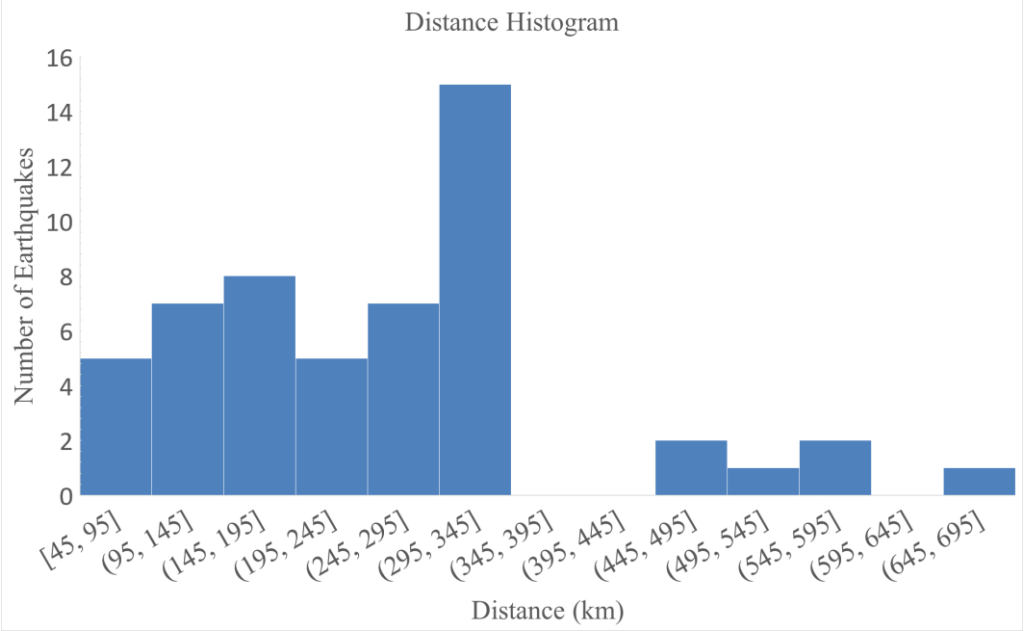

Figure 2.3. Distance histogram.

Table 2.1. Earthquake recorded between 2015 (July) and 2017 (December) in the Sapphire Building.

Event Date (dd.mm.yy)	Time (UTC/local time)	Event Coordinates		Event Location	Magnitude (M_L)	Magnitude (M_w)	Depth (km)	Distance (km)	Peak Ground Acceleration (cm/sec^2)			
		Latitude	Longitude						Southern B9 NS	Southern B9 EW	Northern B9 NS	Northern B9 EW
20171231	20:12:02/23:12:02	40.5658	27.8670	ERDEK ACIKLARI-BALIKESIR (MARMARA DENIZI)	4.1	3.8	12.6	112	0.085	0.072	0.103	0.101
20170721	22:31:00/01:31:00	36.9693	27.4057	GOKOVA KORFEZI (AKDENIZ)	6.6	6.6	7.1	478	0.145	0.145	0.145	0.145
20170617	19:50:04/22:50:04	38.8508	26.4465	EGE DENIZI	5.6	5.4	12.7	331	0.098	0.095	0.089	0.092
20170612	12:28:38/15:28:38	38.8468	26.3252	EGE DENIZI	6.3	6.1	14.4	338	0.385	0.406	0.414	0.436
20170308	20:09:58/23:09:58	39.9755	27.6600	ÇATAK GÖNEN (BALIKESIR)	4.0	3.8	7.5	168	0.115	0.045	0.048	0.041
20170212	13:48:15/16:48:15	39.4997	26.1167	KOCAKOY AYVACIK (ÇANAKKALE)	5.2	5.2	13.3	302	0.118	0.119	0.122	0.135
20170207	02:24:02/05:24:02	39.5235	26.1242	GULPINAR AYVACIK (ÇANAKKALE)	5.3	5.2	12.7	300	0.125	0.085	0.095	0.088
20170206	10:58:01/13:58:00	39.5248	26.0997	GULPINAR AYVACIK (ÇANAKKALE)	5.3	5.1	13.9	301	0.099	0.065	0.073	0.075
20170206	03:51:39/06:51:39	39.5453	26.1087	GULPINAR AYVACIK (ÇANAKKALE)	5.4	5.2	11.0	299	0.147	0.152	0.141	0.154
20161227	23:20:56/02:20:56	45.7140	26.5280	NEREJU-ROMANIA	5.9	5.0	85.4	552	0.090	0.060	0.044	0.042
20161025	21:04:47/00:04:47	39.7947	28.6662	HACIAHMET-MUSTAFAKEMALPASA (BURSA)	4.1	3.9	8.0	146	0.095	0.039	0.044	0.047
20161015	08:18:32/11:18:32	42.1512	30.6945	KARADENIZ	5.0	4.8	10.2	184	0.175	0.232	0.205	0.264
20160717	08:55:41/11:55:41	40.7032	29.1660	KORU-CINARCIK (YALOVA)	3.9	4.1	11.4	50	0.733	0.800	0.684	0.724
20160625	05:40:11/08:40:11	40.7068	29.2122	YALOVA ACIKLARI (MARMARA DENIZI)	4.5	4.4	9.3	50	2.142	2.172	1.873	1.892
20160607	04:09:45/07:09:45	40.2652	29.1523	KAZIKLI-GURSU (BURSA)	4.6	4.3	15.8	92	0.275	0.328	0.233	0.240
20151028	16:20:02/19:20:02	40.822	27.7642	MARMARA DENIZI	4.5	4.3	14.3	108	0.128	0.116	0.136	0.142
20151027	01:25:50/04:25:50	38.9305	24.3465	EGE DENIZI	4.4	4.3	7.9	463	0.012	0.030	0.045	0.036
20151026	20:07:59/23:07:59	39.7903	26.2667	GOKCEBAYIR-EZINE (CANAKKALE)	4.3	4.6	6.7	273	0.018	0.023	0.038	0.023
20151013	23:18:10/02:18:10	39.1407	29.0298	AHLATLICESME-SIMAV (KUTAHYA)	4.3	4.2	10.4	216	0.085	0.018	0.075	0.021
20150922	06:25:04/09:25:04	39.1505	29.1297	INLICE-SIMAV (KUTAHYA)	4.1	3.7	10.7	215	0.086	0.024	0.072	0.016
20150922	07:11:11/10:11:11	39.1495	29.1292	INLICE-SIMAV (KUTAHYA)	4.1	4.1	11.7	215	0.066	0.035	0.045	0.030
20150919	22:30:28/01:30:28	39.8122	30.4488	TEPEBAŞI (ESKISEHIR)	4.0	3.7	8.7	187	0.068	0.026	0.076	0.025
20150910	08:12:45/11:12:45	38.8395	26.2778	SAKIZ ADASI (EGE DENIZI)	4.9	4.7	15.4	341	0.071	0.029	0.040	0.034
20150903	08:23:29/11:23:19	39.1485	29.1310	INLICE-SIMAV (KUTAHYA)	4.1	4.0	10.5	216	0.056	0.033	0.031	0.018
20150724	02:39:42/05:39:42	40.2435	26.2873	KOCADERE-ECEABAT (CANAKKALE)	4.9	4.8	11.9	248	0.069	0.029	0.039	0.034
20150724	06:54:09/09:54:09	40.2513	26.3053	KOCADERE-ECEABAT (CANAKKALE)	4.6	4.2	10.7	246	0.073	0.039	0.052	0.042
20150724	01:26:00/04:26:00	40.2427	26.3025	KOCADERE-ECEABAT (CANAKKALE)	4.5	4.1	11.2	246	0.090	0.019	0.020	0.024

Table 2.2. Earthquake recorded between 2015 (July) and 2013 (January) in the Sapphire Building.

Event Date (dd.mm.yy)	Time	Event Coordinates		Event Location	Magnitude (M_L)	Magnitude (M_w)	Depth (km)	Distance (km)	Peak Ground Acceleration (cm/sec^2)			
		Latitude	Longitude						Southern B9 NS	Southern B9 EW	Northern B9 NS	Northern B9 EW
20150715	20:30:36/22:30:36	43.3475	28.3355	BULGARISTAN	4.1	3.8	15.5	258	0.075	0.017	0.024	0.023
20150702	22:22:25/01:22:25	39.6805	27.8470	KABAKDERE (BALIKESIR)	4.0	3.8	5.5	184	0.080	0.026	0.024	0.024
20150429	04:40:52/07:40:52	42.0845	29.3045	KARADENIZ	4.0	3.9	15.2	114	0.101	0.084	0.136	0.106
20150416	18:07:44/21:07:44	35.1613	26.9055	GIRIT ADASI ACIKLARI (AKDENIZ)	6.1	5.8	29.4	684	0.131	0.030	0.023	0.019
20150123	10:19:42/12:19:42	40.0657	28.5903	UGURLUPINAR-MUSTAFAKEMALPASA (BURSA)	4.5	4.2	5.0	119	0.124	0.134	0.102	0.128
20141216	09:02:13/11:02:13	40.14798	27.0835	CELTIK-BIGA (CANAKKALE)	4.4	4.3	12.9	193	0.102	0.056	0.041	0.046
20141206	01:45:06/03:45:06	38.8917	26.2603	EGE DENIZI	5.2	5.1	13.7	338	0.074	0.043	0.036	0.038
20141206	06:20:53/08:20:53	38.8912	26.2602	EGE DENIZI	5.0	4.9	15.2	338	0.111	0.041	0.048	0.066
20141128	02:30:06/04:30:06	39.3465	29.0165	ASAGIDOLAYLAR-SIMAV (KUTAHYA)	4.5	4.6	3.9	193	0.139	0.036	0.036	0.031
20141122	19:14:15/21:14:15	45.7770	27.2605	ROMANYA	5.6	5.6	19.4	540	0.148	0.127	0.137	0.133
20141117	23:05:55/01:05:55	38.6722	23.4262	YUNANISTAN	5.1	5.1	14.1	546	0.010	0.012	0.027	0.038
20141022	17:11:05/20:11:05	40.4065	30.1147	TASOLUK-GEYVE (SAKARYA)	4.5	4.5	7.5	120	0.238	0.250	0.270	0.268
20140811	22:23:31/01:23:31	40.3735	25.8525	KALEKOY-GOKCEADA (CANAKKALE)	4.0	4.1	7.7	277	0.014	0.024	0.019	0.049
20140803	22:22:44/01:22:44	40.6075	29.1652	TERMAL (YALOVA)	4.1	3.8	11.5	55	0.111	0.112	0.100	0.103
20140703	05:04:46/08:04:46	40.2088	27.9333	KUS GOLU	4.5	4.3	11.8	133	0.119	0.118	0.127	0.113
20140524	09:25:01/12:25:01	40.3043	25.4580	EGE DENİZİ	6.5	6.8	21.2	311	0.024	0.027	0.027	0.024
20140524	11:33:07/14:33:07	40.2942	25.6150	EGE DENİZİ	4.7	4.3	5.4	299	2.297	2.426	2.466	2.503
20131127	04:13:37/06:13:37	40.8455	27.9187	MARMARA EREGLISI ACIKLARI-TEKIRDAG (MARMARA DENIZI)	4.7	4.6	10.8	95	0.160	0.162	0.178	0.171
20131124	20:49:37/22:49:37	40.7848	31.8763	ULUMESCİT(BOLU)	4.8	4.6	7.6	243	0.078	0.080	0.097	0.090
20130829	06:20:34/09:20:34	40.3478	27.4458	GERLENGEC-BIGA (CANAKKALE)	4.2	4.1	14.8	155	0.065	0.042	0.069	0.045
20130730	05:33:08/08:33:08	40.3102	28.8067	KALEKÖY-GÖKÇEADA (ÇANAKKALE)	5.3	4.9	13.2	88	0.185	0.197	0.199	0.213
20130712	00:36:57/03:36:57	40.3860	25.9683	SAROS KÖRFEZİ (EGE DENİZİ)	4.3	4.2	16.5	267	0.046	0.030	0.019	0.022
20130113	08:55:13/10:55:13	39.6697	25.4790	EGE DENİZİ	5.0	4.6	6.0	338	0.024	0.020	0.035	0.018
20130111	00:30:19/02:30:19	39.6860	25.4987	EGE DENİZİ	4.7	4.5	7.6	335	0.055	0.017	0.020	0.015
20130109	15:41:33/17:41:33	39.6728	25.6705	EGE DENİZİ	5.0	4.6	4.0	323	0.031	0.030	0.055	0.036
20130108	14:16:06/16:16:06	39.6482	25.4957	EGE DENİZİ	6.2	5.7	8.0	338	0.617	0.644	0.581	0.619

2.2. Wind Data

Strong wind excitations caused financial loses and injuries in Istanbul were recorded thanks to the real-time recording system and are analyzed how Sapphire response for these excitations. The most destructive storm excitation was recorded on 27 July 2017. The storm with a speed of 80km/hours lasted just 20 minutes but was enough to cause significant damage and flooding (Reuters). According to officials, 7350 emergency workers were deployed to help in the aftermath of the storm, which destroyed 296 roofs and uprooted 389 trees, one of which is a monumental tree with 26 meters height and 176 years old, across the city. During the storm, the minaret of Çarsı Mosque was destroyed, Marmaray tube tunnel and Avrasya tunnel were closed. (IBB, 2017). In addition to the wind of 27 July 2017, three additional wind excitations which are occurred on 23 September 2014, 09 April 2015, 07 May 2015, are also analyzed.

2.3. Data Processing

The recorded accelerations don't always reflect actual behaviors due to both technical problems and secondary effects. There are many factors affecting the recorded motion in accelerometers. For example, objects can hit accelerometers during earthquakes, and an unrealistic peak can be observed. Therefore, the observation and processing of recorded motion is an obligation. At this point, all records are checked in acceleration time histories, as shown in Figure 3.1 in order to detect whether there is an irrelevant peak or there is a gap in records.

In nature, there are numerous vibrations ranging from birds to vehicles and structures are exposed to these unwanted or unknown vibrations and frequencies. Therefore, it is avoidable to eliminate undesirable vibrations to focus on what to research. Band-pass filters, removing mean value from recorded data according to chosen low and high corner frequencies, are preferred in the data processing. Whereas low corner frequency removes the mean and low-frequency errors, high corner frequency removes high frequencies that are usually dominated by noise. That all significant modes of the structure are within that bandwidth take account in the selection of corner frequencies. The low corner frequency is chosen as 0.05 Hz and high corner frequency is chosen as 10 Hz. Raw data is filtered firstly

from the beginning of the motion to the end of the motion and then from the end of the motion to the beginning of the motion in order to prevent the phase change distorted by digital filters. In addition, both before and after filtering operations, linear trends in the data eliminated. This operation is named as “baseline correction”. In this process, the record is fitted by performing a straight line and then the difference is subtracted. In this way, before and after, linear trends are removed (Boore and Bommer, 2004).

It is necessary to smooth data collected via accelerometers to identify dynamic properties in some cases. For instance, little discrepancies can be seen in the case of natural frequencies. Therefore, smoothing enhances to choose genuine natural frequencies. This little difference in natural frequencies affect the mode shapes. Therefore, in the determination of mode shapes, smoothing is used.

2.4. Methodology

After the determination of events and gather from real-time recorded data sets, acceleration records for each event (earthquakes or winds) are turned into from raw data to corrected acceleration records in accordance with signal processing methods explained in chapter 2 by means of MATLAB software. In order to that raw data turn into corrected data; baseline correction is carried out with *detrend* command in MATLAB software. Filtering operations are carried out in MATLAB with using *filtfilt* command filtering raw data firstly from the beginning of the motion to end of the motion and then from the end of the motion to the beginning of the motion prevent the phase change. In addition, smoothing is carried out in MATLAB with *smooth* function developed by Safak E.

Corrected accelerations were plotted and evaluated, velocities that are the first integration of corrected accelerations and displacements which are the second integration of corrected accelerations for each selected event were computed and plotted.

Torsional accelerations are derived from the difference of two parallel records at locations on the northern and southern sides of each floor levels in order to estimate how much dominant of torsional behavior is in Sapphire Building.

Average drift ratios are computed from displacement time histories by considering relative displacements any two floors on both the northern and southern sides of the building.

Fourier Amplitude Spectrum (FAS) is used to detect natural frequencies. This operation is performed in MATLAB with *fft* command. Torsional FAS is derived from subtracting two parallel accelerations in the EW and NS directions.

After the determination of natural frequencies for EW, NS, and torsional directions, corrected acceleration time histories are filtered considering natural frequencies in order to focus just mode shapes. Following, modal displacement time histories are estimated and modal displacements corresponding to each story are selected for a random while. After that, particle motions and mode shape profiles are plotted.

Two damping estimation methods as logarithmic decrement and half-power bandwidth are used in this study. These calculations are carried out in MATLAB by means of developed functions.

3. DYNAMIC RESPONSE CHARACTERISTICS

Dynamic response characteristics of wind and earthquake events are studied under 4 different titles about as time domain characteristics, frequency domain characteristics, average drift ratios, and damping.

3.1. Time Domain Characteristics

PAs, PVs, and PDs are estimated for selected wind and earthquake records at the 52nd, 36th, 25th, 14th, 9th, B1 and B9 floor levels on the northern and southern sides of the Sapphire Building. Correlations between PAs, PVs, and PDs, at the 52nd floor level; and magnitude and distance are estimated.

3.1.1 Earthquake Response

Dynamic response characteristics due to 51 earthquakes, shown in Table 2.1 and Table 2.2 are summarized in this section. The biggest response on the building is recorded after the main shock of the M_w = 6.9 Aegean Sea Turkey earthquake of 24 May 2014 (called as Aegean Sea earthquake hereafter) at an epicentral distance of 311 km. Figure 3.1 and Figure 3.2 show the corrected acceleration time histories due to the Aegean Sea earthquake. Figure 3.3 and Figure 3.4 show the velocity time histories. Figure 3.5 and Figure 3.6 show corresponding displacement time histories on 7 different floor levels in the EW and NS directions. PAs, PGs, and PDs on seven different floor levels recorded during the Aegean Sea Earthquake are summarized in Table 3.1.

The structural system is more slender in the EW direction when compared with the NS direction. Since, EW direction is the shortest side of the building and cores, shown in Figure 1.4, are more effective in the NS direction when compared with shear-walls, placed on the EW side. Therefore, the displacement response of the structure, shown in Figure 3.5 in the EW direction is longer than in the NS direction, shown in Figure 3.6.

Table 3.1. PAs, PVs, and PDs in the EW and NS directions recorded on the southern side of the building during M_w = 6.9 Aegean Sea Turkey earthquake of 24 May 2014.

Aegean Sea Turkey, earthquake of 24 May 2014						
Magnitude				M_w = 6.9		
Epicentral Coordinate (Latitude/Longitude)				40.2942 25.615		
Epicentral Distance (km)				311		
	NS Direction			EW Direction		
Number of Storey	PA (cm/s^2)	PV (cm/s)	PD (cm)	PA (cm/s^2)	PV (cm/s)	PD (cm)
52	12.54	2.83	2.30	9.41	3.09	3.06
36	8.58	1.97	1.75	7.98	1.97	1.95
25	9.33	1.85	1.65	7.77	1.34	1.32
14	13.53	1.92	1.42	11.75	1.08	0.73
9	9.96	1.61	1.28	8.61	0.91	0.65
B1	4.20	0.72	0.93	3.92	0.42	0.49
B9	2.47	0.41	0.50	2.50	0.43	0.52

Although torsional accelerations can be identified in acceleration time histories, lateral deformations are highly larger than those in torsional deformations and so torsional behavior is not dominant when compared with lateral behavior as seen in Figure 3.7.

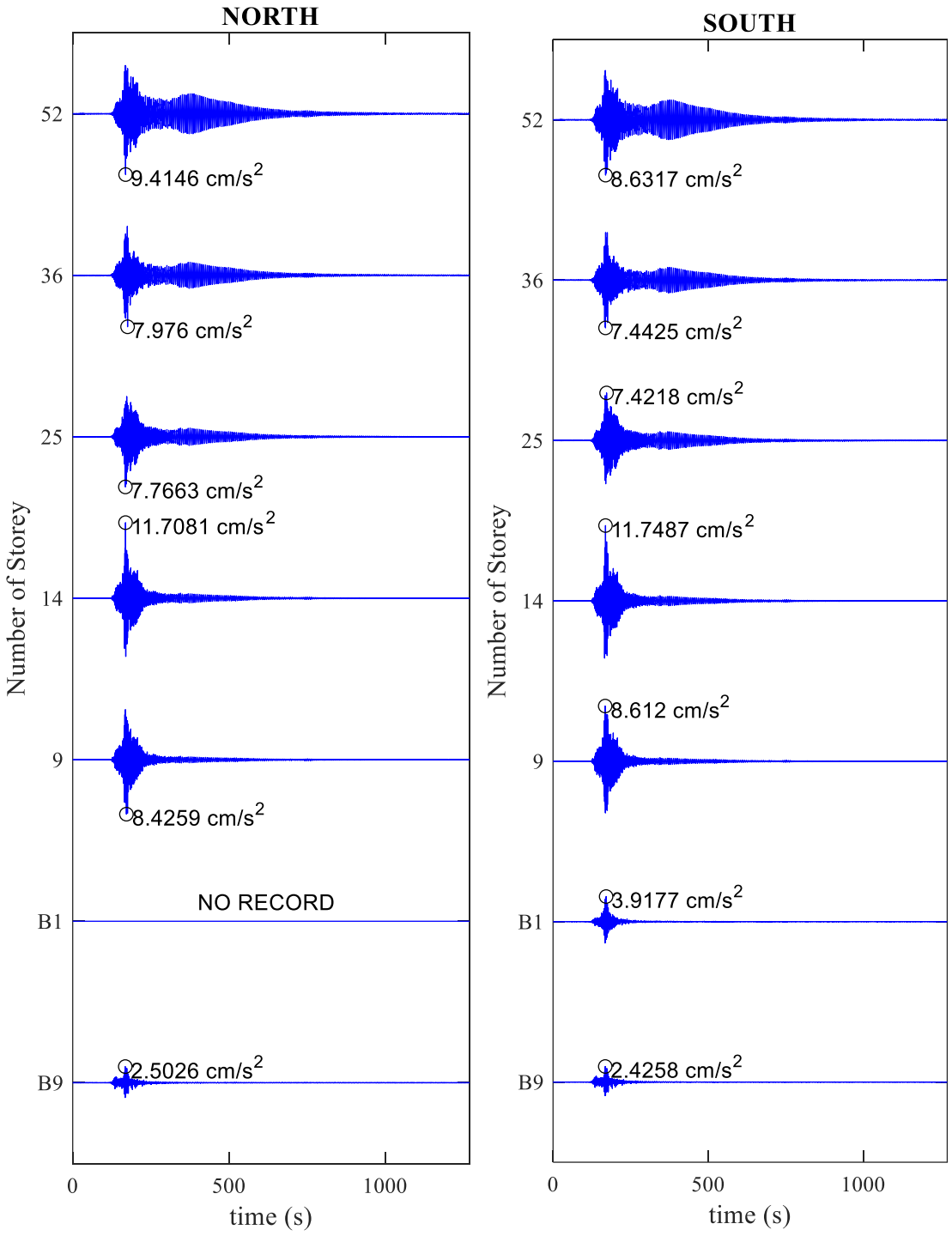

Figure 3.1. Acceleration time histories in the EW direction, recorded at B9, B1, 9th, 14th, 25th, 36th, 52nd floor levels on the northern and southern sides of the building during the Aegean Sea earthquake.

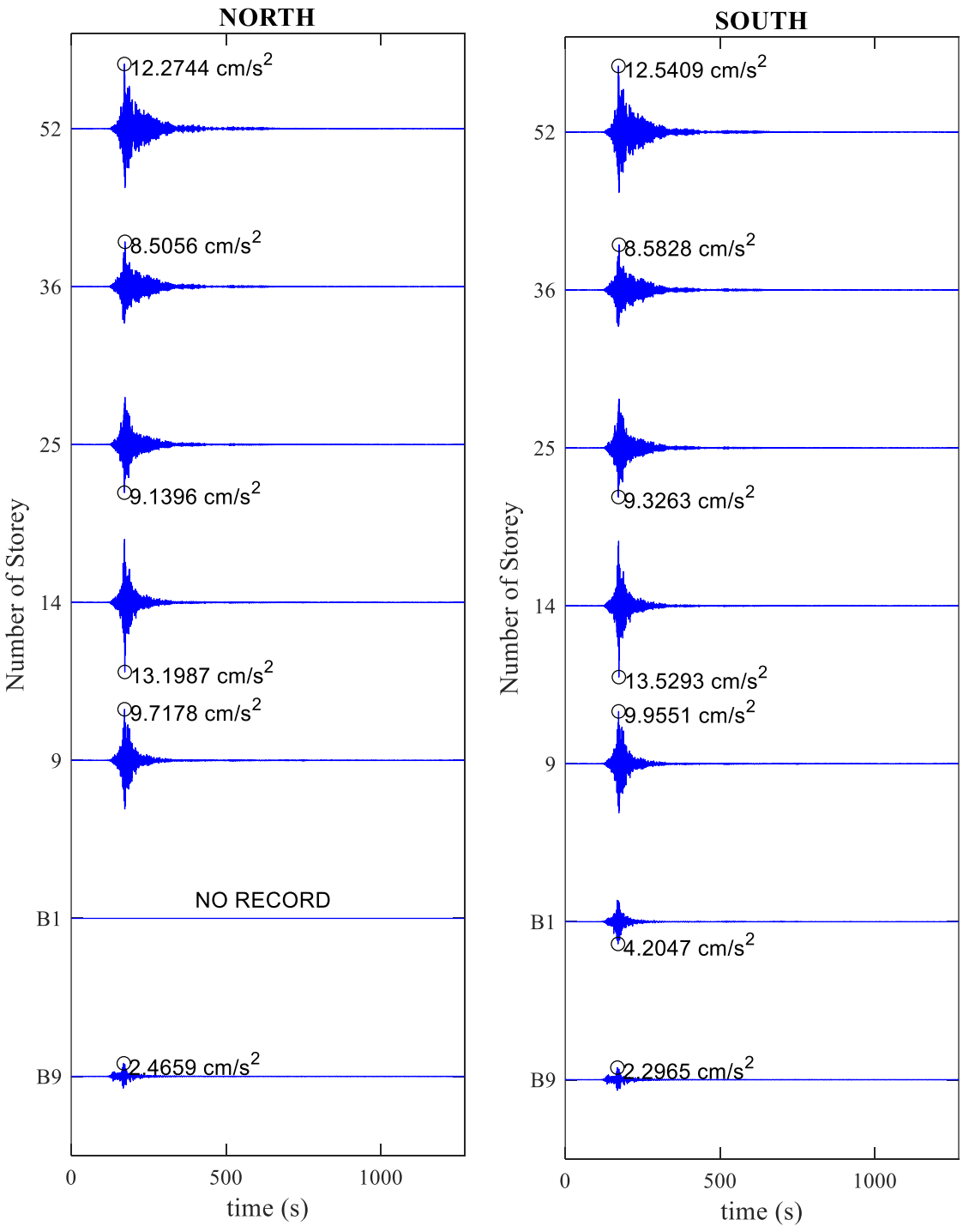

Figure 3.2. Acceleration time histories in the NS direction, recorded at B9, B1, 9th, 14th, 25th, 36th, 52nd floor levels on the northern and southern sides of the building during the Aegean Sea earthquake.

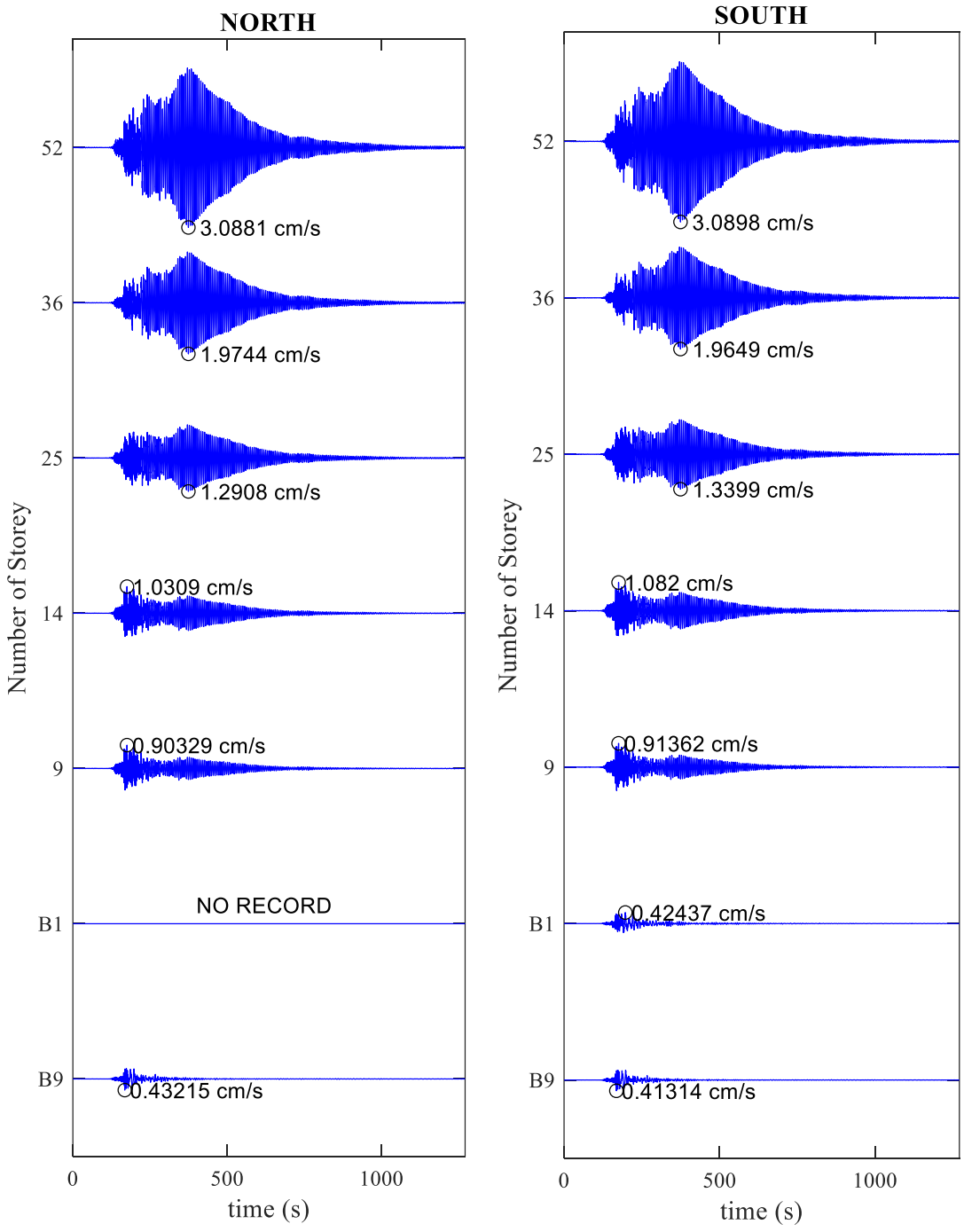

Figure 3.3. Velocity time histories in the EW direction, recorded at B9, B1, 9th, 14th, 25th, 36th, 52nd floor levels on the northern and southern sides of the building during the Aegean Sea earthquake.

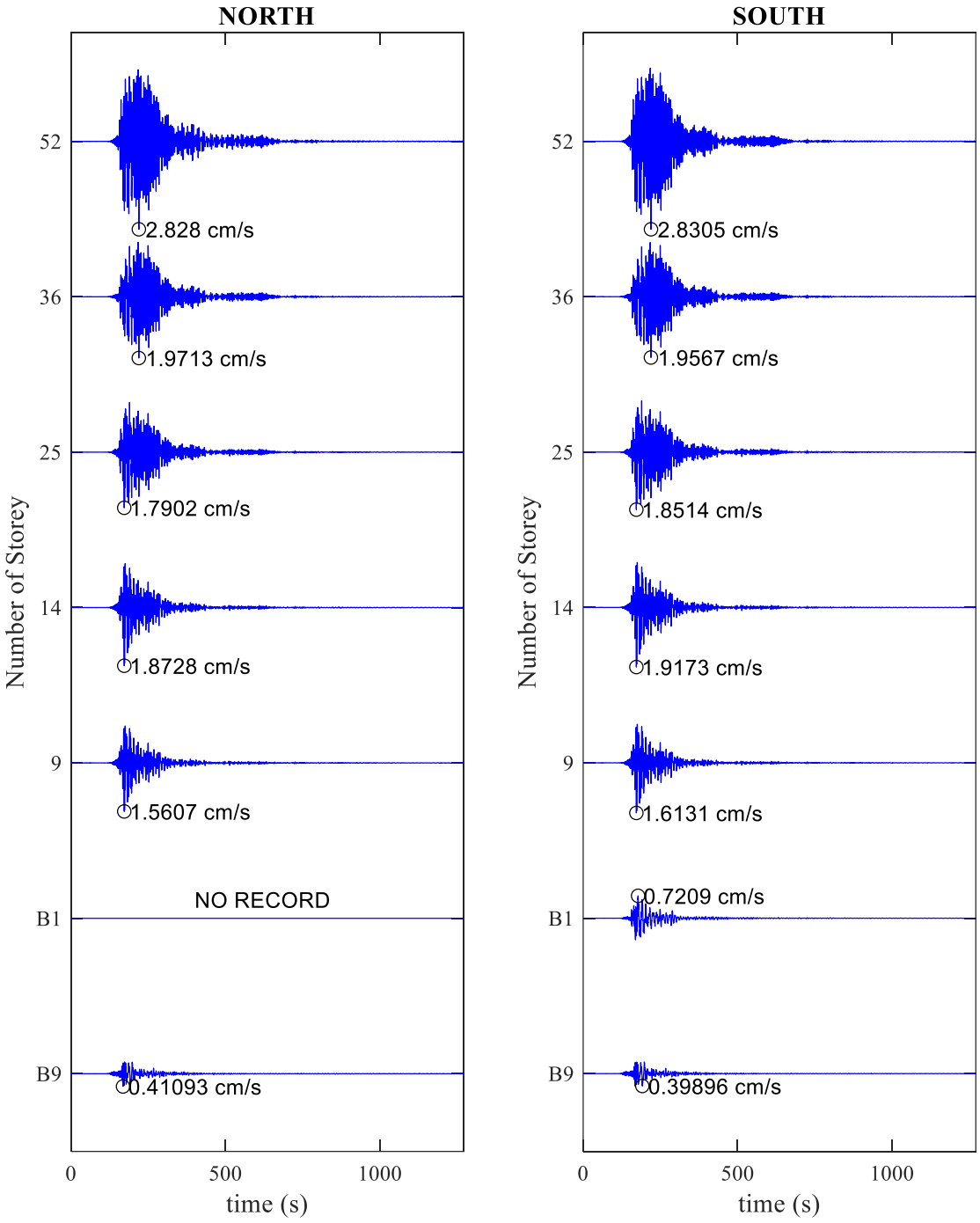

Figure 3.4. Velocity time histories in the NS direction, recorded at B9, B1, 9th, 14th, 25th, 36th, 52nd floor levels on the northern and southern sides of the building during the Aegean Sea earthquake.

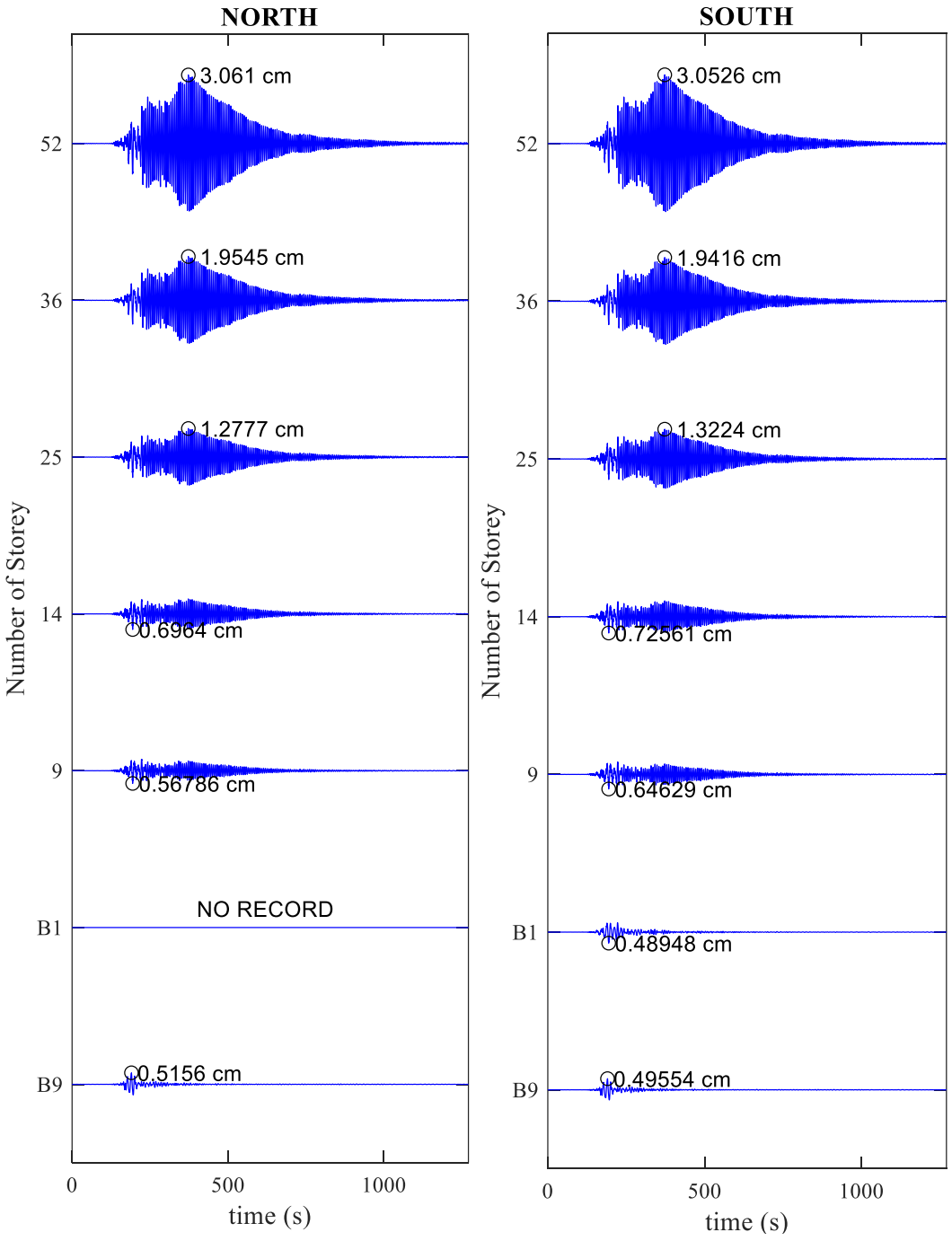

Figure 3.5. Displacement time histories in the EW direction, recorded at B9, B1, 9th, 14th, 25th, 36th, 52nd floor levels on the northern and southern sides of the building during the Aegean Sea earthquake.

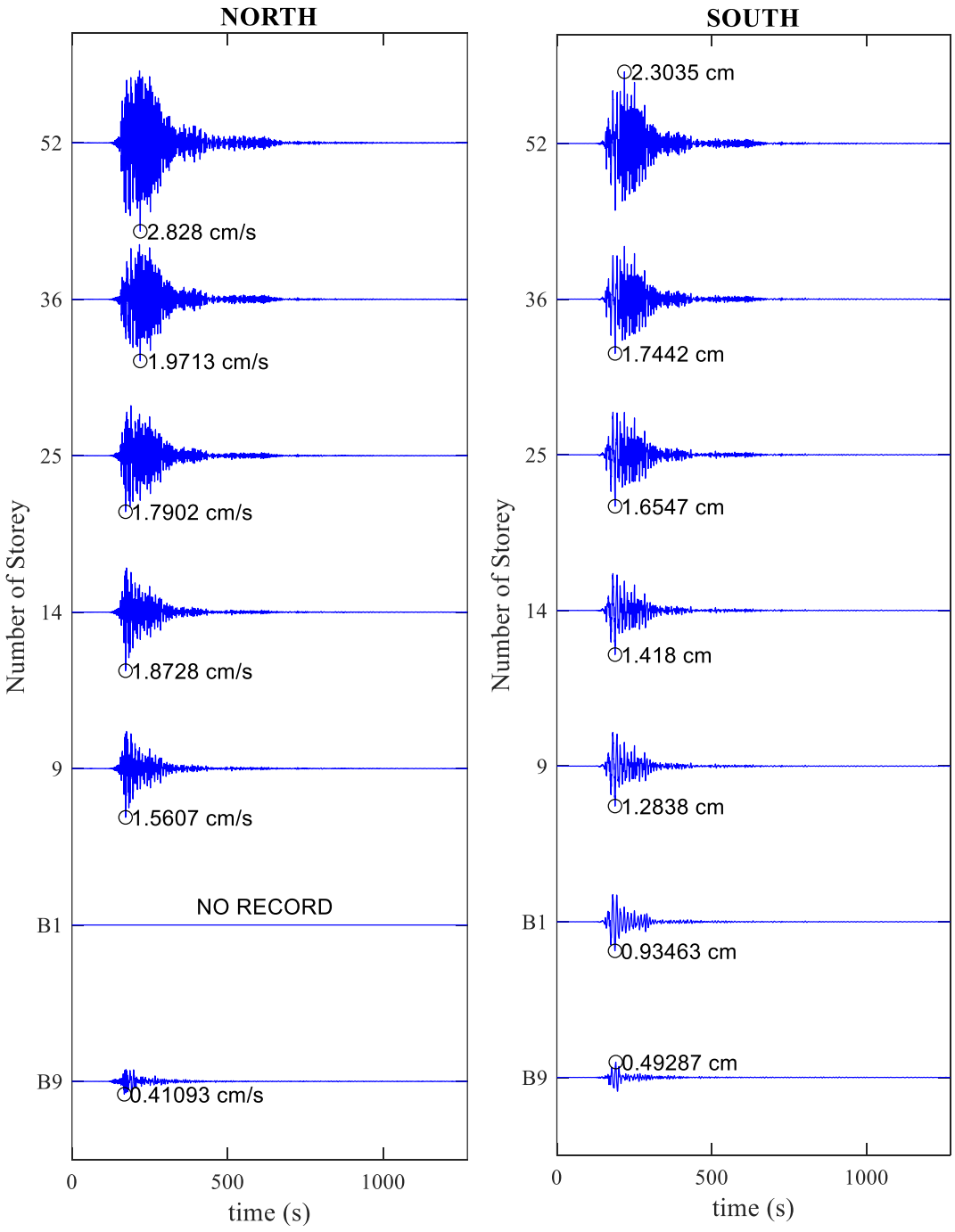

Figure 3.6. Displacement time histories in the NS direction, recorded at B9, B1, 9th, 14th, 25th, 36th, 52nd floor levels on the northern and southern sides of the building during the Aegean Sea earthquake.

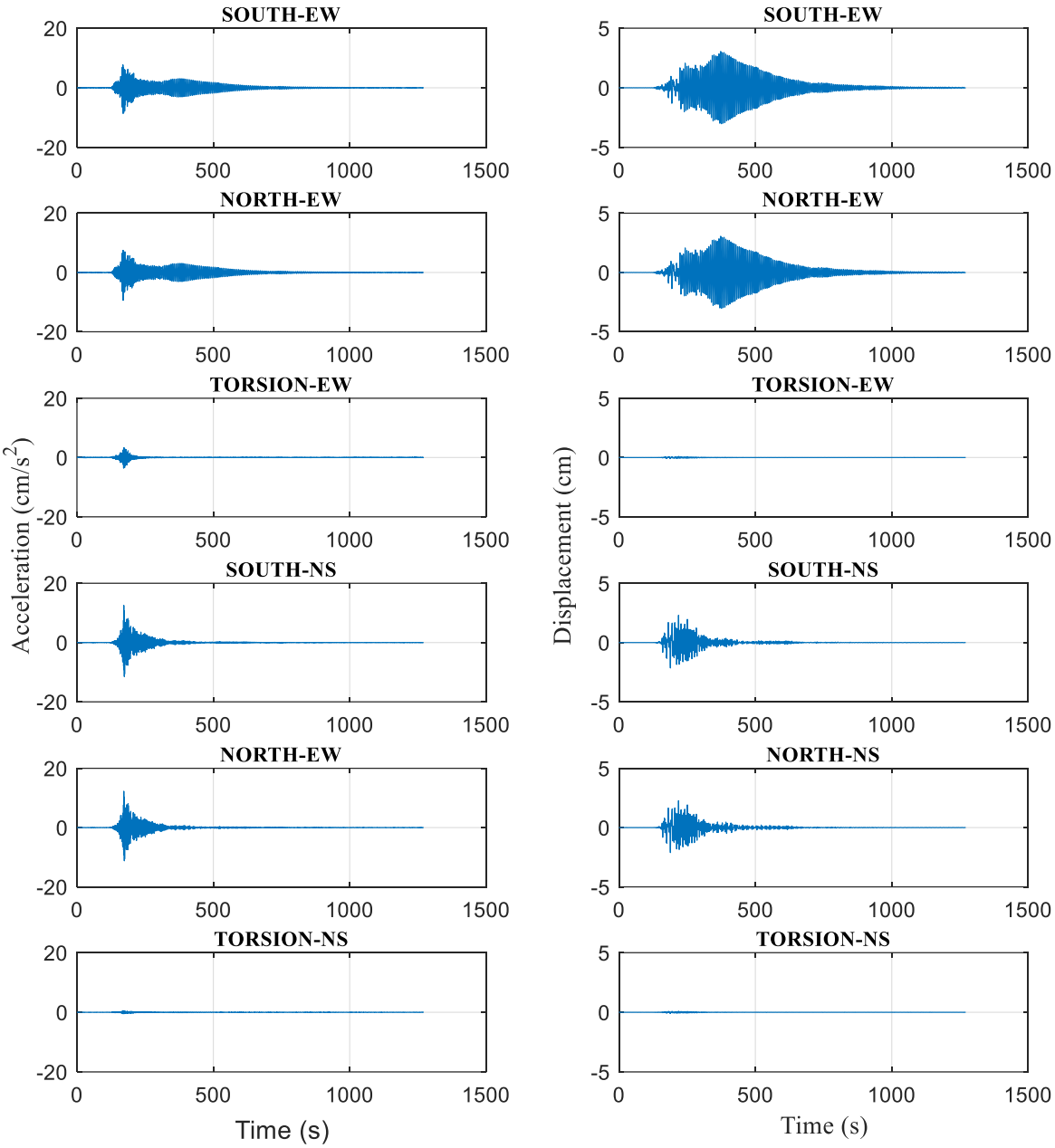

Figure 3.7. The acceleration and displacement time histories in the EW and NS direction, recorded at the 52nd floor level on the northern and southern sides of the building during the Aegean Sea Earthquake. Torsional time histories are estimated from the difference of two parallel records on the northern and southern sides of the 52nd floor level.

There is a difference between the arrival time of the earthquake excitation, which occurred in the Aegean Sea earthquake which is a faraway earthquake, and the beginning time of displacements. This behavior is shown in Figure 3.8, Figure 3.9 and Figure 3.10. When earthquake excitation arrives at the building, displacement response has also begun but it is a very small amplitude. Displacements in the free response range are much higher than those in the arrival time of the earthquake.

While the ground response is observed at B9 and B1, the free response of the building begins at 9^{th} floor level, as seen in Figure 3.8 and Figure 3.9. However, the dynamic characteristics profile, comprising acceleration, velocity, and displacement, along with the height dramatically change at the level of the 9^{th} of the building. This behavior can be seen in logarithmic scale profiles shown in Figure 3.19 and Figure 3.20.

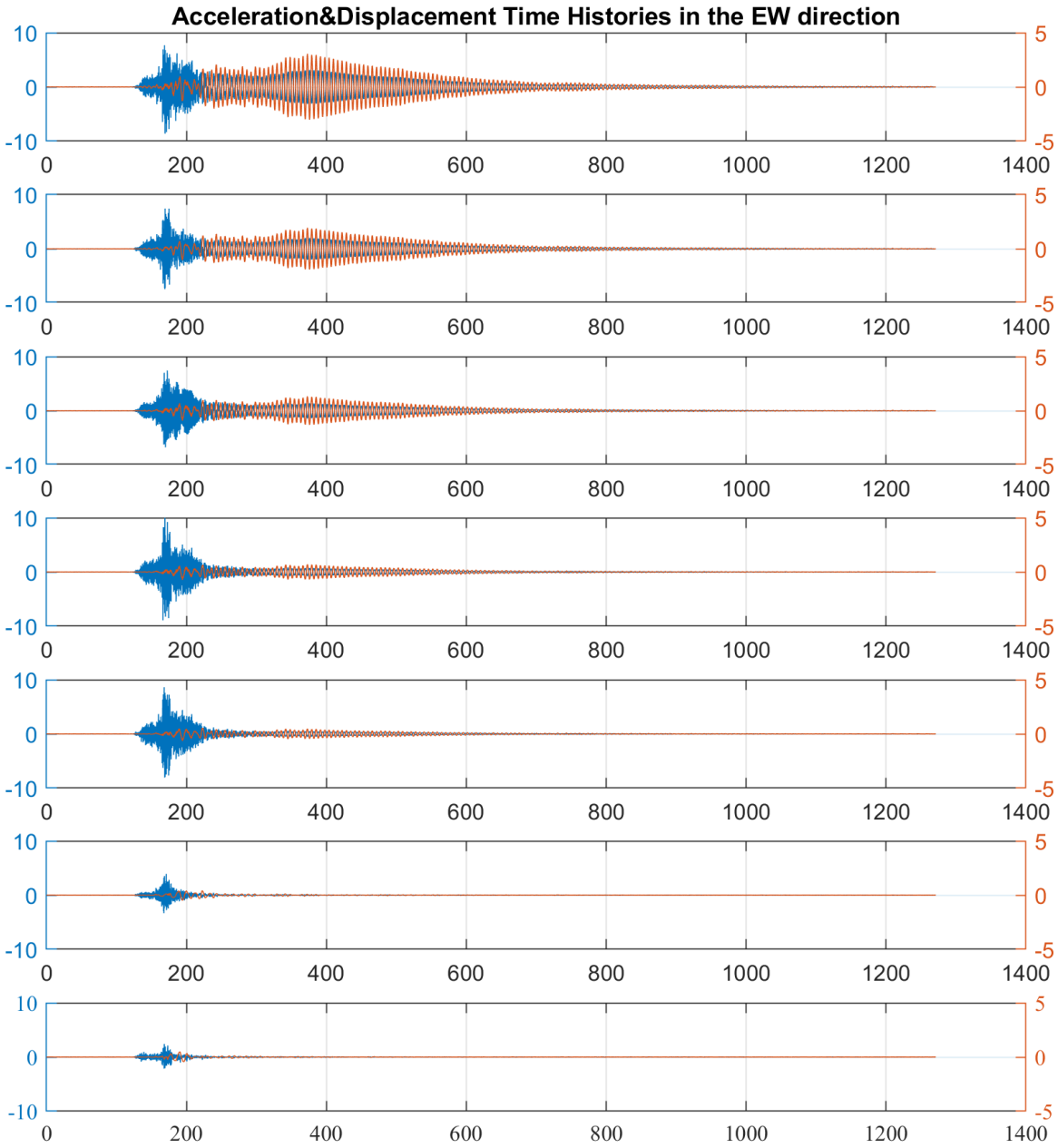

Figure 3.8. Recorded acceleration [blue line] and estimated displacement [orange line] time histories in the EW direction at B9, B1, 9th, 14th, 25th, 36th, 52nd floor levels on the southern side of the building, during the Aegean Sea earthquake.

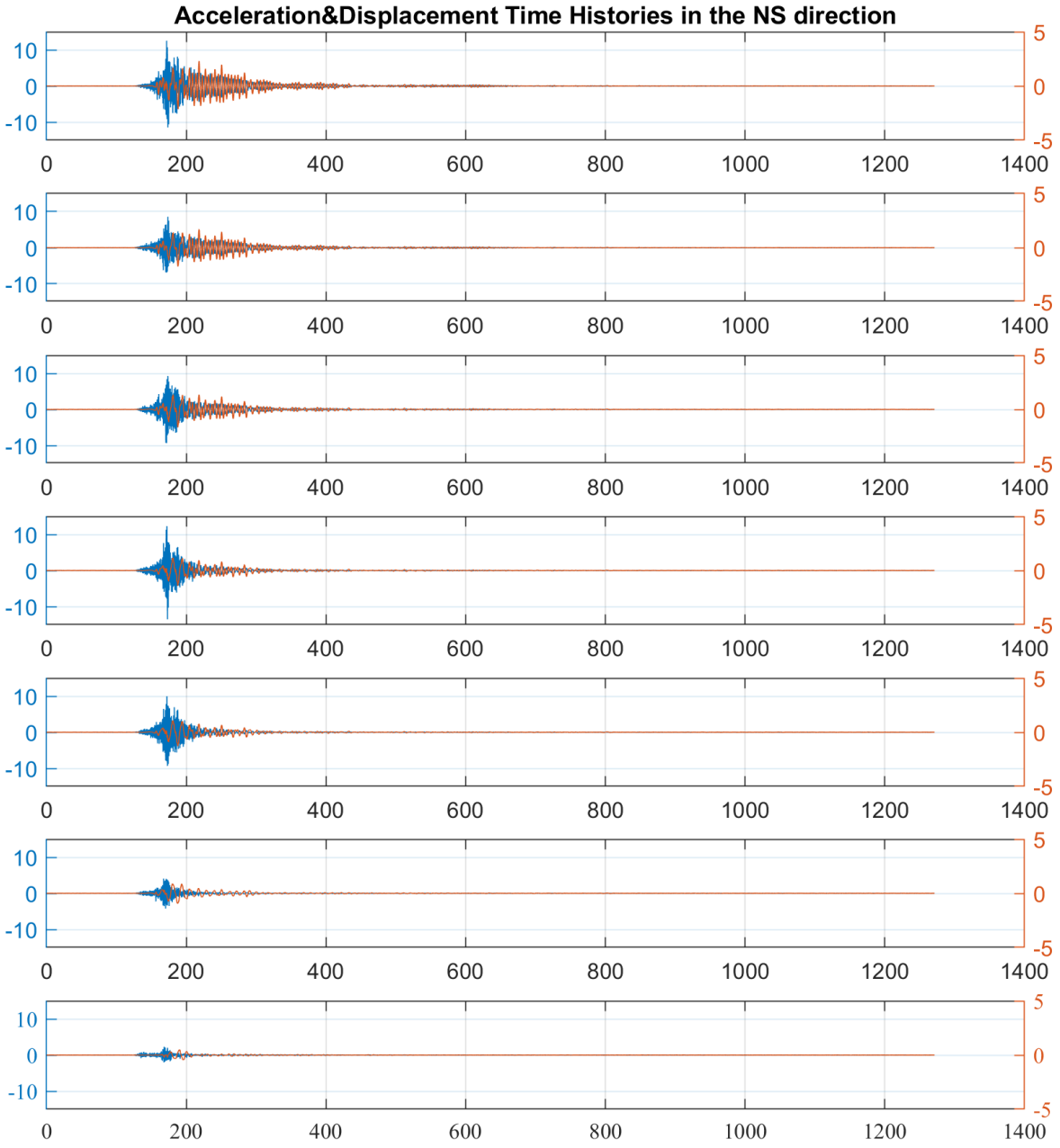

Figure 3.9. Recorded acceleration [blue line] and estimated displacement [orange line] time histories in the NS direction at B9, B1, 9th, 14th, 25th, 36th, 52nd floor levels on the southern side of the building, during the Aegean Sea Earthquake.

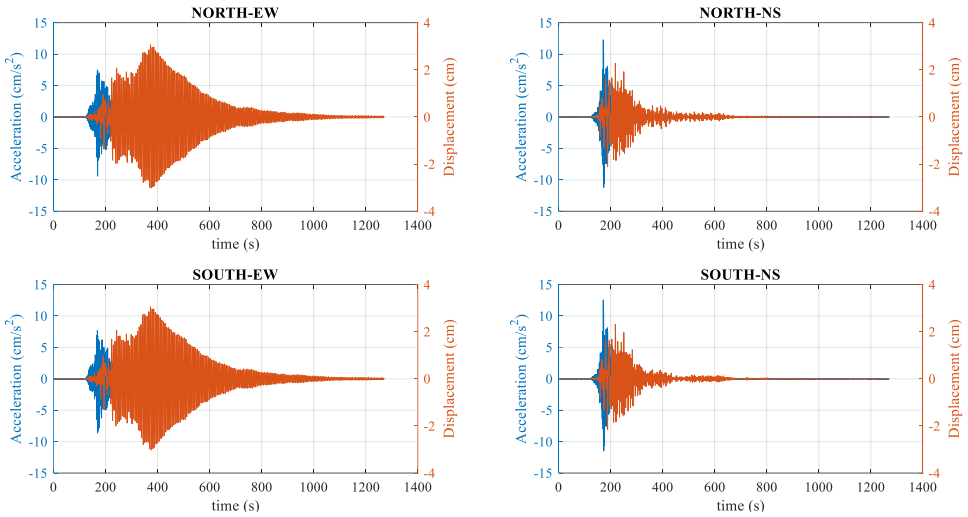

Figure 3.10. Recorded roof acceleration [blue line] and estimated roof displacement [orange line] time histories in the EW and NS directions at the 52nd floor level on the northern and southern sides of the building, during the Aegean Sea earthquake

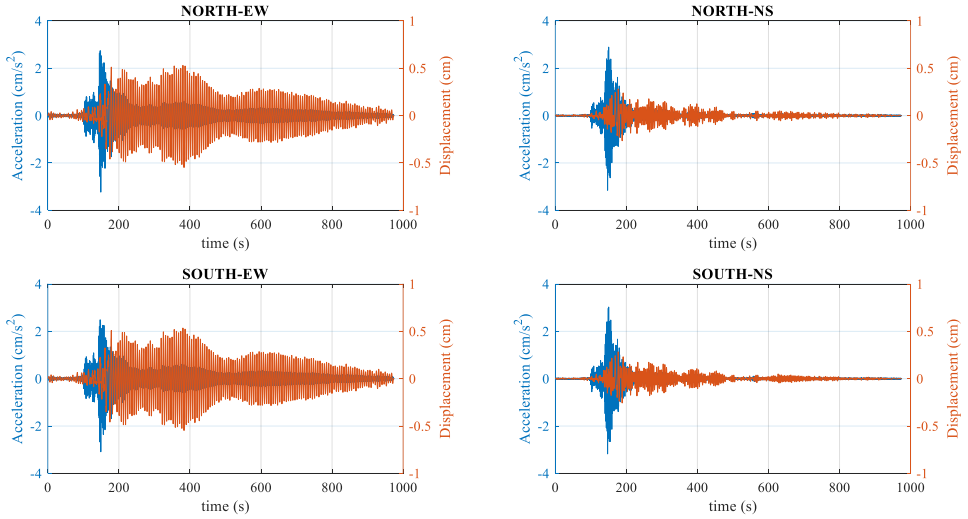

Figure 3.11. Recorded roof acceleration [blue line] and estimated roof displacement [orange line] time histories in the EW and NS directions at the 52nd floor level on the northern and southern sides of the building, during M_w = 6.1 Aegean Sea Turkey earthquake of 12 June 2017.

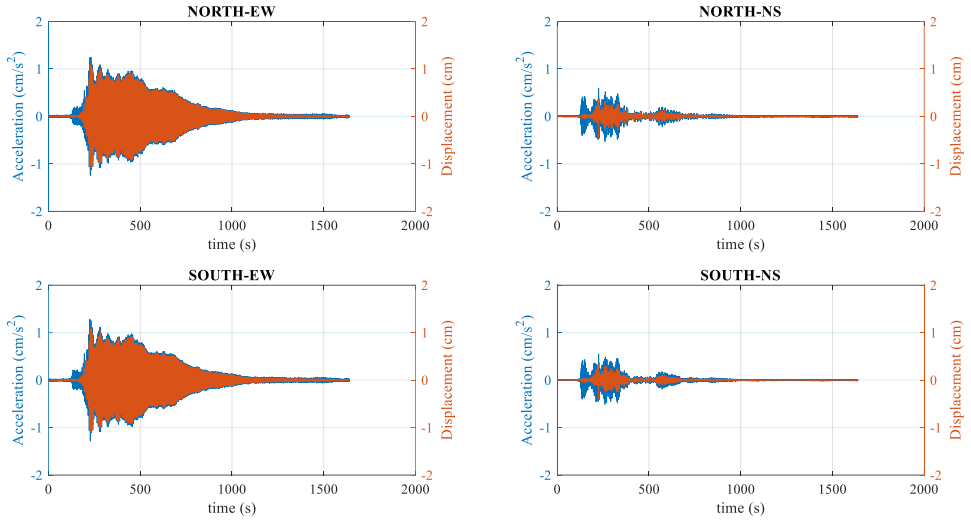

Figure 3.12. Recorded roof acceleration [blue line] and estimated roof displacement [orange line] time histories in the EW and NS directions at the 52nd floor level on the northern and southern sides of the building, during M_w = 6.6 Gökova Körfezi (Akdeniz) Turkey earthquake of 21 July 2017.

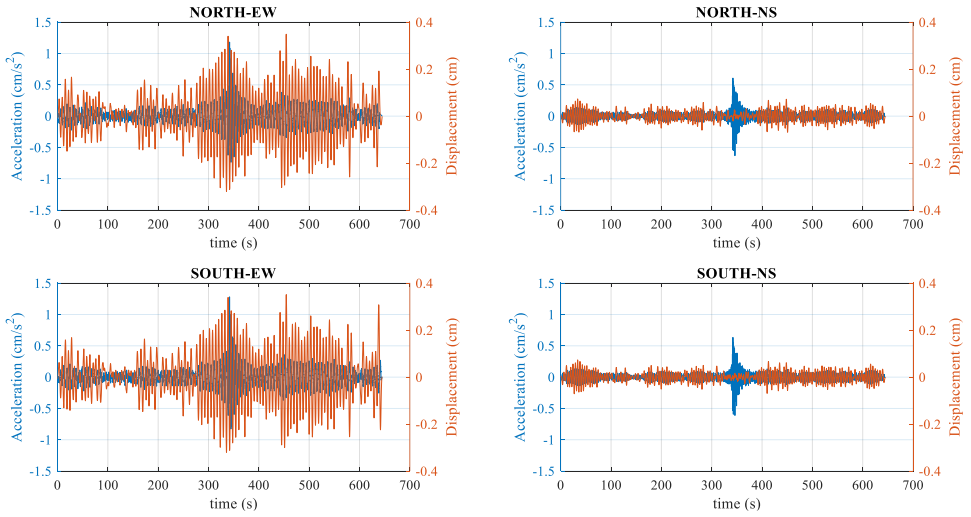

Figure 3.13. Recorded roof acceleration [blue line] and estimated roof displacement [orange line] time histories in the EW and NS directions at the 52nd floor level on the northern and southern sides of the building, during M_w = 4.5 Taşoluk-Geyve Turkey, earthquake of 22 October.

As mentioned before, the structural system is less rigid in the EW direction. The structural system behaves bending deformation in the EW direction, whereas in the NS direction does shear deformations. This behavior can be seen in Figure 3.14.

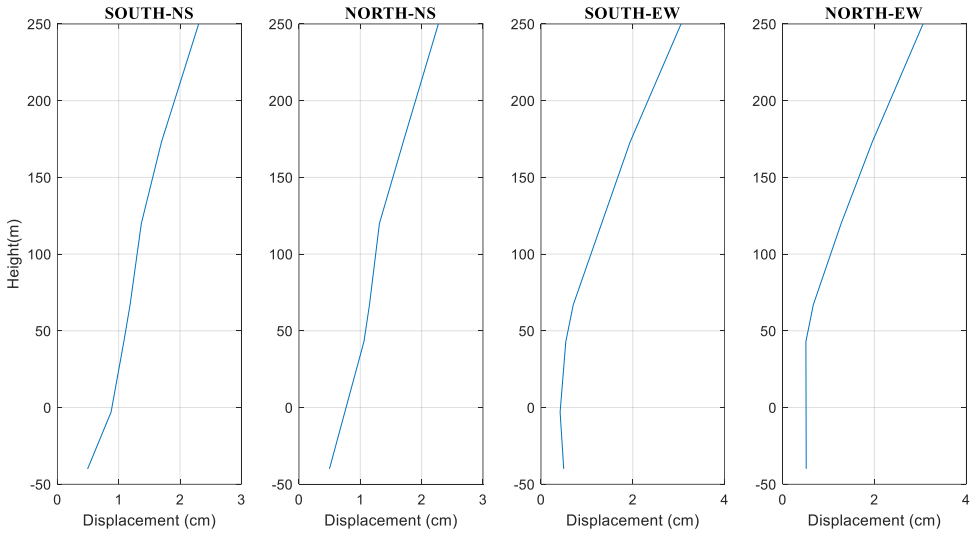

Figure 3.14. Peak horizontal displacement profiles at the B9, B1, 9th, 14th, 25th, 36th, 52nd floor levels on the northern and southern sides of the building, during the Aegean Sea earthquake.

Most of the recorded earthquakes are far away, consequently, their effects on Sapphire are less when compared to stronger earthquakes as it can be seen in displacement time histories shown in Figure 3.19 and Figure 3.20. Four earthquake excitations differ from others easily as seen in these figures. In addition to the Aegean Sea earthquake, following, M_w = 6.1 Aegean Sea Turkey earthquake of 12 June 2017, M_w = 6.6 Gökova Körfezi (Akdeniz) Turkey earthquake of 21 July 2017 (called as Gökova earthquake hereafter) and M_w = 4.5 Taşoluk-Geyve Turkey earthquake of 22 October 2014 have a significant response on Sapphire. PAs, PVs, and PDs on seven different floor levels recorded on southern sides due to these 4 largest earthquakes are shown also in Table 3.2.

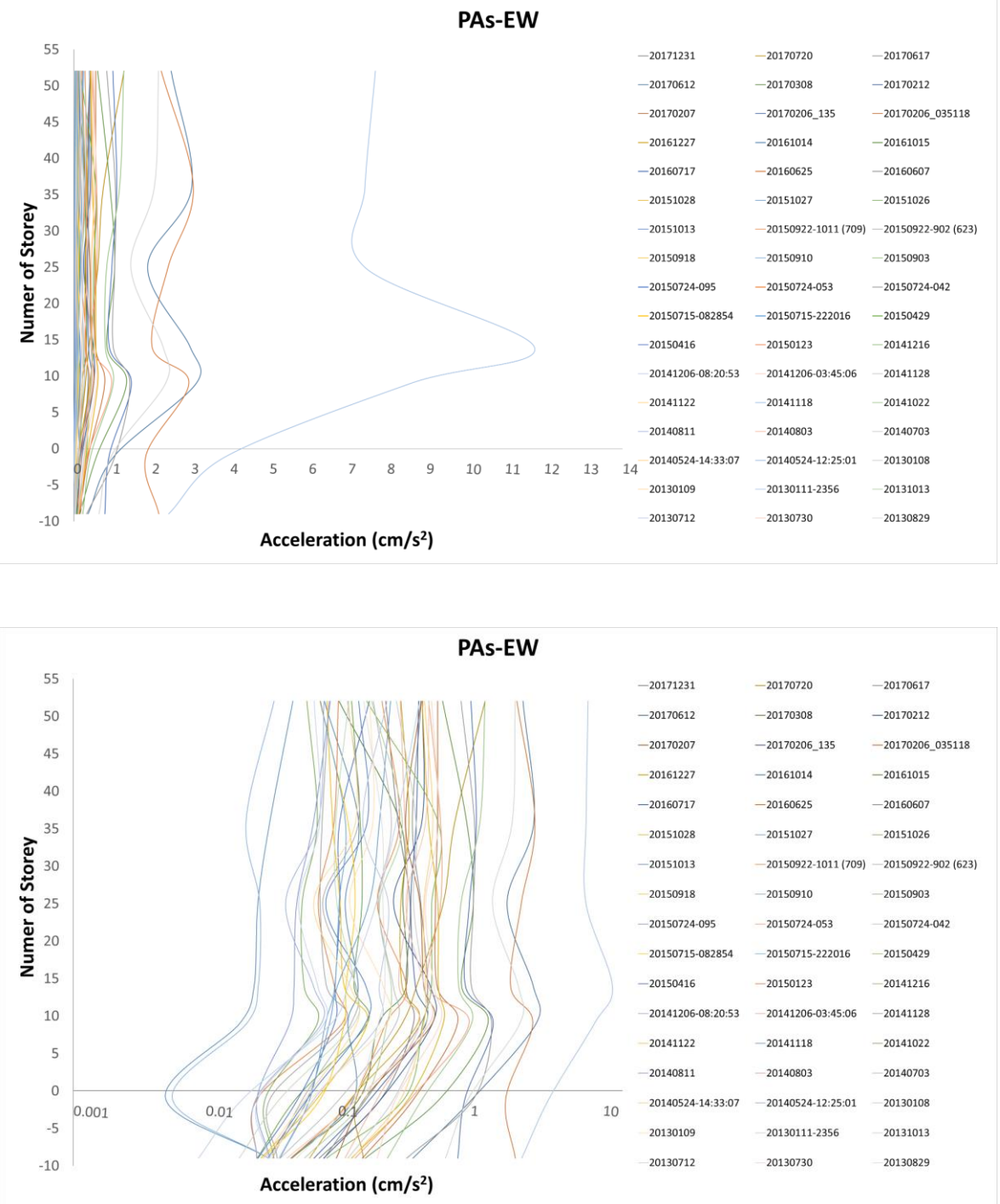

Figure 3.15. Peak horizontal accelerations, recorded at the B9, B1, 9th, 14th, 25th, 36th, 52nd floor levels on the southern side of the building, due to earthquake excitations in the EW direction, shown in the linear scale (top) and in the logarithmic scale (bottom).

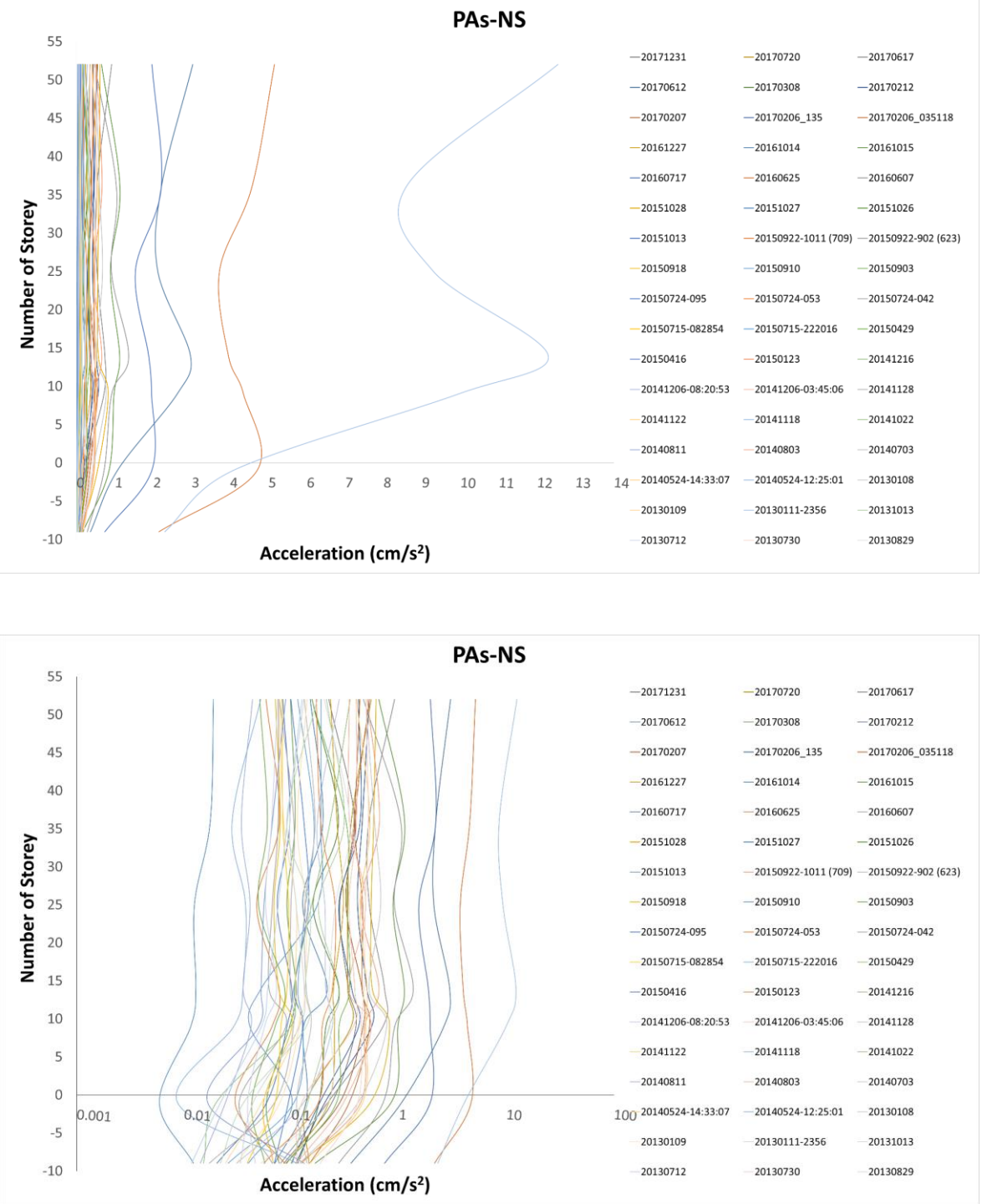

Figure 3.16. Peak horizontal accelerations, recorded at the B9, B1, 9th, 14th, 25th, 36th, 52nd floor levels on the southern side of the building, due to earthquake excitations in the NS direction, shown in the linear scale (top) and in the logarithmic scale (bottom).

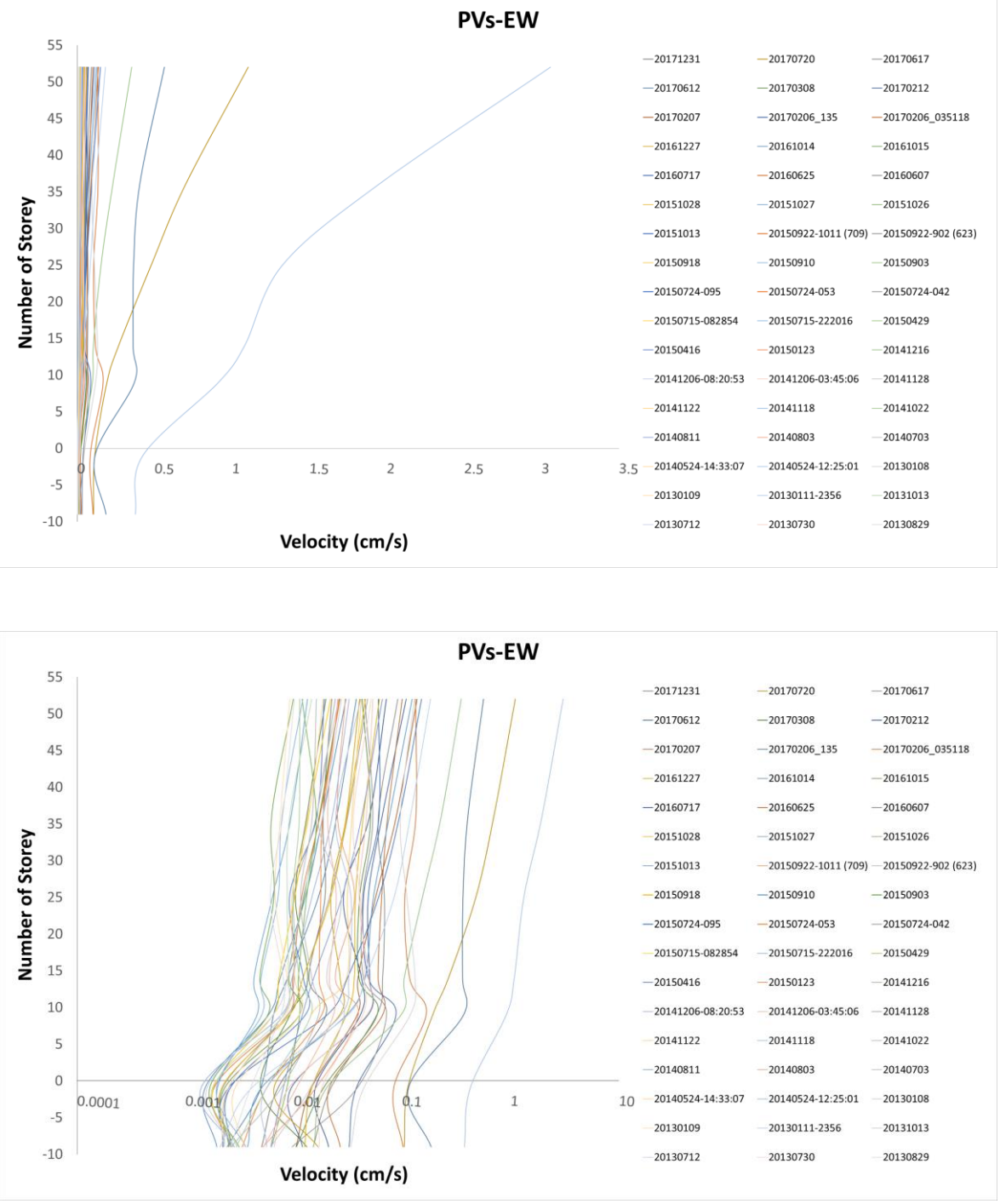

Figure 3.17. Peak horizontal velocities, recorded at the B9, B1, 9th, 14th, 25th, 36th, 52nd floor levels on the southern side of the building, due to earthquake excitations in the EW direction, shown in the linear scale (top) and in the logarithmic scale (bottom).

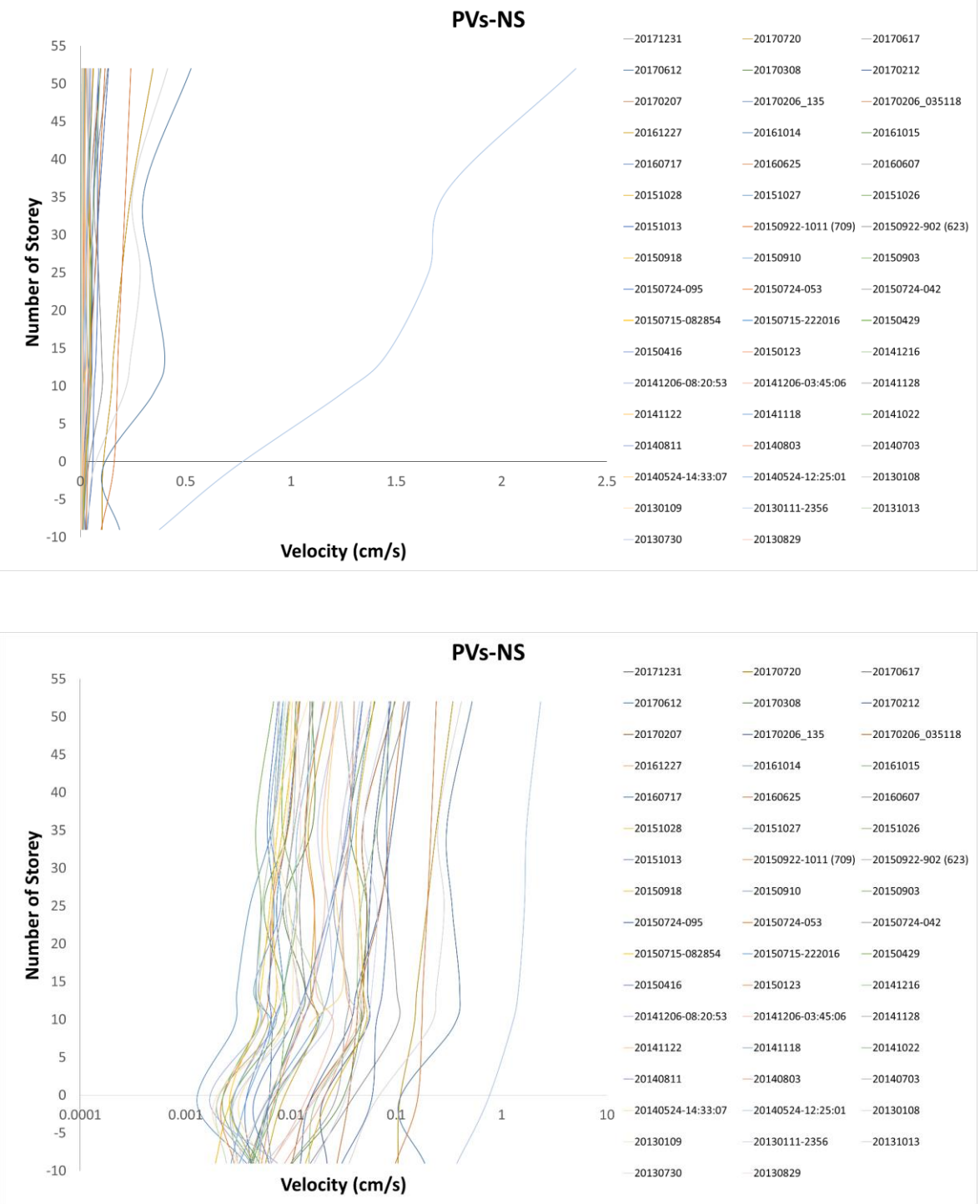

Figure 3.18. Peak horizontal velocities, recorded at the B9, B1, 9th, 14th, 25th, 36th, 52nd floor levels on the southern side of the building, due to earthquake excitations in the NS direction, shown in the linear scale (top) and in the logarithmic scale (bottom).

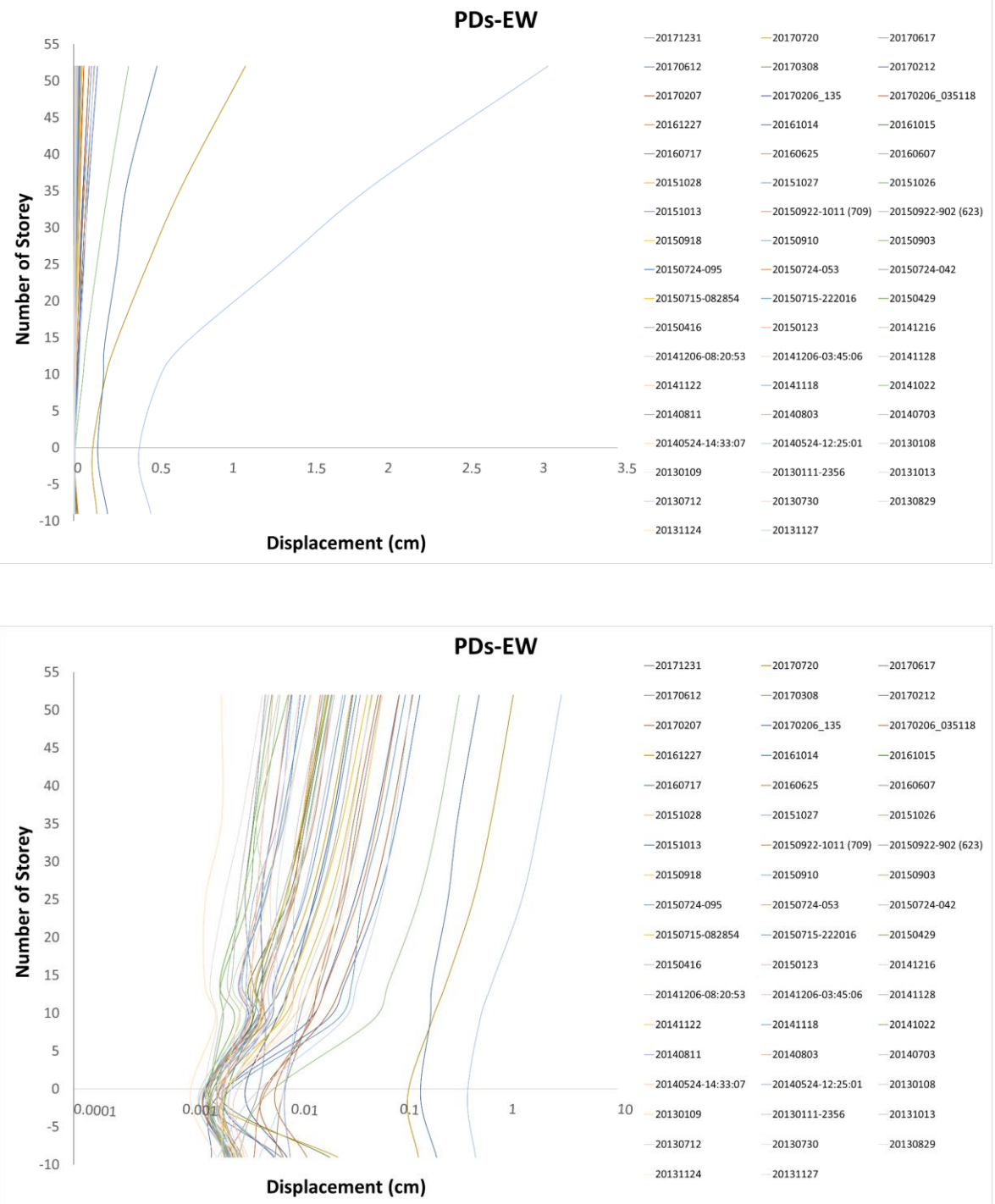

Figure 3.19. Peak horizontal displacements, recorded at the B9, B1, 9th, 14th, 25th, 36th, 52nd floor levels on the southern side of the building, due to earthquake excitations in the EW direction, shown in the linear scale (top) and in the logarithmic scale (bottom).

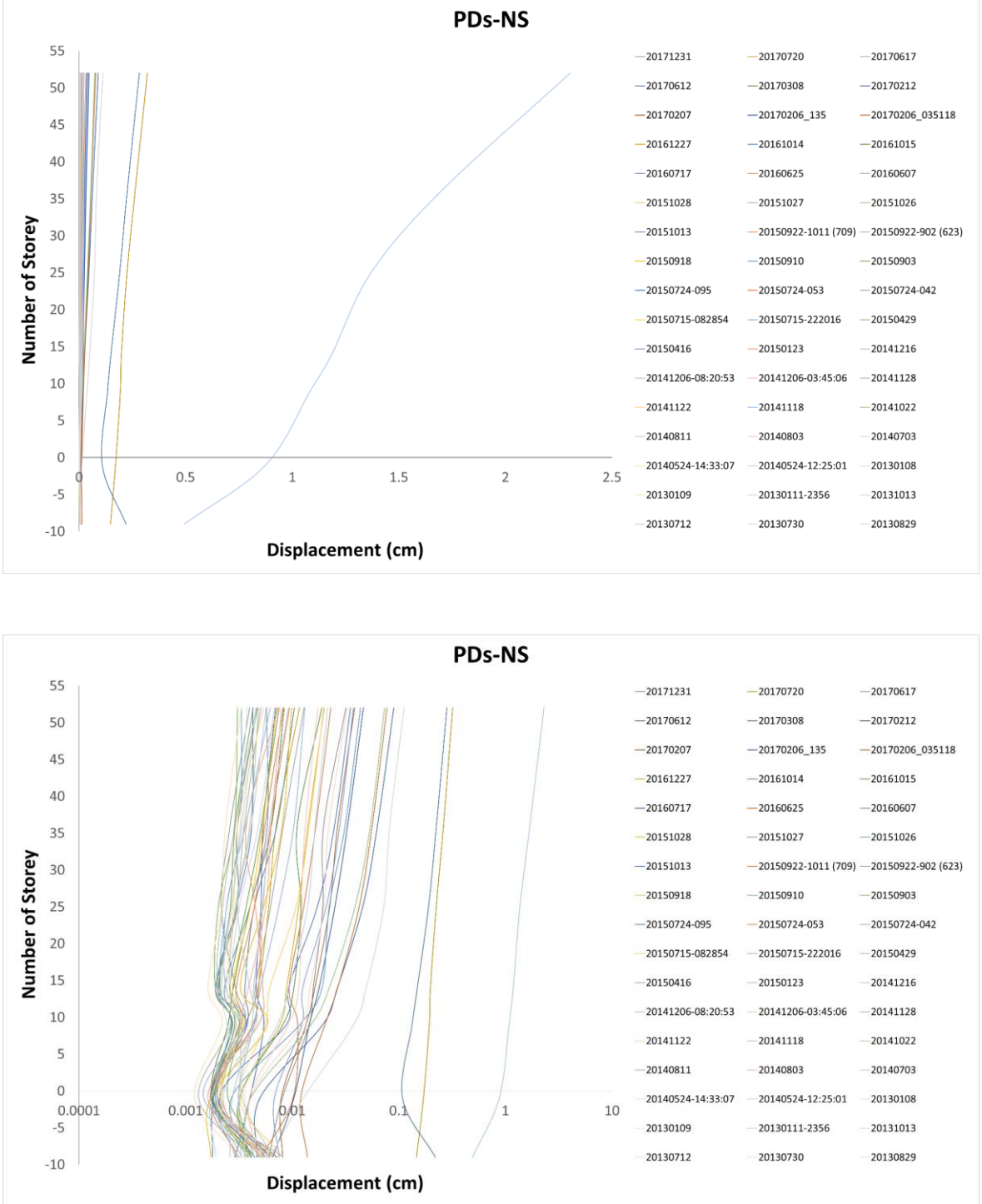

Figure 3.20. Peak horizontal displacements, recorded at the B9, B1, 9th, 14th, 25th, 36th, 52nd floor levels on the southern side of the building, due to earthquake excitations in the NS direction, shown in the linear scale (top) and in the logarithmic scale (bottom).

Table 3.2. Maximum PAs, PVs, and PDs, recorded on the southern sides of the building, during the Aegean Sea earthquake, the Gökova earthquake, M_w = 6.1 Aegean Sea Turkey earthquake of 12 June 2017, and M_w = 4.5 Taşoluk-Geyve Turkey earthquake of 22 October 2014.

Aegean Sea Turkey, earthquake of 24 May 2014

Magnitude			M_w = 6.9			
Epicentral Coordinate (Latitude/Longitude)			40.2942	25.615		
Epicentral Distance (km)			311			
	NS Direction			EW Direction		
Number of Storey	PA (cm/s^2)	PV (cm/s)	PD (cm)	PA (cm/s^2)	PV (cm/s)	PD (cm)
52	12.54	2.83	2.30	9.41	3.09	3.06
36	8.58	1.97	1.75	7.98	1.97	1.95
25	9.33	1.85	1.65	7.77	1.34	1.32
14	13.53	1.92	1.42	11.75	1.08	0.73
9	9.96	1.61	1.28	8.61	0.91	0.65
B1	4.20	0.72	0.93	3.92	0.42	0.49
B9	2.47	0.41	0.50	2.50	0.43	0.52

Gökova Körfezi(Akdeniz) Turkey, earthquake of 21 July 2017

Magnitude			M_w = 6.6			
Epicentral Coordinate (Latitude/Longitude)			36.9693	27.4057		
Epicentral Distance (km)			478			
	NS Direction			EW Direction		
Number of Storey	PA (cm/s^2)	PV (cm/s)	PD (cm)	PA (cm/s^2)	PV (cm/s)	PD (cm)
52	0.55	0.34	0.32	1.28	1.11	1.10
36	0.36	0.24	0.26	0.76	0.70	0.70
25	0.33	0.20	0.22	0.62	0.48	0.47
14	0.33	0.16	0.20	0.39	0.27	0.27
9	0.36	0.15	0.19	0.30	0.19	0.20
B1	0.14	0.11	0.17	0.14	0.11	0.12
B9	0.14	0.10	0.15	0.15	0.10	0.15

Aegean Sea Turkey, earthquake of 12 June 2017

Magnitude			M_w = 6.1			
Epicentral Coordinate (Latitude/Longitude)			38.8468	26.3252		
Epicentral Distance (km)			338			
	NS Direction			EW Direction		
Number of Storey	PA (cm/s^2)	PV (cm/s)	PD (cm)	PA (cm/s^2)	PV (cm/s)	PD (cm)
52	3.03	0.53	0.28	2.49	0.56	0.53
36	2.21	0.30	0.23	3.01	0.40	0.34
25	2.11	0.34	0.19	1.89	0.36	0.28
14	2.97	0.40	0.15	2.97	0.36	0.20
9	2.62	0.35	0.13	3.13	0.37	0.19
B1	1.06	0.11	0.11	1.04	0.11	0.15
B9	0.36	0.19	0.22	0.37	0.19	0.22

Taşoluk-Geyve Turkey, earthquake of 22 October 2014

Magnitude			M_w = 4.5			
Epicentral Coordinate (Latitude/Longitude)			45.7770	27.2605		
Epicentral Distance (km)			120			
	NS Direction			EW Direction		
Number of Storey	PA (cm/s^2)	PV (cm/s)	PD (cm)	PA (cm/s^2)	PV (cm/s)	PD (cm)
52	0.63	0.10	0.07	1.28	0.35	0.35
36	0.73	0.07	0.05	1.18	0.23	0.23
25	0.58	0.05	0.04	0.84	0.15	0.15
14	0.95	0.04	0.02	0.81	0.10	0.08
9	0.79	0.04	0.02	1.01	0.10	0.06
B1	0.45	0.02	0.00	0.43	0.02	0.01
B9	0.23	0.01	0.00	0.24	0.02	0.00

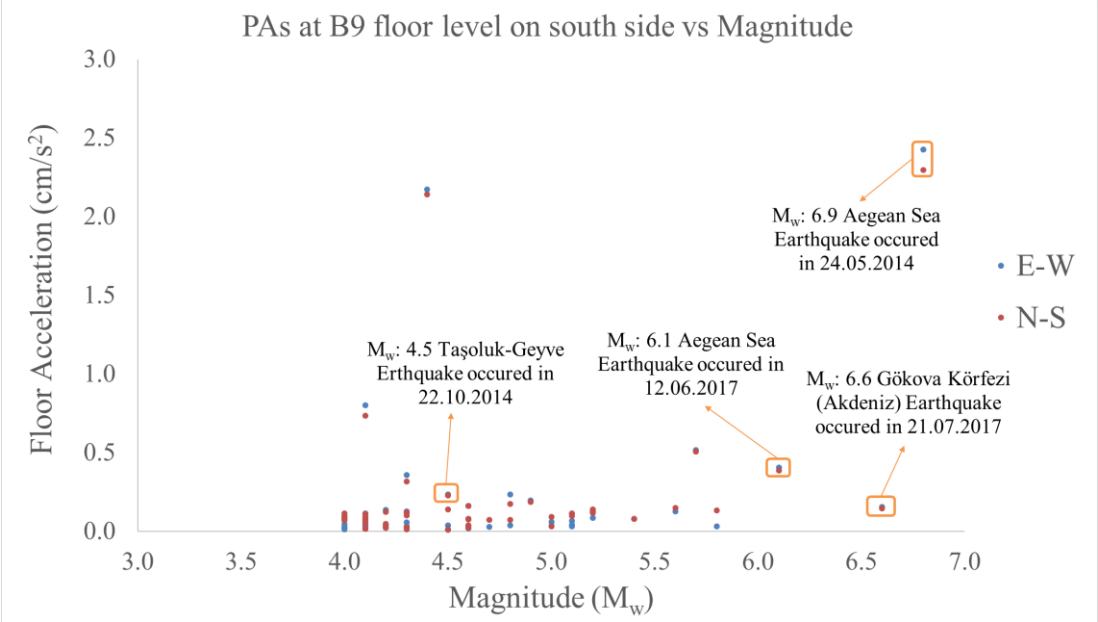

Figure 3.21. Peak ground accelerations, recorded at the B9 floor level on the southern side of the building, versus magnitudes.

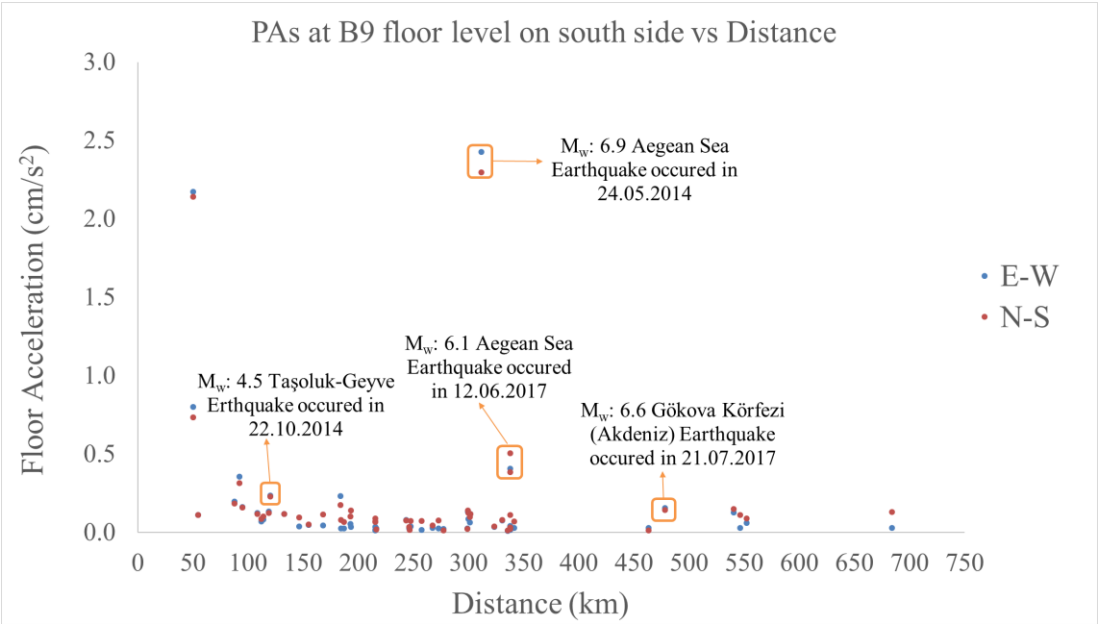

Figure 3.22. Peak ground accelerations, recorded at the B9 floor level on the southern side of the building, versus distances.

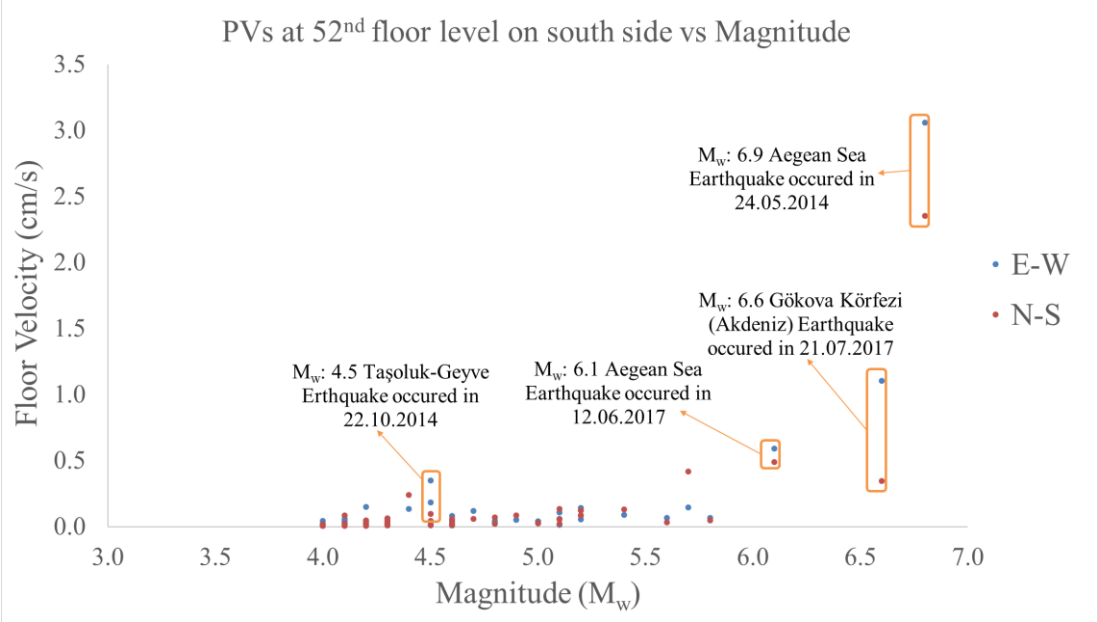

Figure 3.23. Peak velocities, recorded at the 52nd floor level on the southern side of the building, versus magnitudes.

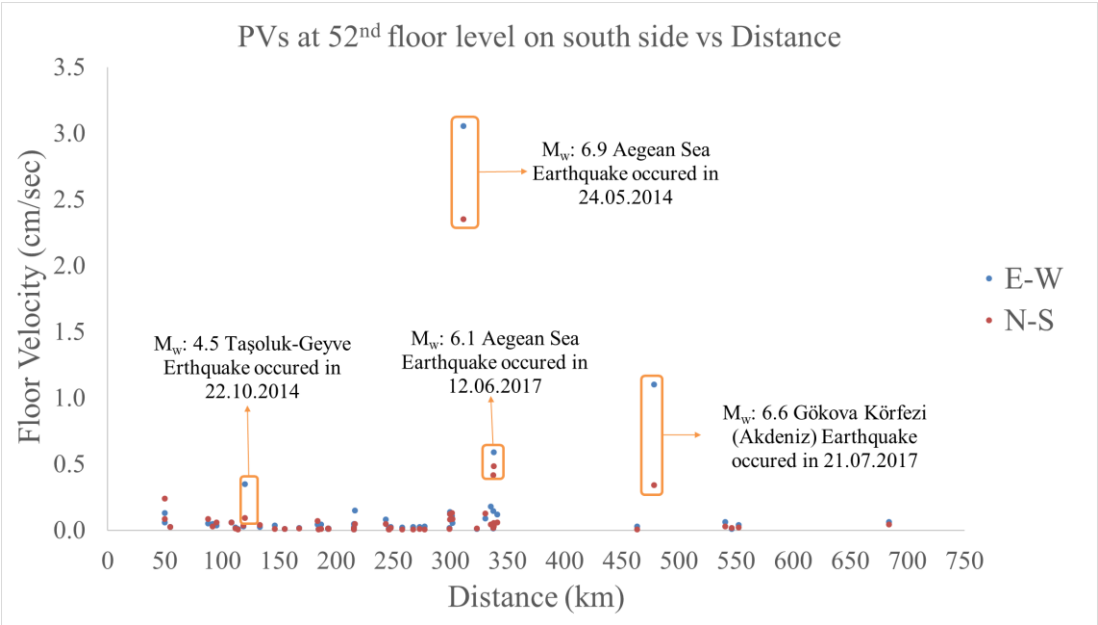

Figure 3.24. Peak velocities, recorded at the 52nd floor level on the southern side of the building, versus distances.

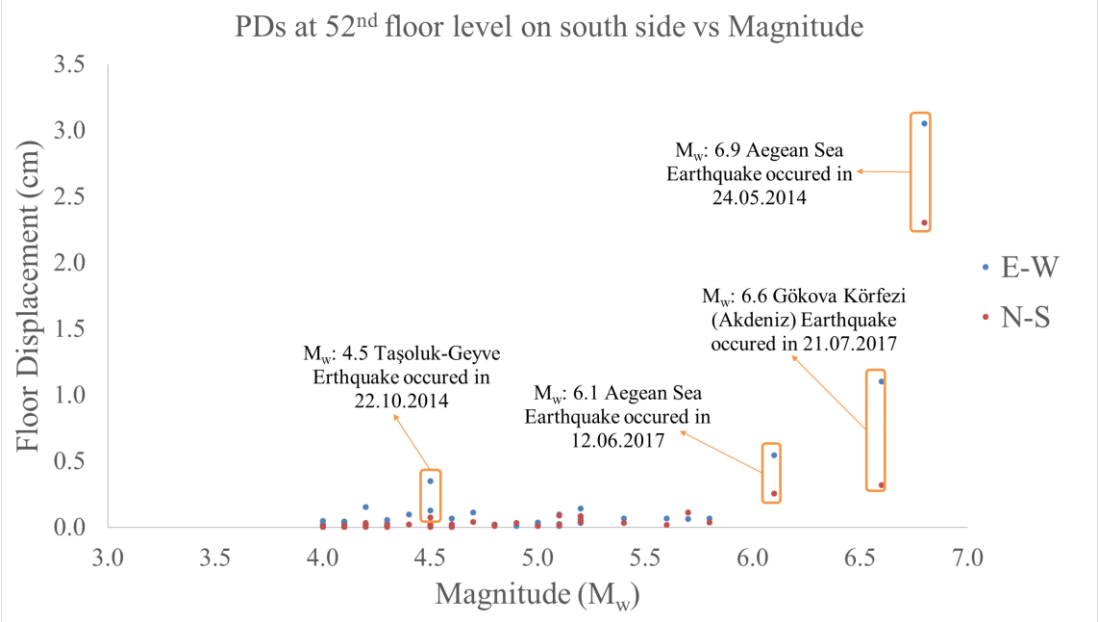

Figure 3.25. Peak displacements, recorded at the 52nd floor level on the southern side of the building, versus magnitudes.

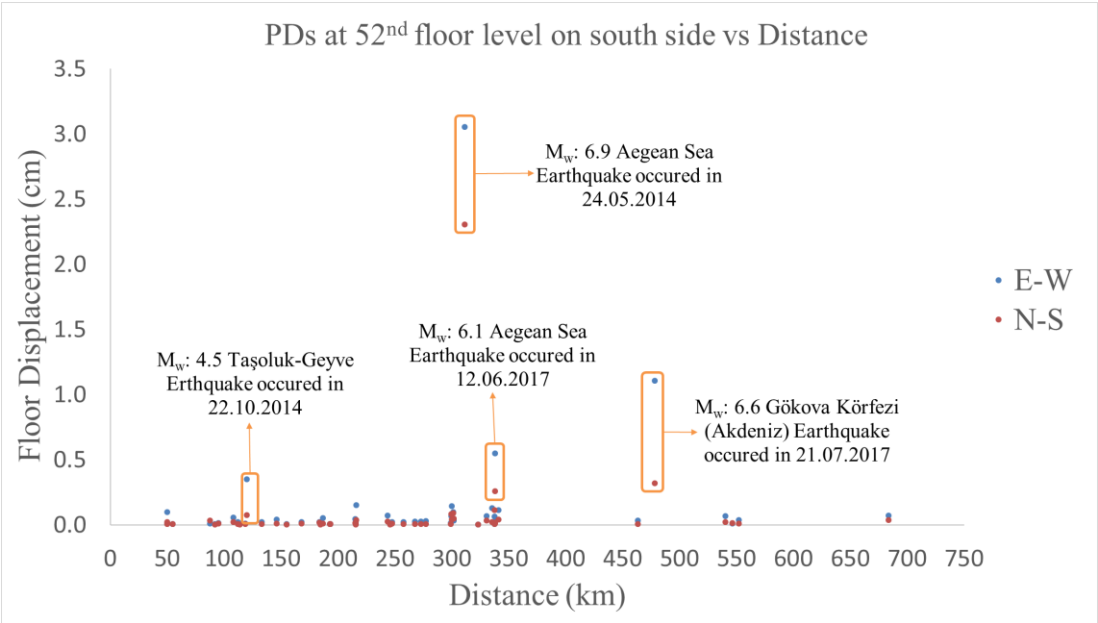

Figure 3.26. Peak displacements, recorded at the 52nd floor level on the southern side of the building, versus distances.

3.1.2 Wind Response

4 wind events, detailed in Chapter 2.2, are analyzed and their characteristics are detailed in this section. PAs, PVs, and PDs are estimated for selected wind records on seven different floor levels on the northern and southern sides of the building.

The most significant response in the building is derived from the wind of 27 July 2017. Figure 3.27 and Figure 3.28 show corrected acceleration time histories, which occurred during the wind of 27 July 2017 for seven different floor levels. Figure 3.29 and Figure 3.30 show the velocity time histories, estimated from the integration of the corrected accelerations and Figure 3.31 and Figure 3.32 show the displacement time histories, estimated from the double integration of the corrected accelerations for the seven different levels in the EW and NS directions. The biggest peak values occurred on 27 July 2017 are shown in Table 3.3.

Structures are exposed to wind excitations along with the whole length and since displacement and acceleration time histories are overlapping each other, as seen in Figure 3.34 and Figure 3.35.

Lateral deformations are highly larger than those in torsional deformations as seen in Figure 3.33 and, so torsional behavior is not dominant also in wind response when compared with lateral behavior.

Table 3.3. PAs, PVs, and PDs in the EW and NS directions recorded on the southern side of the building during the wind of 27 July 2017.

Number of Storey	Wind of 27 July 2017					
	NS Direction			EW Direction		
	PA (cm/s^2)	PV (cm/s)	PD (cm)	PA (cm/s^2)	PV (cm/s)	PD (cm)
52	2.23	1.59	1.34	3.12	2.83	3.18
36	1.57	1.11	0.94	2.00	1.78	2.02
25	1.13	0.78	0.65	1.41	1.16	1.33
14	0.74	0.44	0.37	0.92	0.60	0.69
9	0.57	0.32	0.27	0.76	0.41	0.47
B1	0.08	0.04	0.04	0.08	0.04	0.05
B9	0.00	0.00	0.00	0.03	0.00	0.01

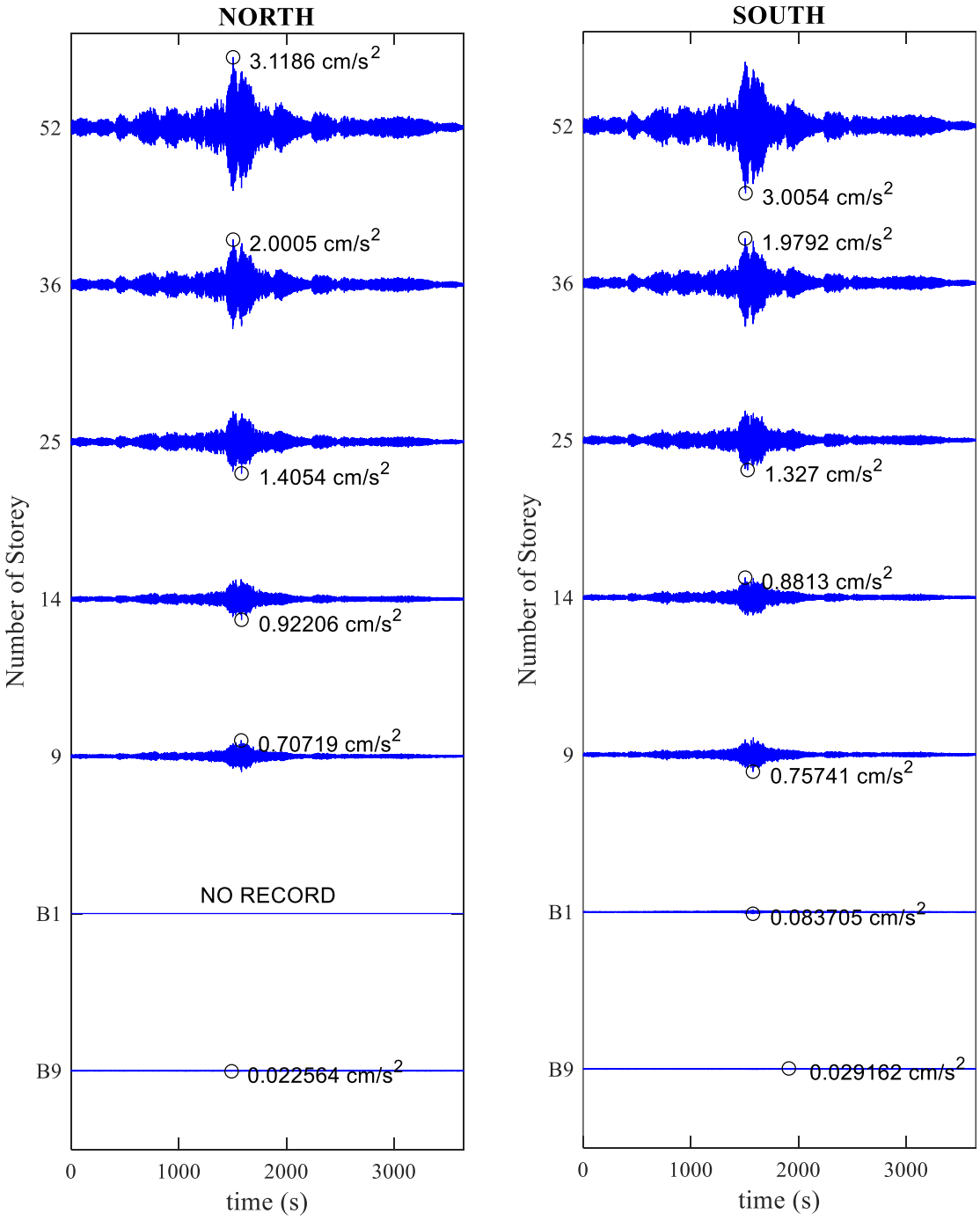

Figure 3.27. Acceleration time histories in the EW direction, recorded at B9, B1, 9th, 14th, 25th, 36th, 52nd floor levels on the northern and southern sides of the building during the wind of 27 July 2017.

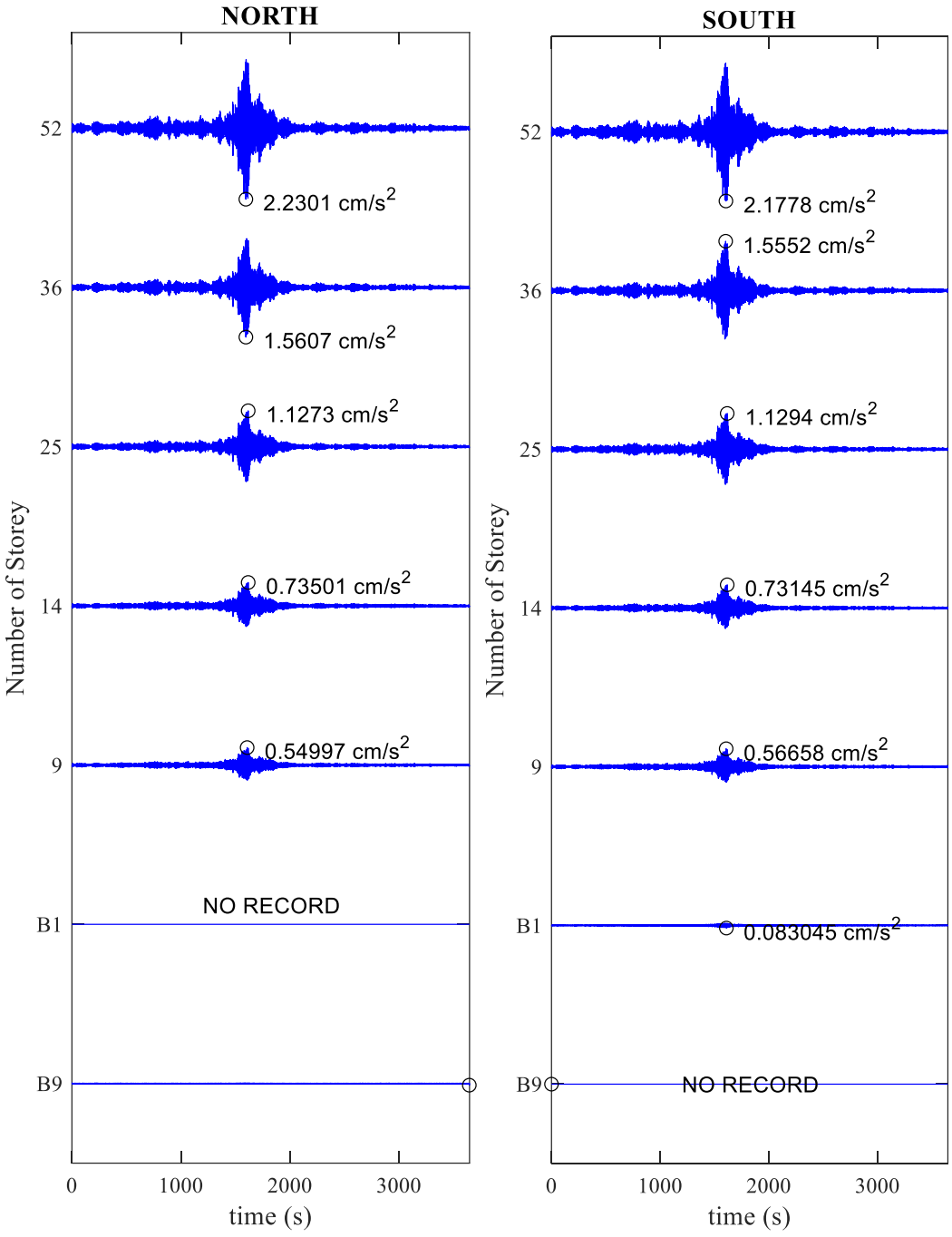

Figure 3.28. Acceleration time histories in the NS direction, recorded at B9, B1, 9th, 14th, 25th, 36th, 52nd floor levels on the northern and southern sides of the building during the wind of 27 July 2017.

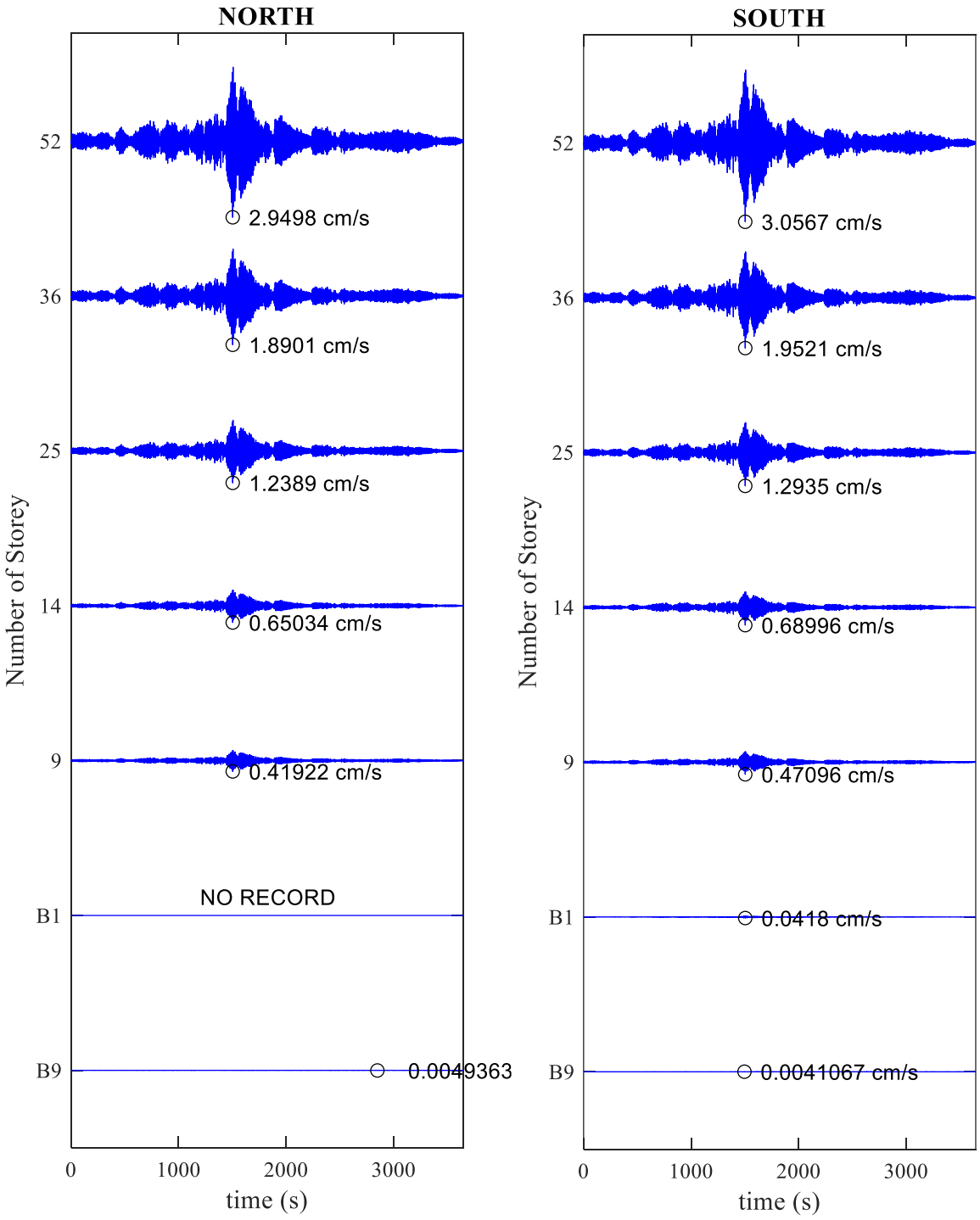

Figure 3.29. Velocity time histories in the EW direction, recorded at B9, B1, 9th, 14th, 25th, 36th, 52nd floor levels on the northern and southern sides of the building during the wind of 27 July 2017.

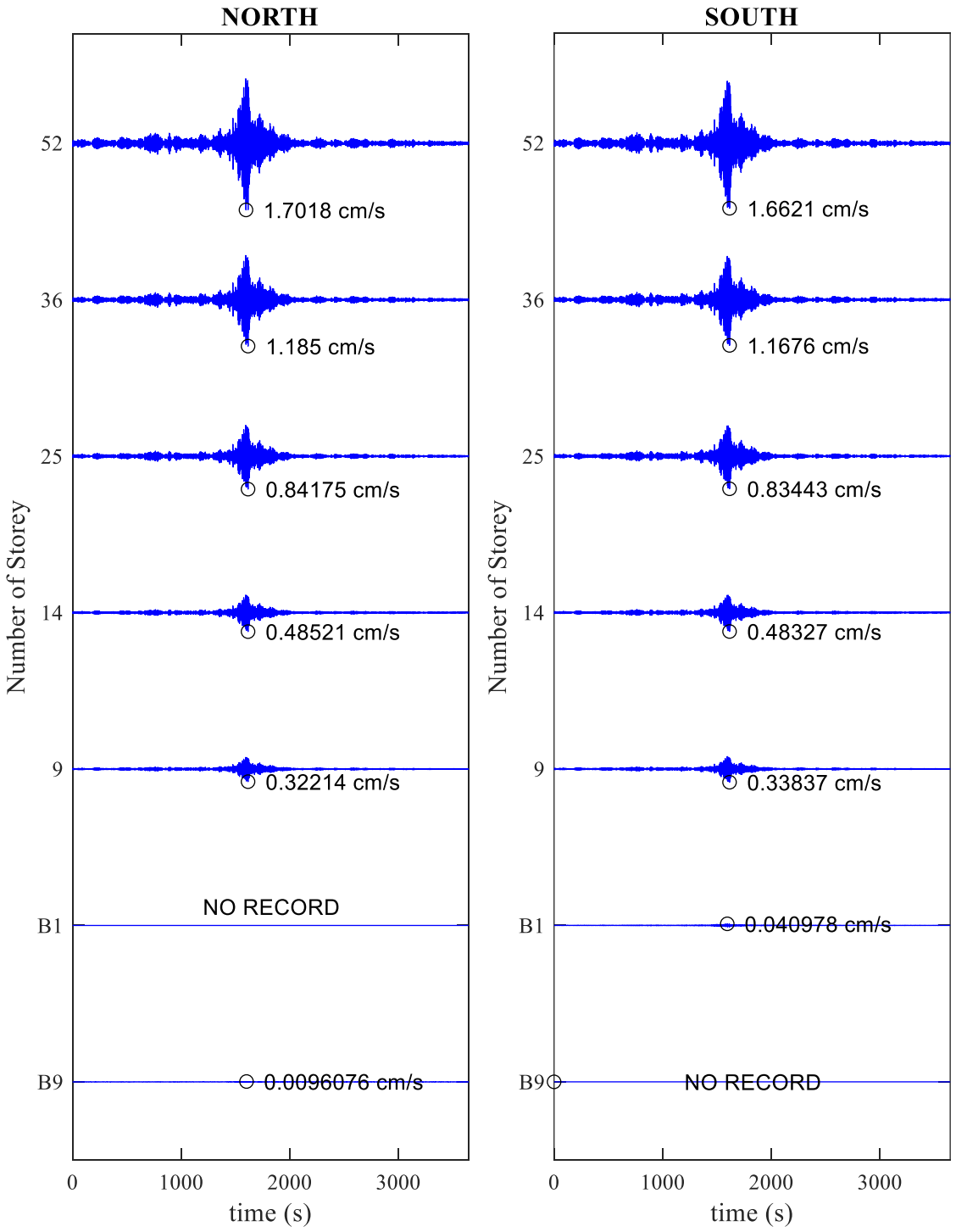

Figure 3.30. Velocity time histories in the NS direction, recorded at B9, B1, 9th, 14th, 25th, 36th, 52nd floor levels on the northern and southern sides of the building during the wind of 27 July 2017.

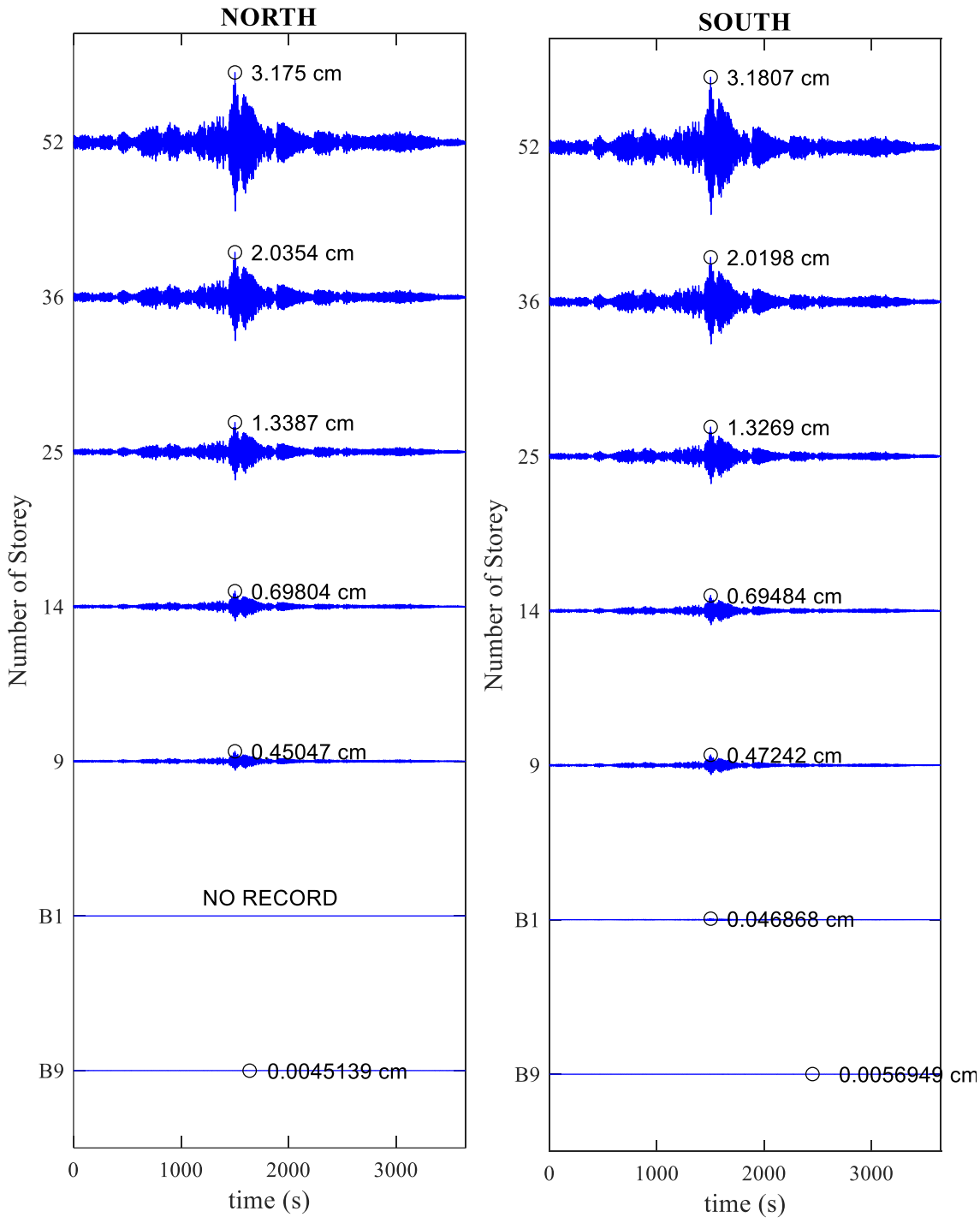

Figure 3.31. Displacement time histories in the EW direction, recorded at B9, B1, 9th, 14th, 25th, 36th, 52nd floor levels on the northern and southern sides of the building during the wind of 27 July 2017.

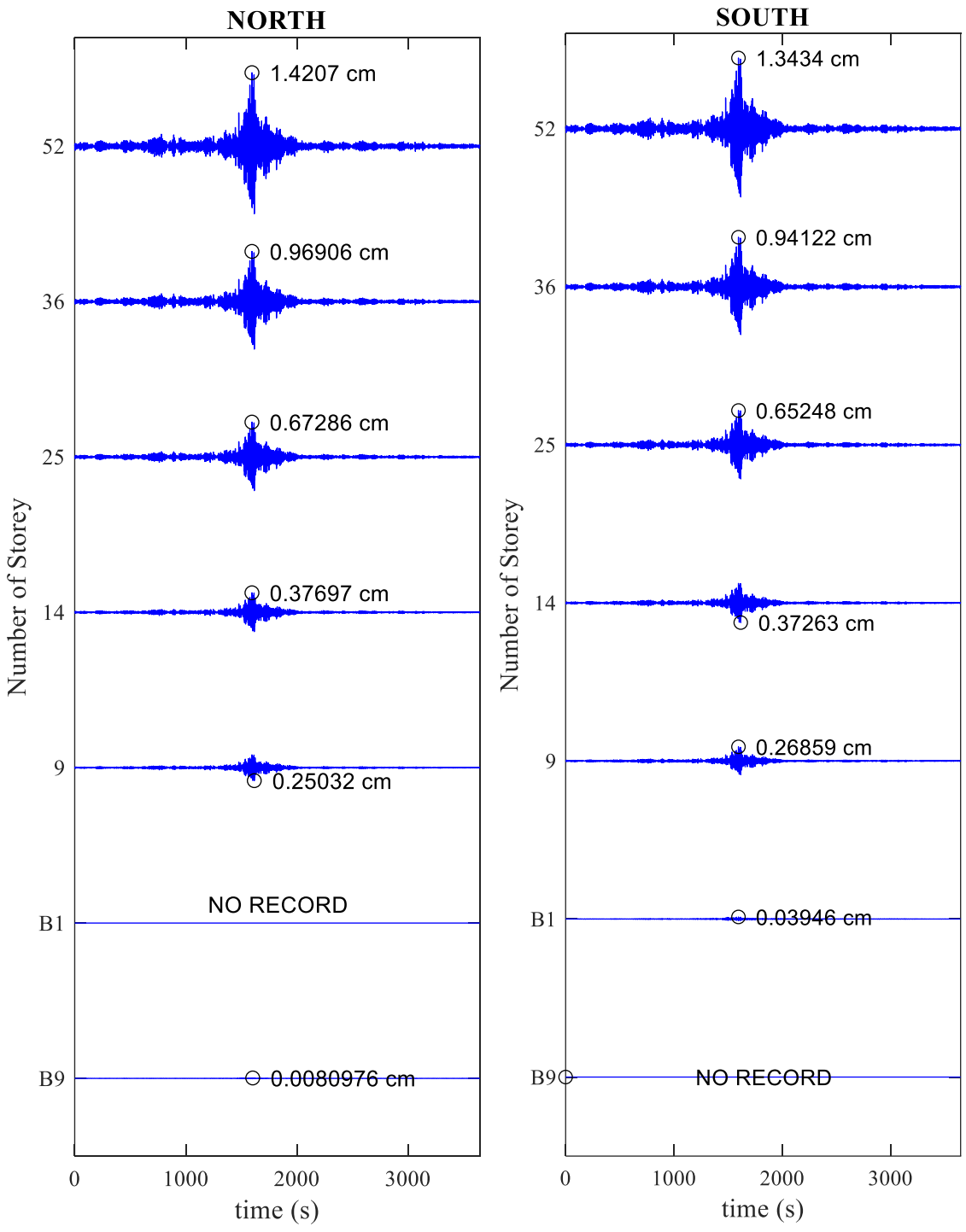

Figure 3.32. Displacement time histories in the NS direction, recorded at B9, B1, 9th, 14th, 25th, 36th, 52nd floor levels on the northern and southern sides of the building during the wind of 27 July 2017.

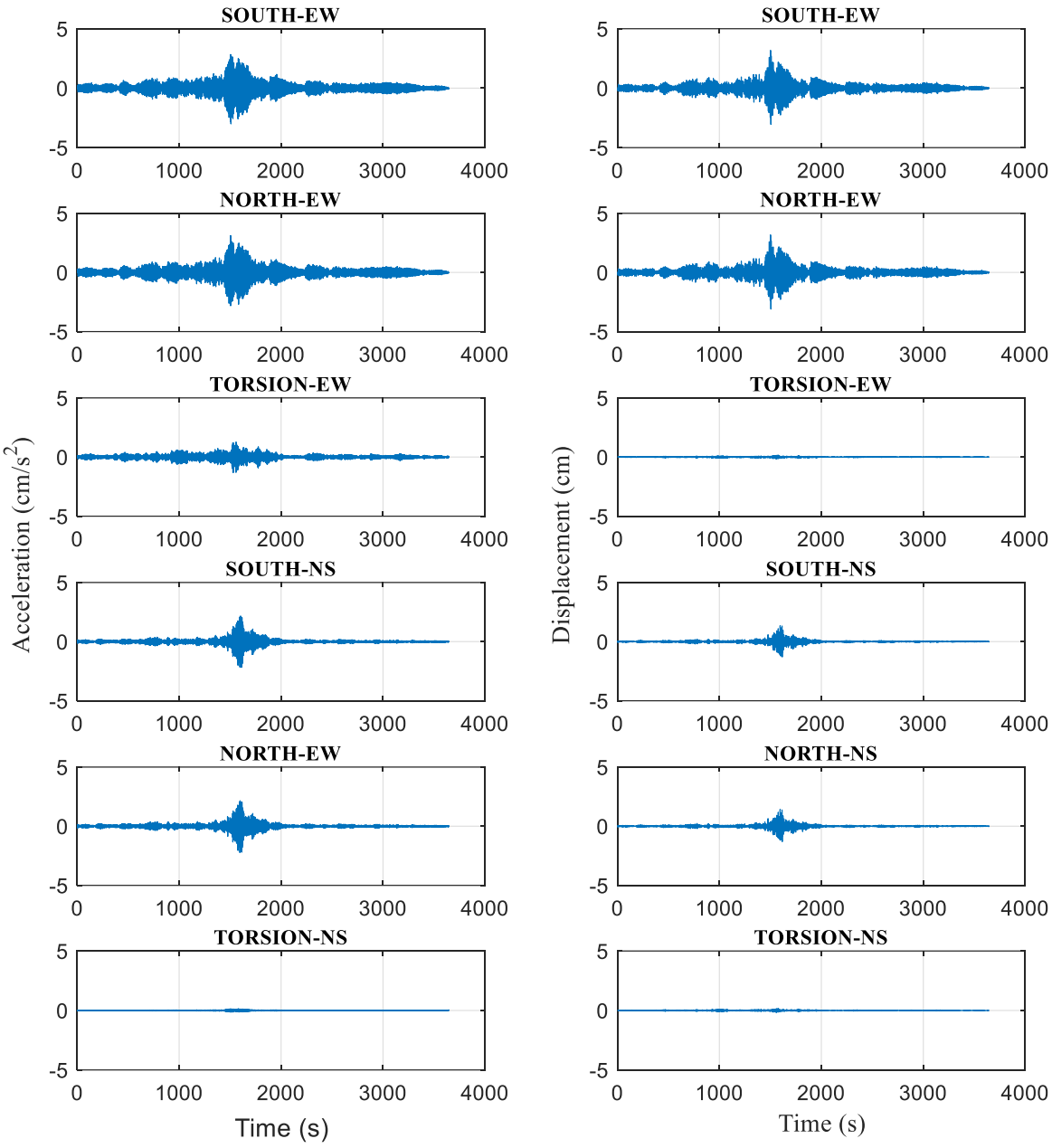

Figure 3.33. The acceleration and displacement time histories in the EW and NS direction, recorded at the 52nd floor level on the northern and southern sides of the building during the wind of 27 July 2017. Torsional time histories are estimated from the difference of two parallel records on the northern and southern sides of the 52nd floor level.

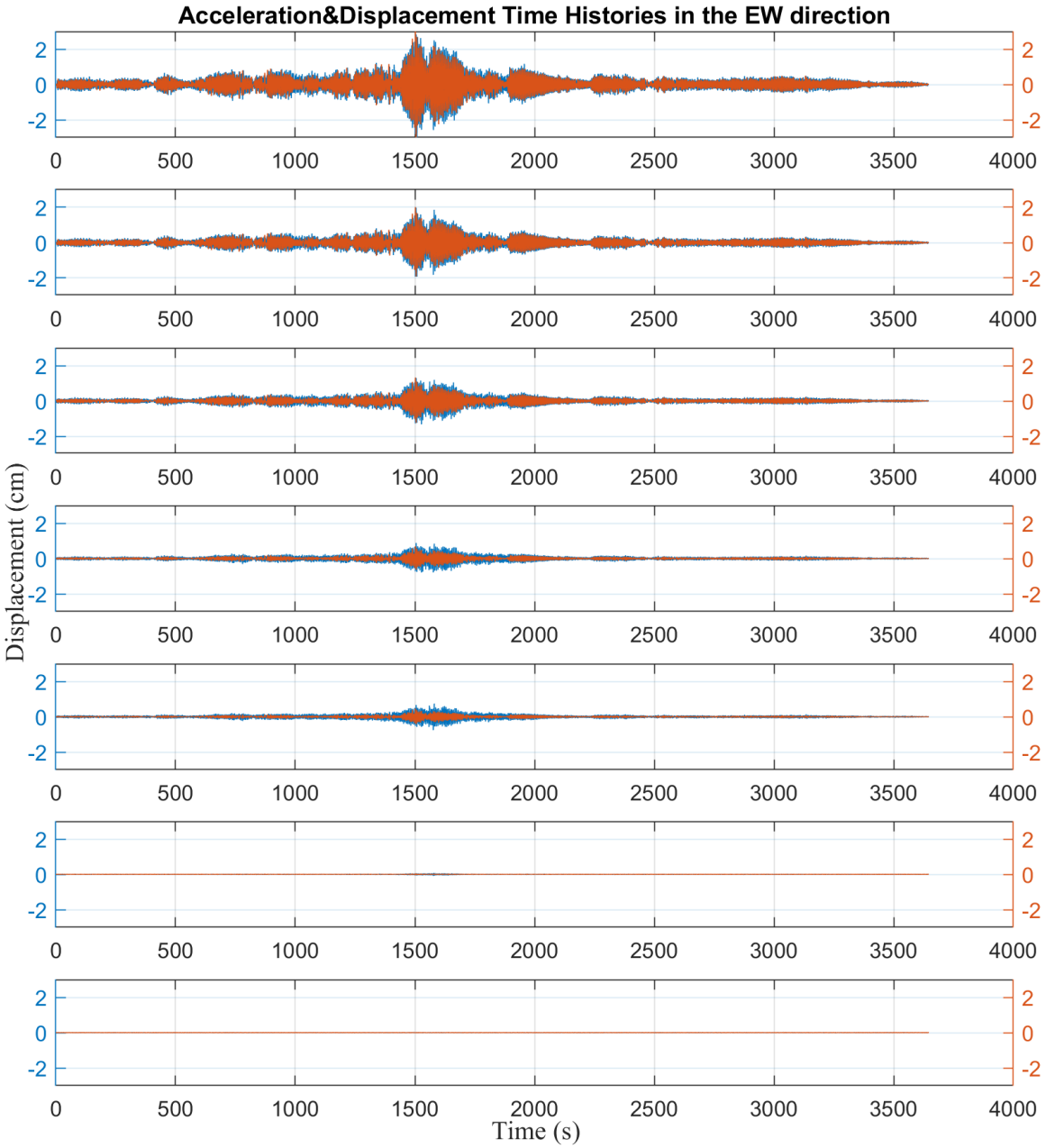

Figure 3.34. Recorded acceleration [blue line] and estimated displacement [orange line] time histories in the EW direction at B9, B1, 9th, 14th, 25th, 36th, 52nd floor levels on the southern side of the building, during the wind of 27 July 2017.

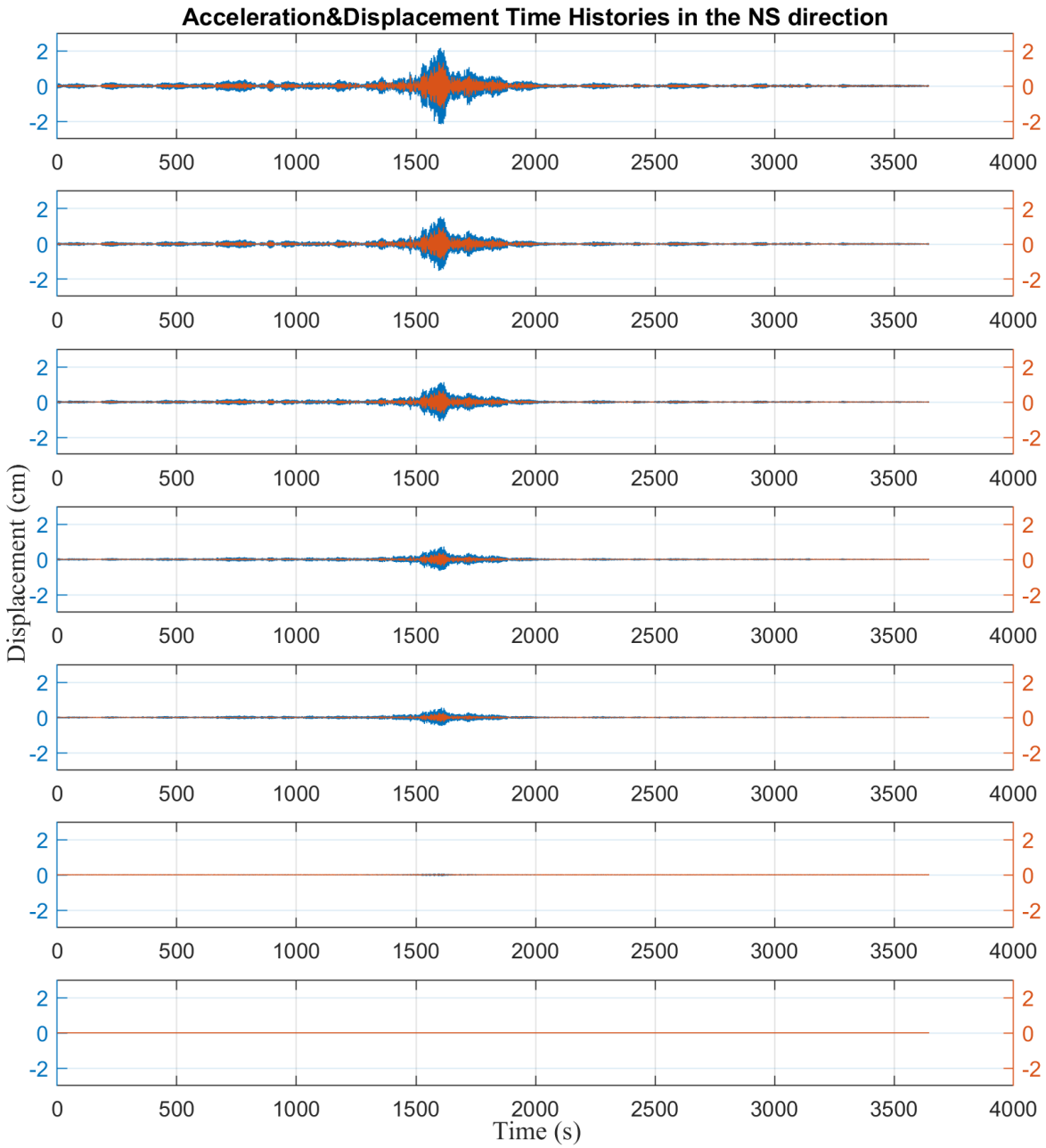

Figure 3.35. Recorded acceleration [blue line] and estimated displacement [orange line] time histories in the NS direction at B9, B1, 9th, 14th, 25th, 36th, 52nd floor levels on the southern side of the building, during the wind of 27 July 2017.

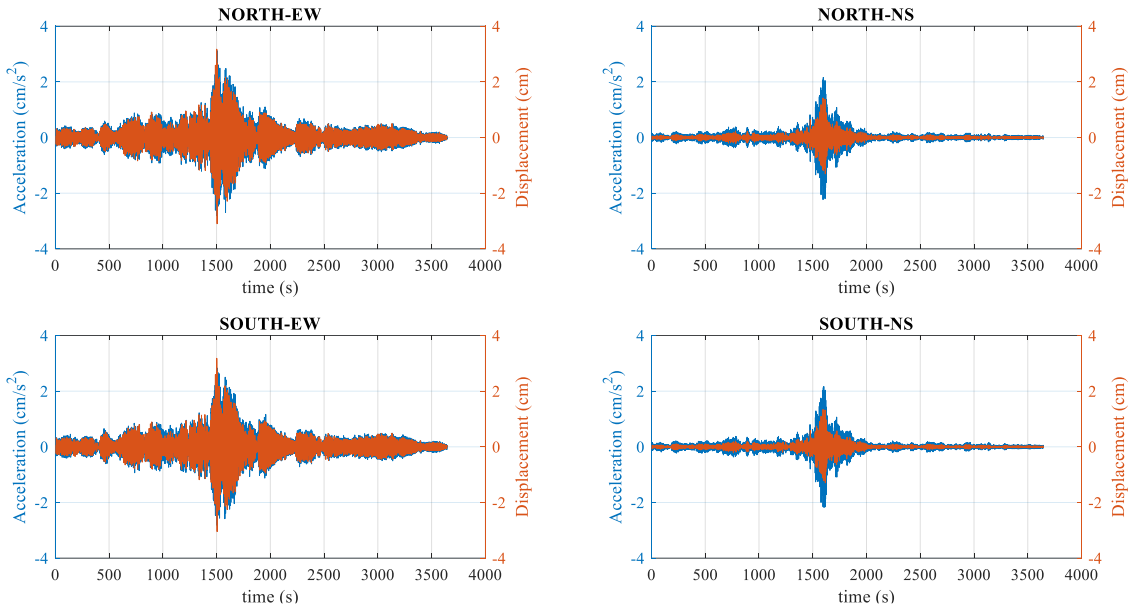

Figure 3.36. Recorded roof acceleration [blue line] and estimated roof displacement [orange line] time histories in the EW and NS directions at the 52nd floor level on the northern and southern sides of the building, during the wind of 27 July 2017.

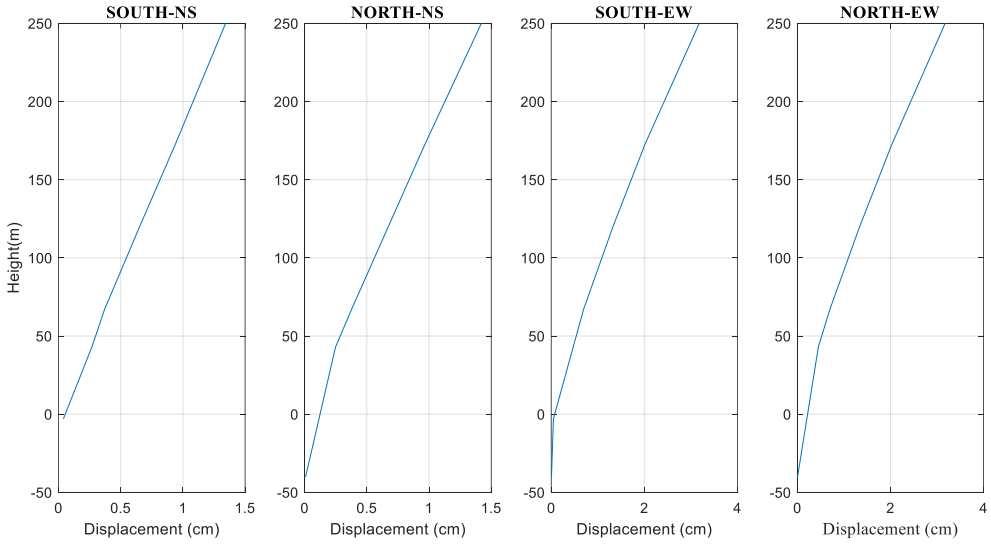

Figure 3.37. Peak horizontal displacement profiles at the B9, B1, 9th, 14th, 25th, 36th, 52nd floor levels on the northern and southern sides of the building, during the wind of 27 July 2017.

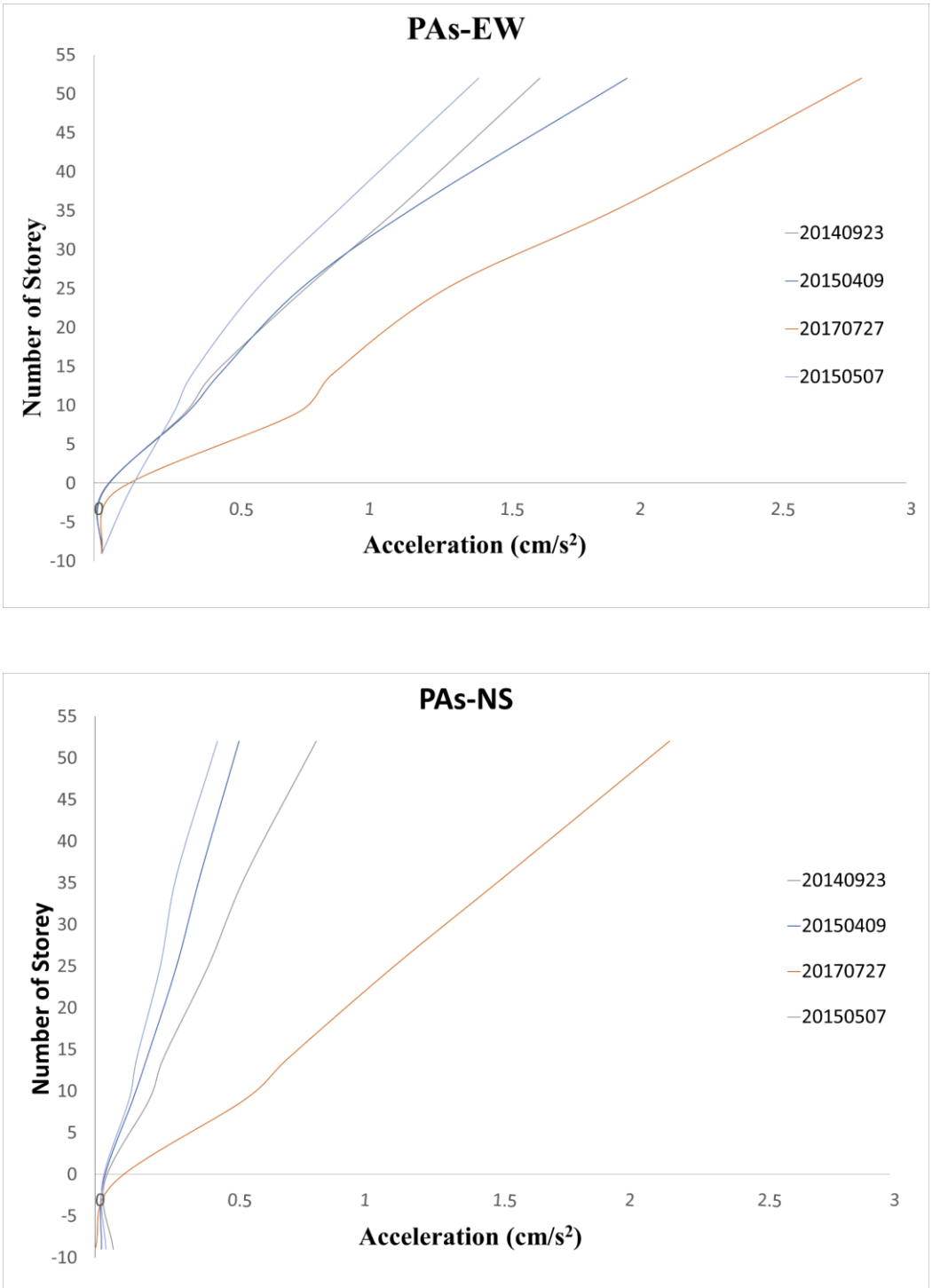

Figure 3.38. Peak horizontal accelerations, recorded at the B9, B1, 9th, 14th, 25th, 36th, 52nd floor levels on the southern side of the building, due to wind excitations in the EW (top) and NS (bottom) directions.

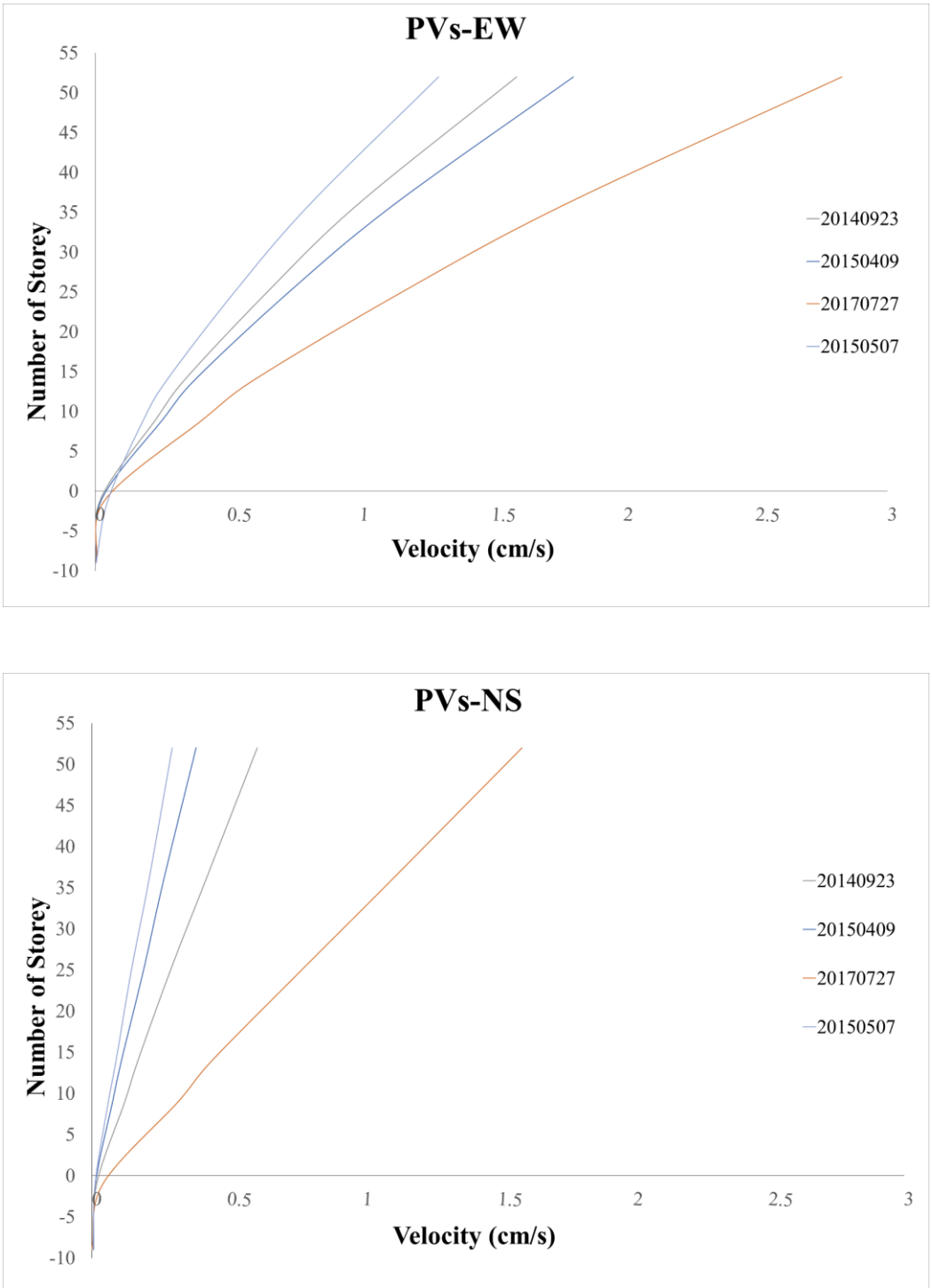

Figure 3.39. Peak horizontal velocities, recorded at the B9, B1, 9th, 14th, 25th, 36th, 52nd floor levels on the southern side of the building, due to wind excitations in the EW (top) and NS (bottom) directions.

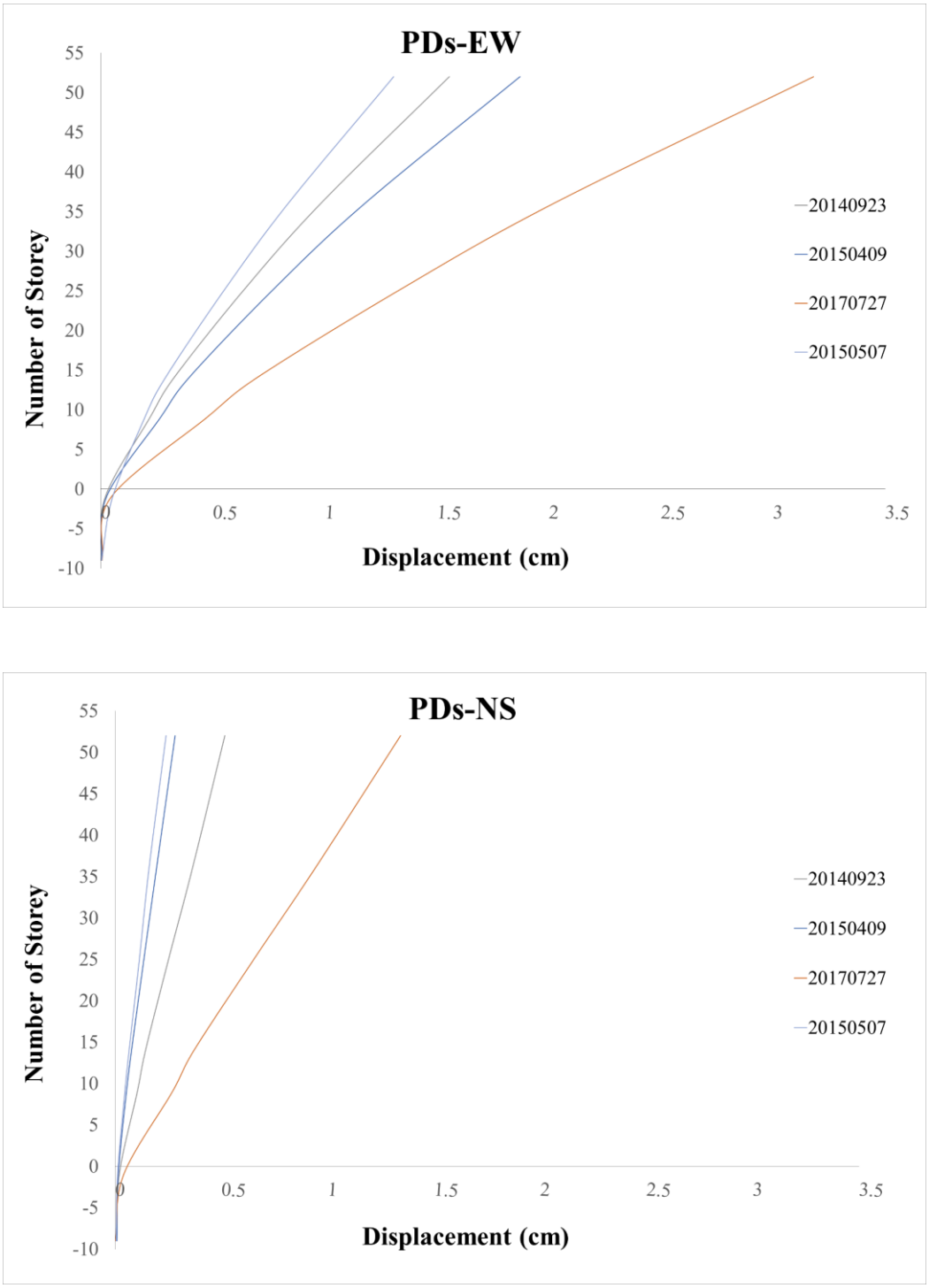

Figure 3.40. Peak horizontal displacements, recorded at the B9, B1, 9th, 14th, 25th, 36th, 52nd floor levels on the southern side of the building, due to wind excitations in the EW (top) and NS (bottom) directions.

Table 3.4. Maximum PAs, PVs and PDs, recorded on the southern sides of the building, during the wind of 23 September 2014 (top left), the wind of 09 April 2015 (top right), the wind of 07 May 2015 (bottom left), the wind of 27 July 2017 (bottom right).

Wind of 23 September 2014

Number of Storey	NS Direction			EW Direction		
	PA (cm/s^2)	PV (cm/s)	PD (cm)	PA (cm/s^2)	PV (cm/s)	PD (cm)
52	0.83	0.61	0.52	1.65	1.60	1.56
36	0.57	0.42	0.36	1.15	0.99	0.98
25	0.43	0.29	0.25	0.78	0.65	0.64
14	0.26	0.17	0.14	0.44	0.34	0.33
9	0.20	0.12	0.10	0.34	0.23	0.22
B1	0.03	0.02	0.02	0.04	0.02	0.02
B9	0.07	0.00	0.01	0.03	0.00	0.00

Wind of 09 April 2015

Number of Storey	NS Direction			EW Direction		
	PA (cm/s^2)	PV (cm/s)	PD (cm)	PA (cm/s^2)	PV (cm/s)	PD (cm)
52	0.54	0.39	0.28	1.97	1.81	1.87
36	0.40	0.27	0.19	1.21	1.13	1.18
25	0.31	0.19	0.13	0.76	0.73	0.76
14	0.20	0.11	0.08	0.46	0.38	0.39
9	0.14	0.08	0.05	0.34	0.26	0.27
B1	0.03	0.01	0.01	0.03	0.02	0.03
B9	0.02	0.01	0.01	0.03	0.00	0.00

Wind of 07 May 2015

Number of Storey	NS Direction			EW Direction		
	PA (cm/s^2)	PV (cm/s)	PD (cm)	PA (cm/s^2)	PV (cm/s)	PD (cm)
52	0.46	0.30	0.24	1.42	1.30	1.31
36	0.31	0.21	0.16	0.93	0.81	0.84
25	0.25	0.15	0.11	0.60	0.53	0.55
14	0.16	0.09	0.07	0.36	0.27	0.29
9	0.13	0.06	0.05	0.29	0.18	0.20
B1	0.03	0.01	0.01	0.13	0.05	0.05
B9	0.04	0.00	0.00	0.03	0.00	0.00

Wind of 27 July 2017

Number of Storey	NS Direction			EW Direction		
	PA (cm/s^2)	PV (cm/s)	PD (cm)	PA (cm/s^2)	PV (cm/s)	PD (cm)
52	2.23	1.59	1.34	3.12	2.83	3.18
36	1.57	1.11	0.94	2.00	1.78	2.02
25	1.13	0.78	0.65	1.41	1.16	1.33
14	0.74	0.44	0.37	0.92	0.60	0.69
9	0.57	0.32	0.27	0.76	0.41	0.47
B1	0.08	0.04	0.04	0.08	0.04	0.05
B9	0.00	0.00	0.00	0.03	0.00	0.01

3.2. Frequency Domain Characteristics

The determination of natural frequencies and mode shapes are essential for the dynamic analysis of structures. The Aegean Sea earthquake, the Gökova Earthquake, M_w = 6.1 Aegean Sea Turkey earthquake of 12 June 2017, M_w = 4.5 Taşoluk - Geyve Turkey earthquake of 22 October 2014 and wind of 23 September 2014, 09 April 2015, 07 May 2015, 27 July 2017 are selected to estimate modal frequencies and mode shapes.

3.2.1 Modal Frequencies

Natural frequencies, which can be calculated via several methods, are key parameters for the determination of the dynamic response of structures. “For building-type structures, it is possible to identify basic dynamic characteristics of a structure by using only Fourier transforms and band-pass filters” (Şafak E. & Çaktı E., 2014). FAS, the widely used method, is used in order to detect natural frequencies in this study.

3.2.1.1 Earthquake Response

FAS of accelerations in the EW and NS directions on the southern side of the building for the Aegean Sea Earthquake from all channels are shown in Figure 3.41 and Figure 3.42. Predominant peaks at several frequencies in the EW and NS directions can be easily seen in these figures. In addition, FAS of differences between two parallel accelerations from all channels recorded on both the southern and northern sides of the building in the EW and NS directions for the Aegean Sea Earthquake are computed and shown in Figure 3.43 and Figure 3.44 to detect torsional frequencies.

Natural frequencies clearly estimated from FAS by peak picking are summarized in Table 3.5. Whereas the first three natural frequencies in the EW direction are 0.16Hz, 0.84Hz, and 1.96-1.98Hz, in the NS direction are 0.22 Hz, 0.84 Hz, and 1.82-1.86 Hz. In addition, the first three torsional frequencies are in between 0.42 Hz, 1.4 Hz, and 2.80-2.84 Hz.

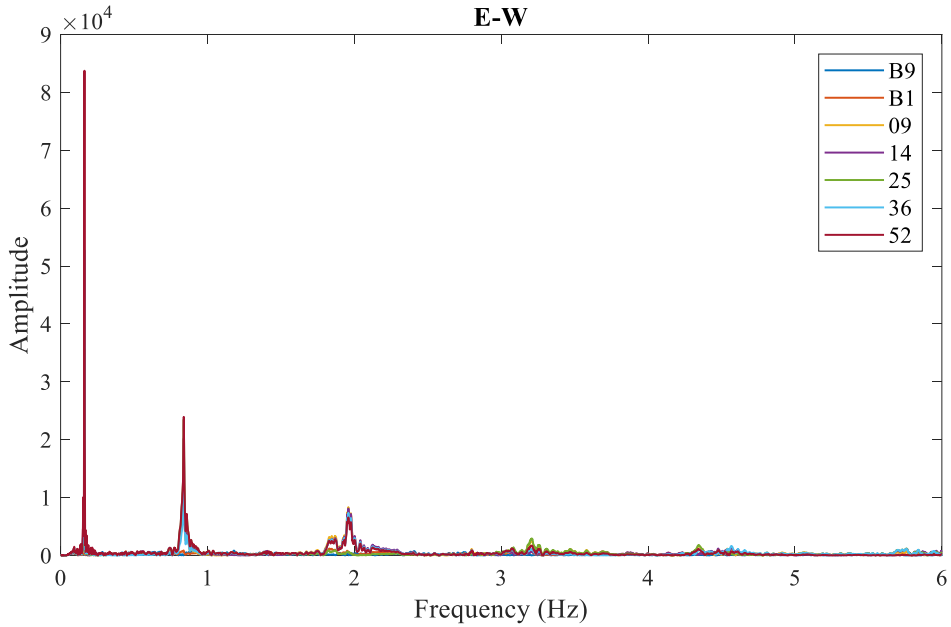

Figure 3.41. Fourier amplitude spectra of accelerations, in the EW direction, recorded on the southern side of the building, during the Aegean Sea earthquake.

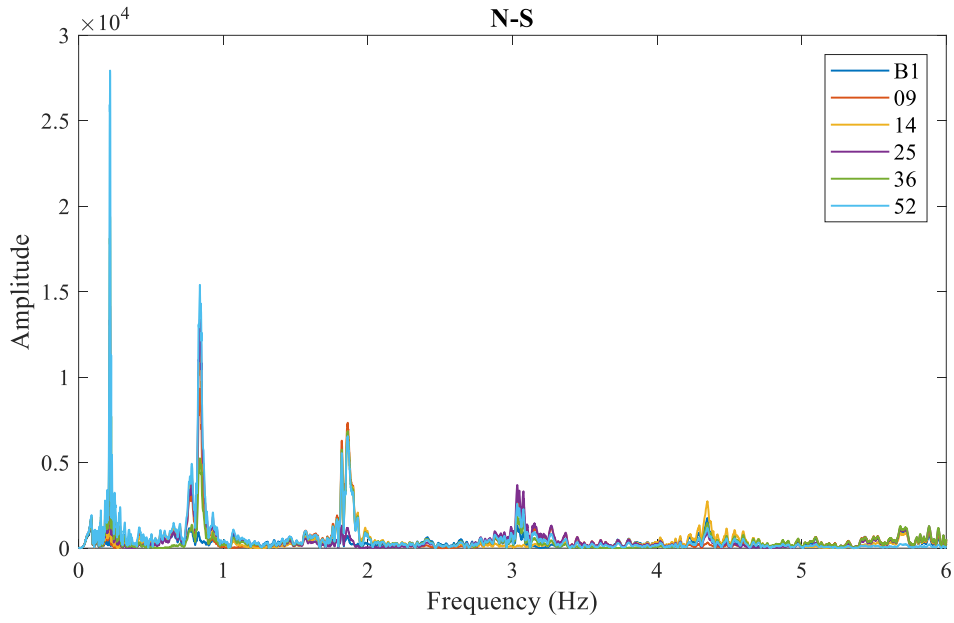

Figure 3.42. Fourier amplitude spectra of accelerations, in the NS direction, recorded on the southern side of the building, during the Aegean Sea earthquake.

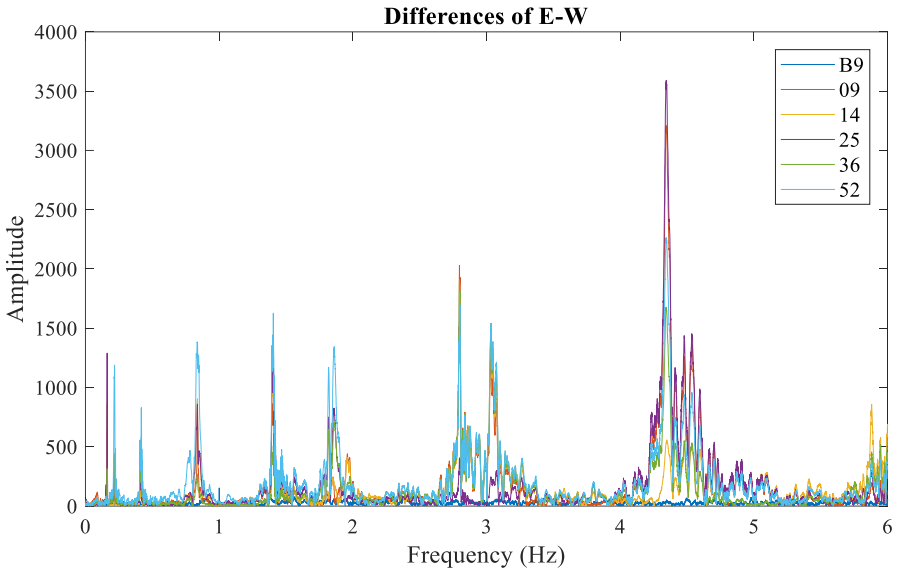

Figure 3.43. Fourier amplitude spectra of differences between two parallel accelerations in the EW direction recorded on the northern and southern sides of the building, during the Aegean Sea earthquake.

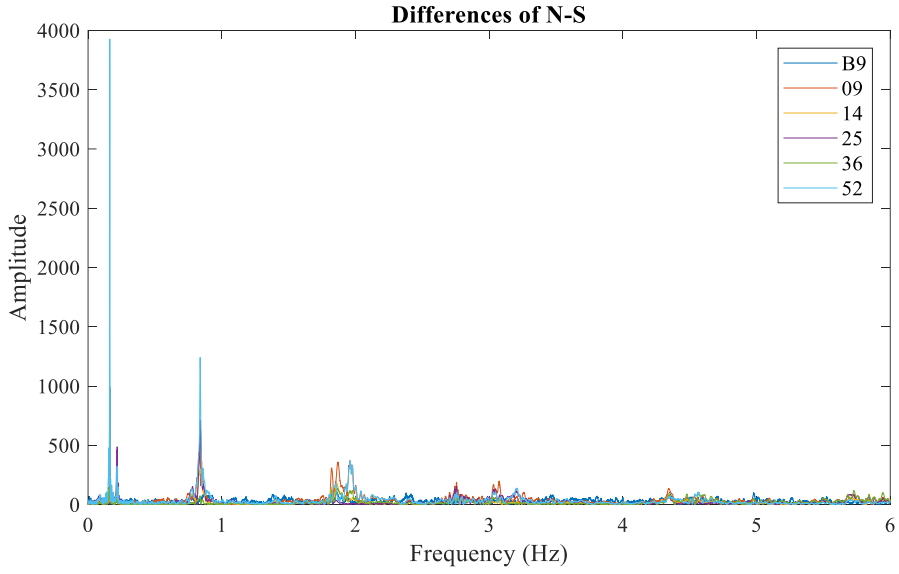

Figure 3.44. Fourier amplitude spectra of differences between two parallel accelerations in the NS direction recorded on the northern and southern sides of the building, during the Aegean Sea earthquake.

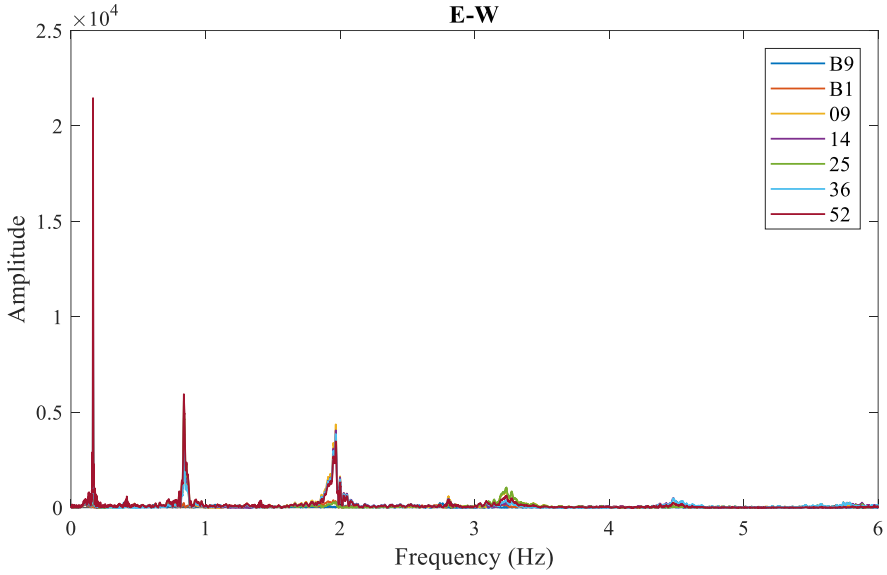

Figure 3.45. Fourier amplitude spectra of accelerations, in the EW direction, recorded on the southern side of the building, during M_w = 6.1 Aegean Sea Turkey earthquake of 12 June 2017.

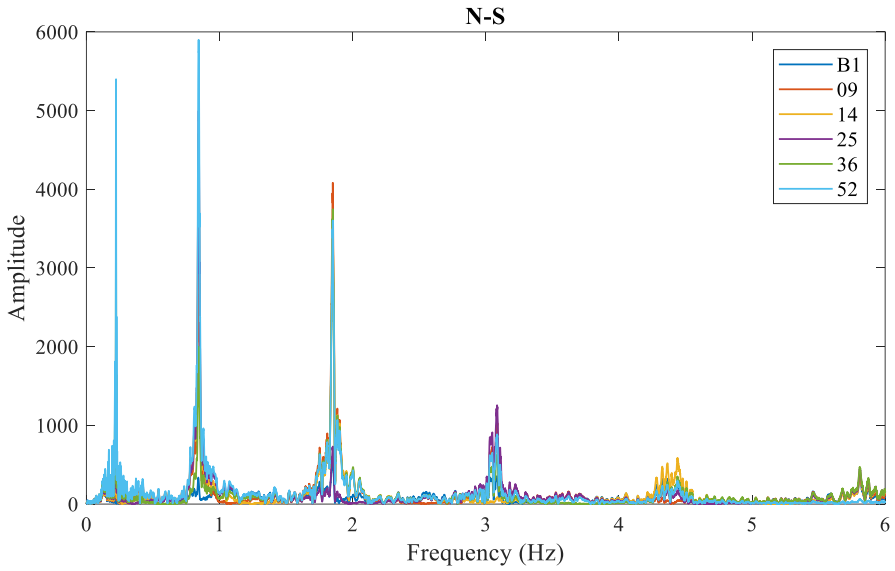

Figure 3.46. Fourier amplitude spectra of accelerations, in the NS direction, recorded on the southern side of the building, during M_w = 6.1 Aegean Sea Turkey earthquake of 12 June 2017.

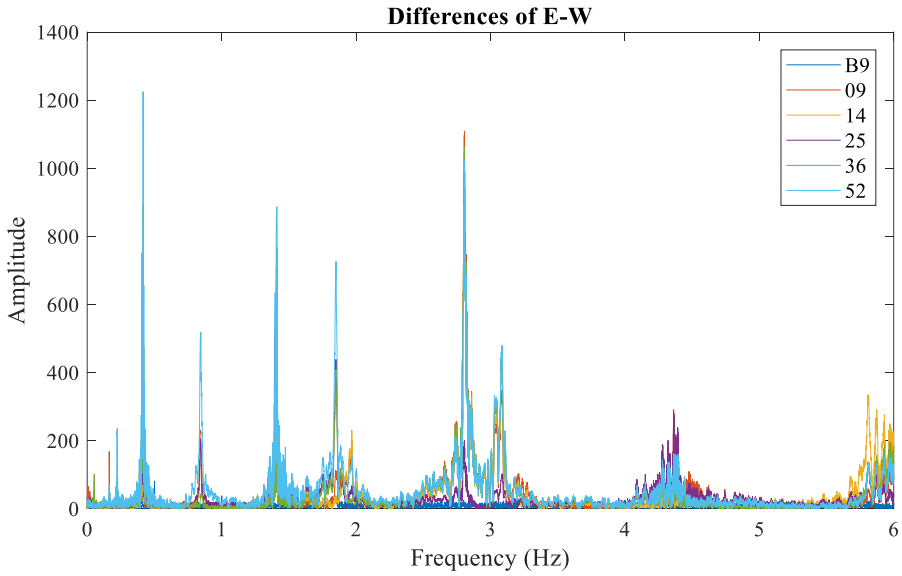

Figure 3.47. Fourier amplitude spectra of differences between two parallel accelerations in the EW direction recorded on the northern and southern side of the building, during M_w = 6.1 Aegean Sea Turkey earthquake of 12 June 2017.

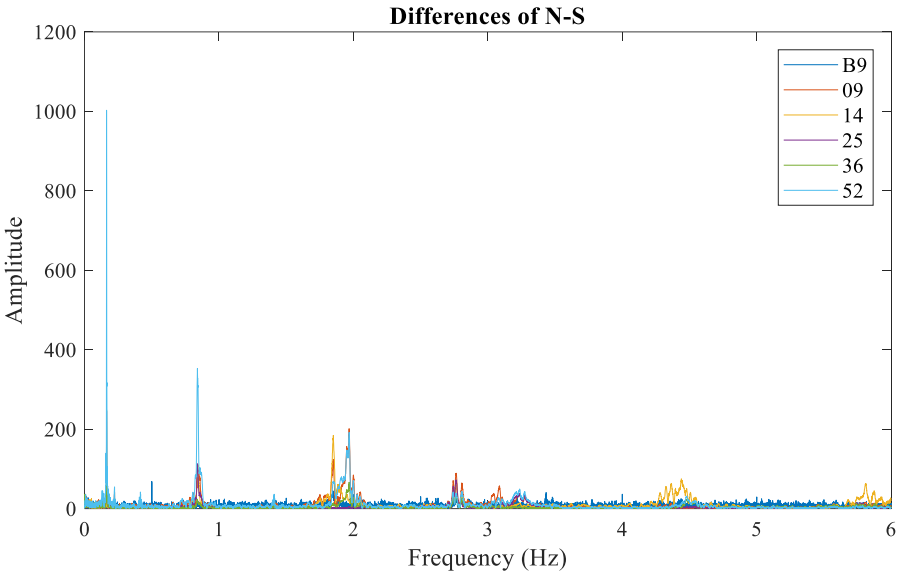

Figure 3.48. Fourier amplitude spectra of differences between two parallel accelerations in the NS direction recorded on the northern and southern side of the building, during M_w = 6.1 Aegean Sea Turkey earthquake of 12 June 2017.

Table 3.5. Modal frequencies (Hz) in the EW direction (top), NS direction (middle), torsional (bottom) of the building, during the Aegean Sea earthquake, M_w = 6.6 Gökova Körfezi (Akdeniz) Turkey earthquake of 21 July 2017, M_w = 6.1 Aegean Sea Turkey earthquake of 12 June 2017, M_w = 4.5 Taşoluk-Geyve Turkey earthquake of 22 October 2014.

	Modal Frequencies (Hz) - EW			
Events	Mode 1	Mode 2	Mode 3	Mode 4
M_w = 6.9 Aegean Sea Turkey, earthquake of 24 May 2014	0.16	0.84	1.96	3.21
M_w = 6.6 Gökova Körfezi(Akdeniz) Turkey, earthquake of 21 July 2017	0.16	0.84	1.96	3.22
M_w = 6.1 Aegean Sea Turkey, earthquake of 12 June 2017	0.16	0.84	1.97	3.24
M_w = 4.5 Taşoluk-Geyve Turkey, earthquake of 22 October 2014	0.16	0.85	1.98	3.25

	Modal Frequencies (Hz) - NS			
Events	Mode 1	Mode 2	Mode 3	Mode 4
M_w = 6.9 Aegean Sea Turkey, earthquake of 24 May 2014	0.22	0.84	1.82	3.03
M_w = 6.6 Gökova Körfezi(Akdeniz) Turkey, earthquake of 21 July 2017	0.22	0.84	1.85	3.09
M_w = 6.1 Aegean Sea Turkey, earthquake of 12 June 2017	0.22	0.84	1.85	3.09
M_w = 4.5 Taşoluk-Geyve Turkey, earthquake of 22 October 2014	0.23	0.85	1.86	3.09

	Modal Frequencies (Hz) - Torsional			
Events	Mode 1	Mode 2	Mode 3	Mode 4
M_w = 6.9 Aegean Sea Turkey, earthquake of 24 May 2014	0.42	1.41	2.80	-
M_w = 6.6 Gökova Körfezi(Akdeniz) Turkey, earthquake of 21 July 2017	0.42	1.41	2.82	-
M_w = 6.1 Aegean Sea Turkey, earthquake of 12 June 2017	0.42	1.41	2.81	-
M_w = 4.5 Taşoluk-Geyve Turkey, earthquake of 22 October 2014	0.42	1.41	2.84	-

3.2.1.2 Wind Response

FASs of accelerations during the wind of 23 September 2014, the wind of 09 April 2015, the wind of 07 May 2015, the wind of 27 July 2017 are computed. FASs of accelerations in the EW and NS directions on the southern side of the building for the wind of 27 July 2017 from all channels are shown in Figure 3.49 and Figure 3.50. Those are also shown for the wind of 09 April 2015 in Figure 3.53 and Figure 3.54. In addition, FASs of differences between two parallel accelerations from all channels recorded on both the northern and southern sides of the building in the EW and NS directions for the wind of 27 July 2017 and for the wind of 09 April 2015 are computed and shown following in Figure 3.51, Figure 3.52 and Figure 3.55, Figure 3.56 to detect torsional frequencies.

Natural frequencies clearly estimated from FAS by peak picking are shown in Table 3.6. Whereas the first three natural frequencies in the EW direction are 0.16Hz, 0.84 Hz, and 1.95-1.98 Hz, in the NS direction are in between 0.22 Hz, 0.85 Hz, and 1.84-1.86 Hz. In addition, the first three torsional frequencies are 0.41 Hz, 1.40-1.42 Hz, and 2.80-2.82 Hz.

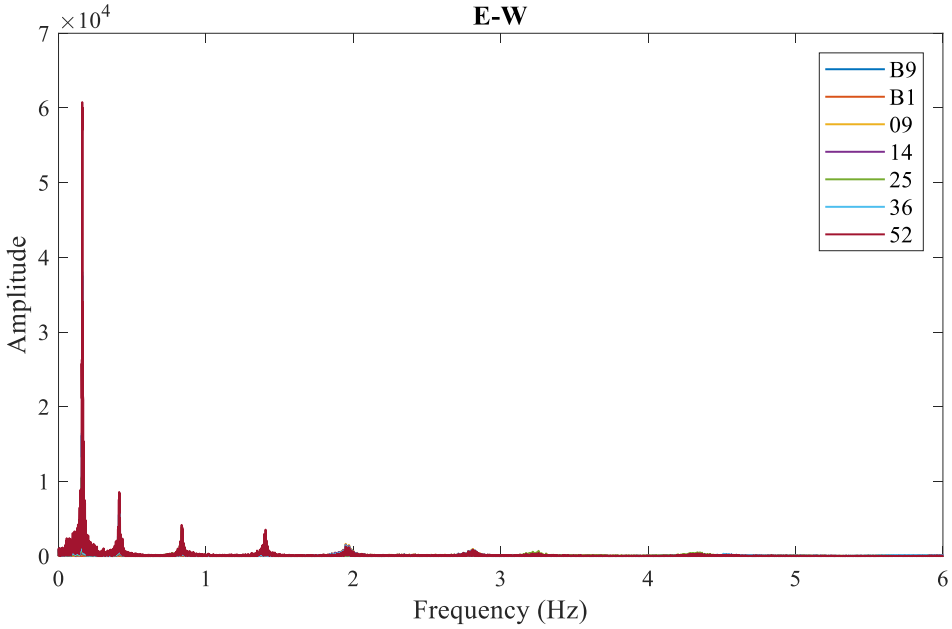

Figure 3.49. Fourier amplitude spectra of accelerations, in the EW direction, recorded on the southern side of the building, during the wind of 27 July 2017.

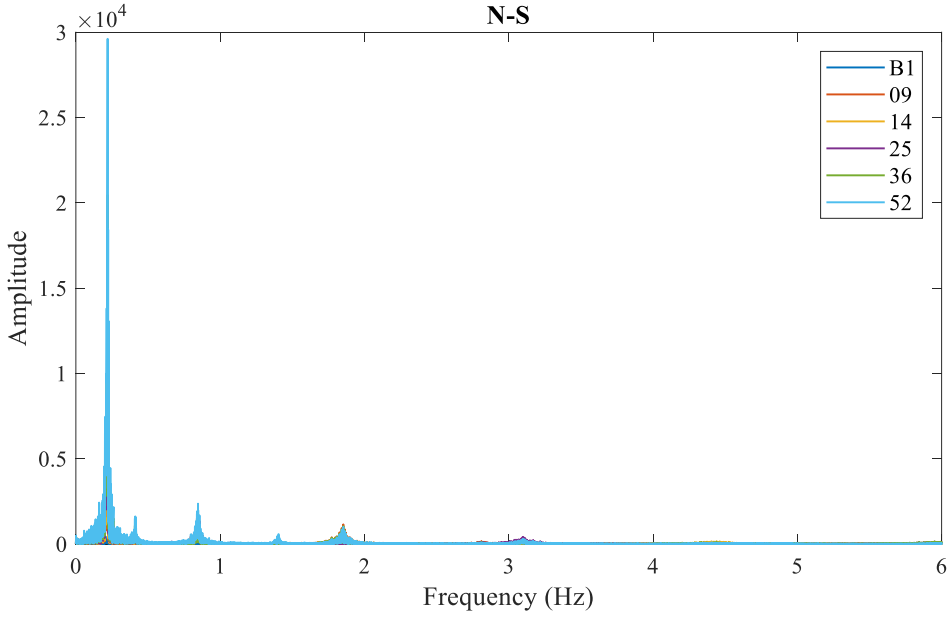

Figure 3.50. Fourier amplitude spectra of accelerations, in the NS direction, recorded on the southern side of the building, during the wind of 27 July 2017.

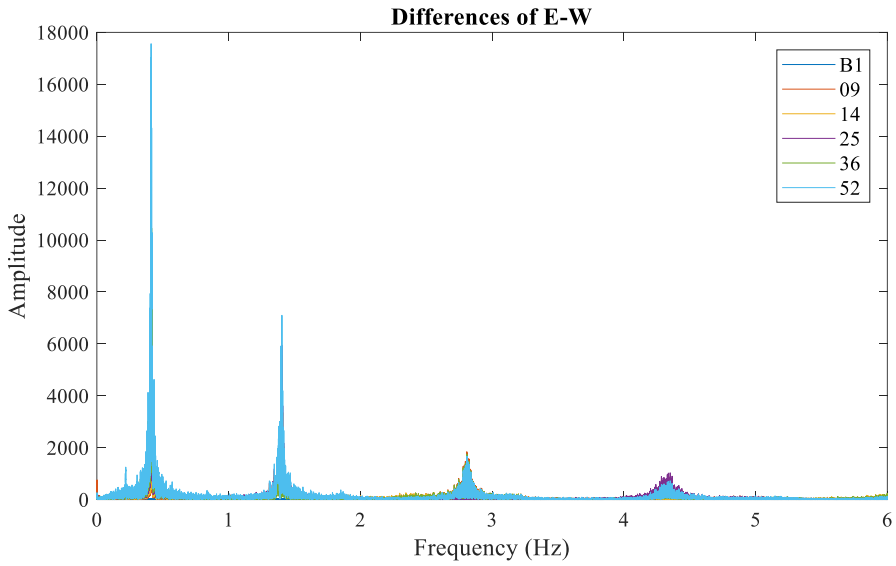

Figure 3.51. Fourier amplitude spectra of differences between two parallel accelerations in the EW direction recorded on the northern and southern sides of the building, during the wind of 27 July 2017.

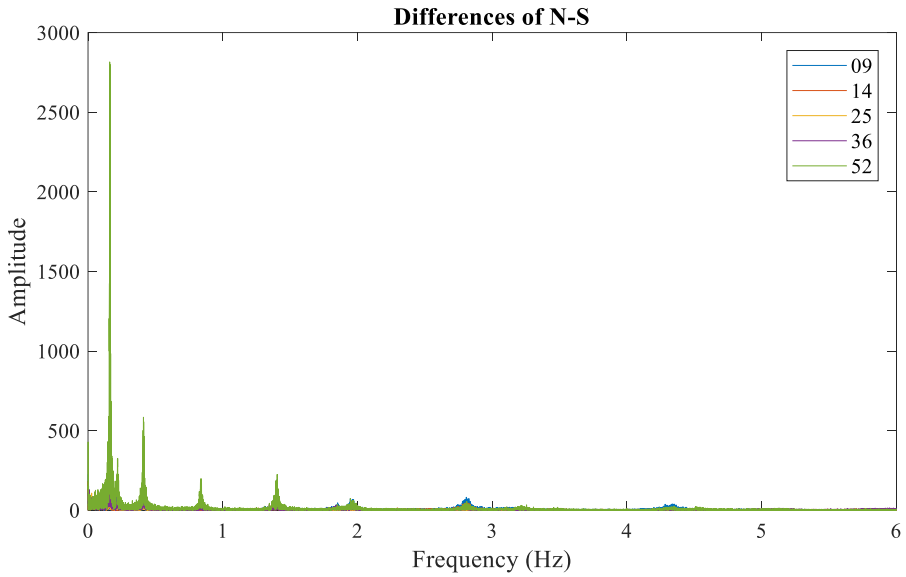

Figure 3.52. Fourier amplitude spectra of differences between two parallel accelerations in the NS direction recorded on the northern and southern sides of the building, during the wind of 27 July 2017.

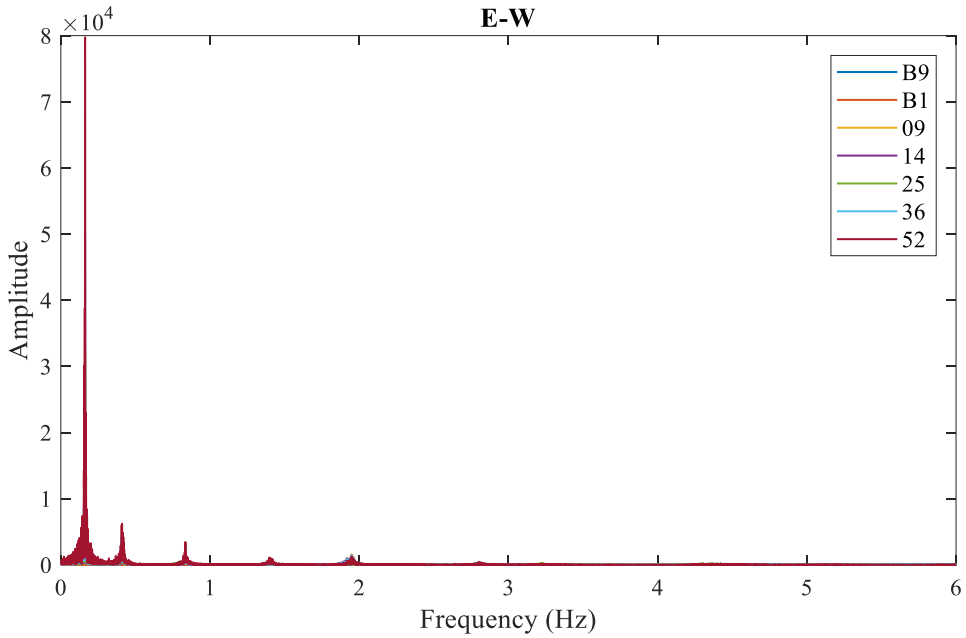

Figure 3.53. Fourier amplitude spectra of accelerations, in the EW direction, recorded on the southern side of the building, during the wind of 09 April 2015.

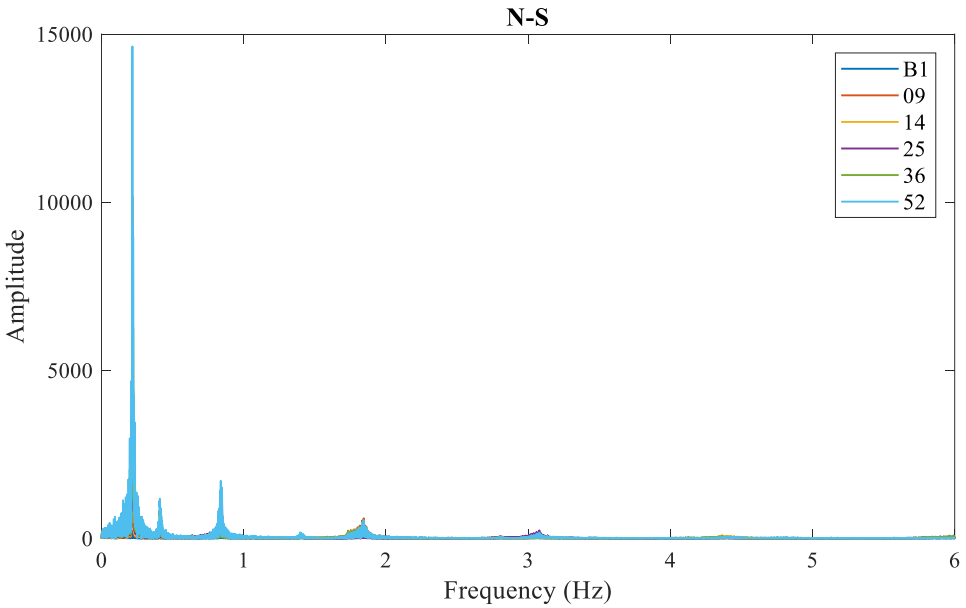

Figure 3.54. Fourier amplitude spectra of accelerations, in the NS direction, recorded on the southern side of the building, during the wind of 09 April 2015.

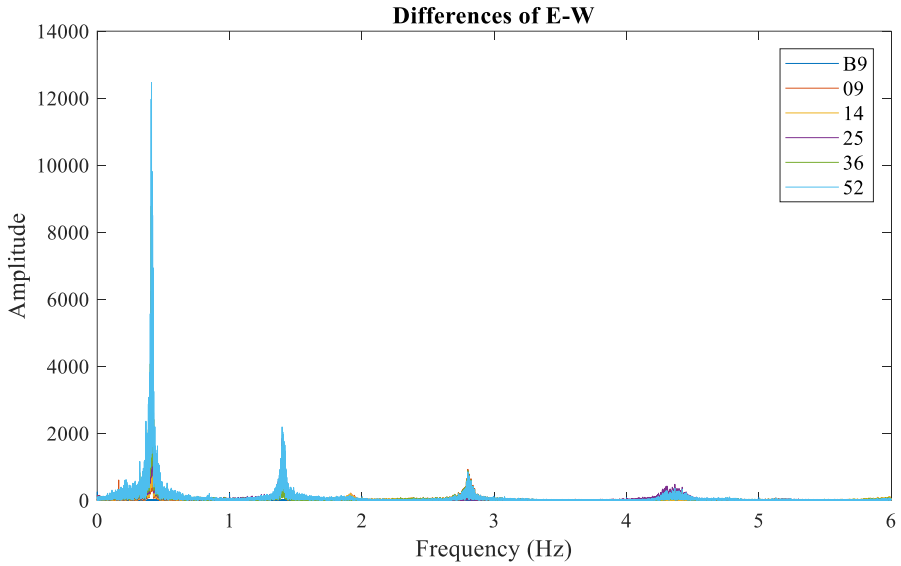

Figure 3.55. Fourier amplitude spectra of differences between two parallel accelerations in the E-W direction recorded on the northern and southern sides of the building, during the wind of 09 April 2015.

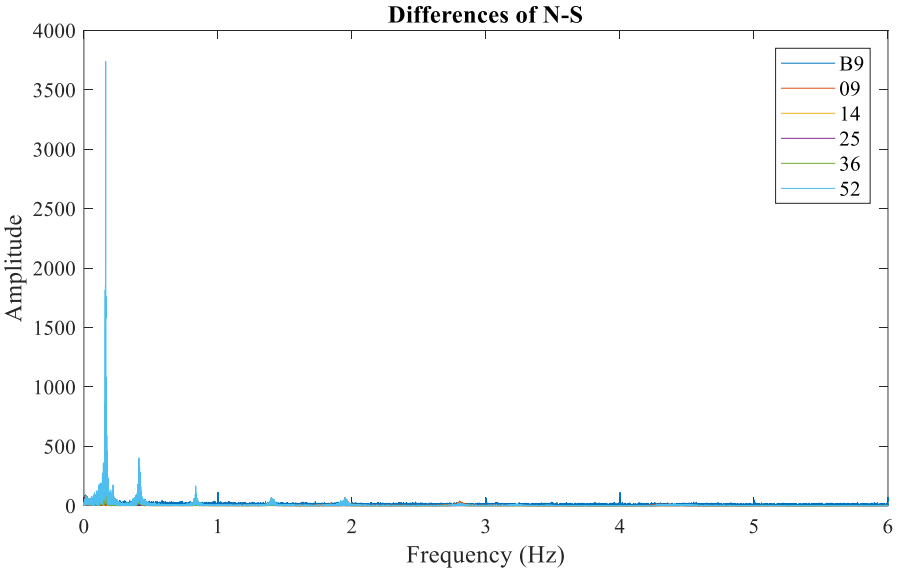

Figure 3.56. Fourier amplitude spectra of differences between two parallel accelerations in the E-W direction recorded on the northern and southern sides of the building, during the wind of 09 April 2015.

Table 3.6. Modal frequencies (Hz) in the EW direction (top), NS direction (middle), torsional (bottom) of the building, during the wind of 09 April 2015, the wind of 07 May 2015, the wind of 27 July 2017.

	Modal Frequencies (Hz) - EW			
Events	Mode 1	Mode 2	Mode 3	Mode 4
Wind of 23 September 2014	0.16	0.84	1.98	3.24
Wind of 09 April 2015	0.16	0.83	1.95	3.23
Wind of 07 May 2015	0.16	0.84	1.96	3.21
Wind of 27 July 2017	0.16	0.84	1.95	3.22

	Modal Frequencies (Hz) - NS			
Events	Mode 1	Mode 2	Mode 3	Mode 4
Wind of 23 September 2014	0.23	0.85	1.86	3.10
Wind of 09 April 2015	0.22	0.85	1.84	3.08
Wind of 07 May 2015	0.22	0.84	1.85	3.09
Wind of 27 July 2017	0.22	0.85	1.84	3.10

	Modal Frequencies (Hz) - Torsional			
Events	Mode 1	Mode 2	Mode 3	Mode 4
Wind of 23 September 2014	0.42	1.42	2.82	-
Wind of 09 April 2015	0.41	1.40	2.80	-
Wind of 07 May 2015	0.41	1.40	2.81	-
Wind of 27 July 2017	0.41	1.41	2.81	-

3.2.2 Mode Shapes

Modal displacements which are the second integration of filtered accelerations are necessary to derive mode shapes. Filtered data represent the response at a chosen mode. After the determination of natural frequencies, corner frequencies used in bandpass filtering for each modal frequency are chosen from the FASs of acceleration records. Table 3.7, for earthquake records, and Table 3.8, for wind records, shows the corner frequencies those are chosen for the bandpass filtering. Particle motions, showing the modal displacements in the EW and NS directions for each mode, are plotted in order to clarify the mode shape.

3.2.2.1 Earthquake

Mode shape profiles, which occurred in M_w = 6.1 Aegean Sea Turkey earthquake of 12 June 2017 are shown in Figure 3.57 for the EW direction and shown in Figure 3.58 for the NS direction. Particle motions occurred in M_w = 6.1 Aegean Sea Turkey earthquake of 12 June 2017 are shown Figure 3.59 for the EW direction, Figure 3.60 for the NS direction, and Figure 3.61 for the torsion. There are 4 modes estimated in the EW, NS direction and for torsion. In EW and NS direction, whereas 1^{st}, 3^{rd} and 4^{th} mode shapes are totally lateral, 2^{nd} mode shape is also lateral but coupled with the other side.

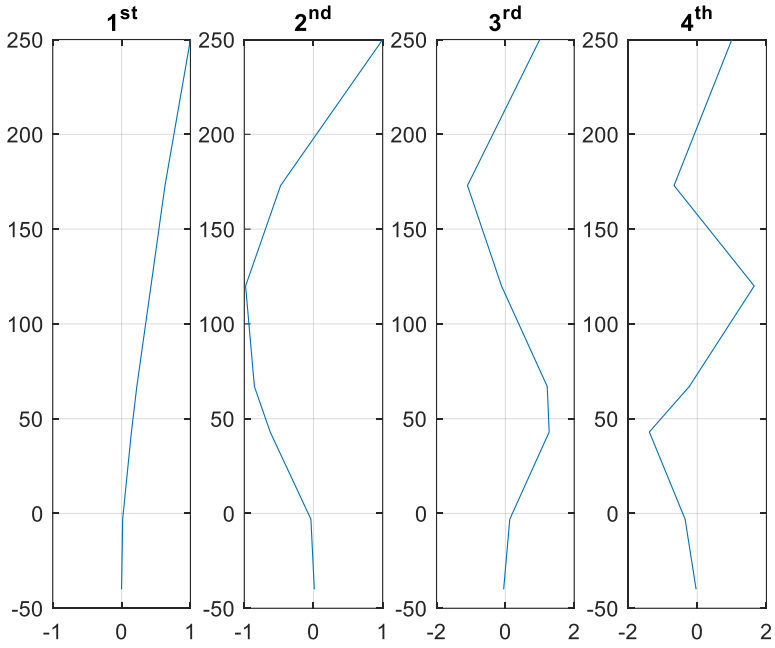

Figure 3.57. First 4 mode shapes in the EW direction, occurred in M_w = 6.1 Aegean Sea Turkey earthquake of 12 June 2017.

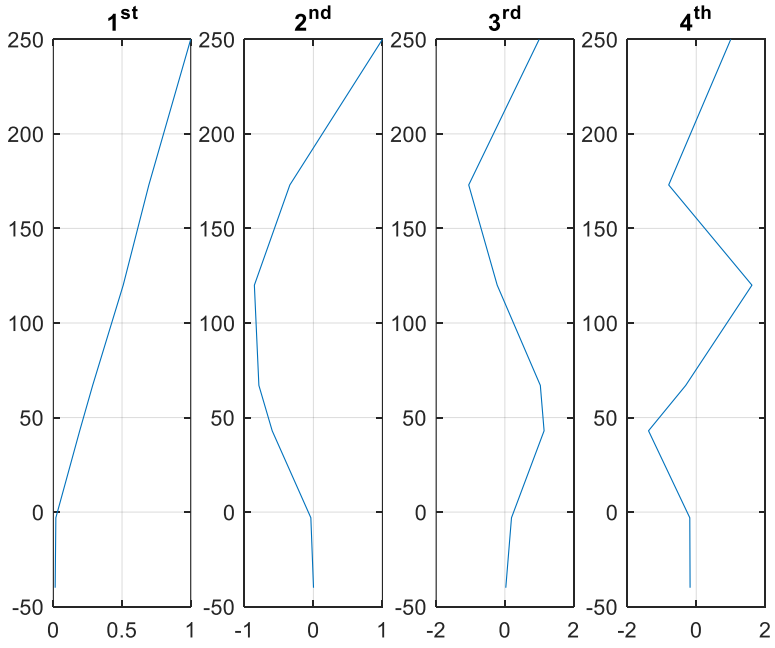

Figure 3.58. First 4 mode shapes in the NS direction, occurred in M_w = 6.1 Aegean Sea Turkey earthquake of 12 June 2017.

Table 3.7. Natural frequencies and corner frequencies used in bandpass filter for earthquake records.

Events	Mode 1			Mode 2			Mode 3			Mode 4		
	Natural Frequency	Corner Frequencies		Natural Frequency	Corner Frequencies		Natural Frequency	Corner Frequencies		Natural Frequency	Corner Frequencies	
M_w = 6.9 Aegean Sea Turkey, earthquake of 24 May 2014	0.1625	0.1549	0.1694	0.8385	0.8118	0.8560	1.9590	1.9510	1.9770	3.2070	3.1560	3.2390
M_w = 6.6 Gökova Körfezi(Akdeniz) Turkey, earthquake of 21 July 2017	0.1633	0.1610	0.1656	0.8438	0.8427	0.8442	1.9640	1.9630	1.9650	3.2210	3.2200	3.2220
M_w = 6.1 Aegean Sea Turkey, earthquake of 12 June 2017	0.1640	0.1610	0.1686	0.8392	0.8133	0.8842	1.9680	1.9510	1.9800	3.2370	3.2350	3.2410
Mw = 4.5 Taşoluk-Geyve Turkey, earthquake of 22 October 2014	0.1648	0.1602	0.1709	0.8484	0.8423	0.8514	1.9760	1.9680	1.9820	3.2500	3.2200	3.2790

Events	Mode 1			Mode 2			Mode 3			Mode 4		
	Natural Frequency	Corner Frequencies		Natural Frequency	Corner Frequencies		Natural Frequency	Corner Frequencies		Natural Frequency	Corner Frequencies	
M_w = 6.9 Aegean Sea Turkey, earthquake of 24 May 2014	0.2174	0.2007	0.2228	0.8385	0.8064	0.8987	1.8200	1.8020	1.8330	3.0330	3.0270	3.0410
M_w = 6.6 Gökova Körfezi(Akdeniz) Turkey, earthquake of 21 July 2017	0.2213	0.2190	0.2235	0.8415	0.8392	0.8461	1.8540	1.8530	1.8550	3.0900	3.0880	3.0910
M_w = 6.1 Aegean Sea Turkey, earthquake of 12 June 2017	0.2228	0.2197	0.2251	0.8430	0.8316	0.8484	1.8510	1.8270	1.8670	3.0850	3.0590	3.0960
Mw = 4.5 Taşoluk-Geyve Turkey, earthquake of 22 October 2014	0.2258	0.2243	0.2274	0.8545	0.8530	0.8560	1.8600	1.8570	1.8650	3.0900	3.0780	3.1250

Events	Mode 1			Mode 2			Mode 3			Mode 4		
	Natural Frequency	Corner Frequencies		Natural Frequency	Corner Frequencies		Natural Frequency	Corner Frequencies		Natural Frequency	Corner Frequencies	
M_w = 6.9 Aegean Sea Turkey, earthquake of 24 May 2014	0.4181	0.4143	0.4211	1.4050	1.4020	1.4100	2.7980	2.7940	2.8030	-	-	-
M_w = 6.6 Gökova Körfezi(Akdeniz) Turkey, earthquake of 21 July 2017	0.4162	0.4150	0.4166	1.4080	1.4070	1.4090	2.8180	2.8170	2.8190	-	-	-
M_w = 6.1 Aegean Sea Turkey, earthquake of 12 June 2017	0.4158	0.4135	0.4173	1.4110	1.4100	1.4120	2.8070	2.8060	2.8080	-	-	-
Mw = 4.5 Taşoluk-Geyve Turkey, earthquake of 22 October 2014	0.4196	0.4150	0.4242	1.4140	1.4080	1.4160	2.8350	2.8320	2.8380	-	-	-

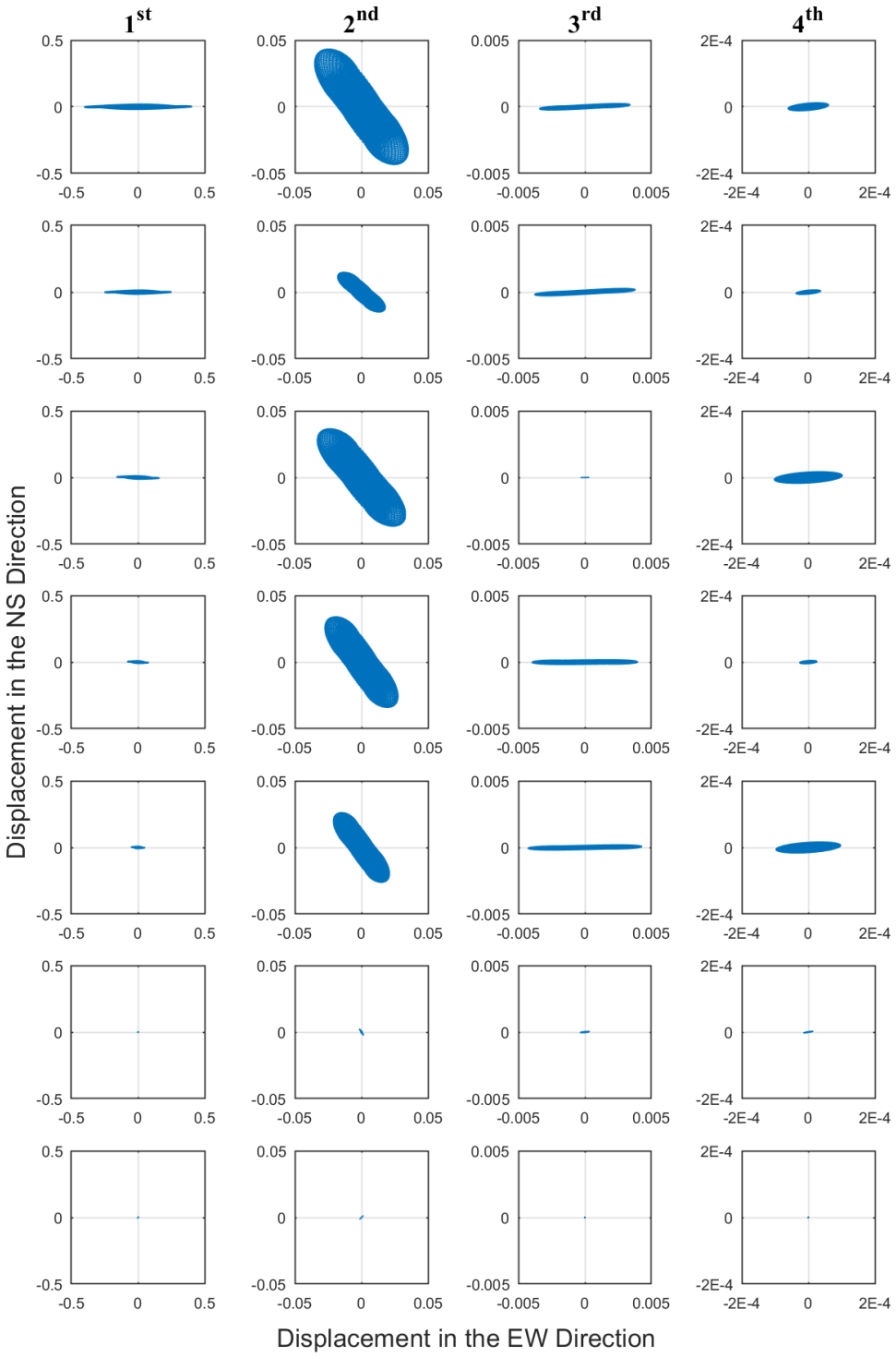

Figure 3.59. Particle motions in the EW direction at B9, B1, 9th, 14th, 25th, 36th, 52nd floors corresponding to respectively 1st, 2nd, 3rd, 4th mode shapes, during M_w = 6.1 Aegean Sea Turkey earthquake of 12 June 2017.

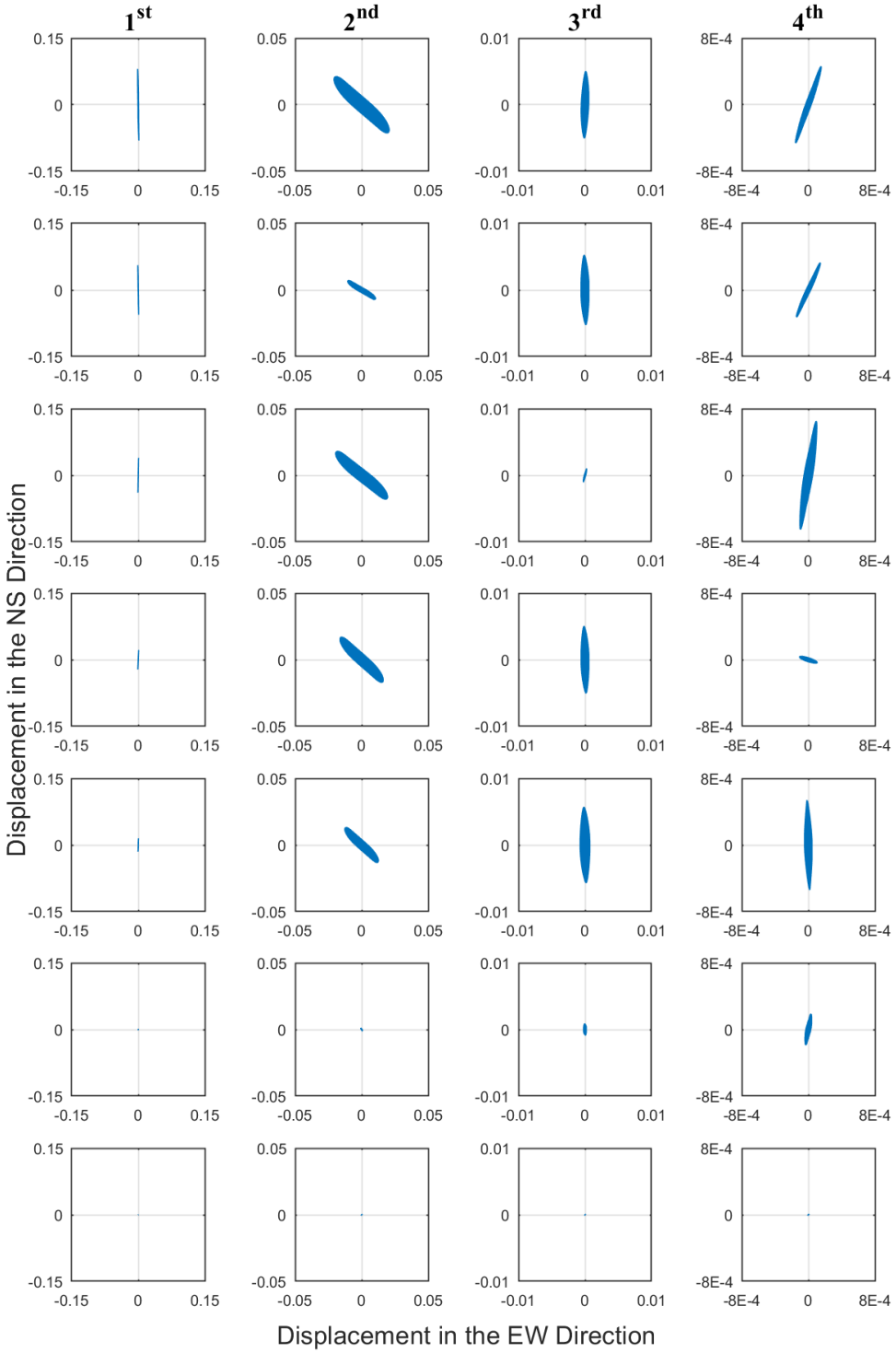

Figure 3.60. Particle motions corresponding to respectively 1st, 2nd, 3rd, 4th mode shapes in the NS direction at B9, B1, 9th, 14th, 25th, 36th, 52nd floors during M_w = 6.1 Aegean Sea Turkey earthquake of 12 June 2017.

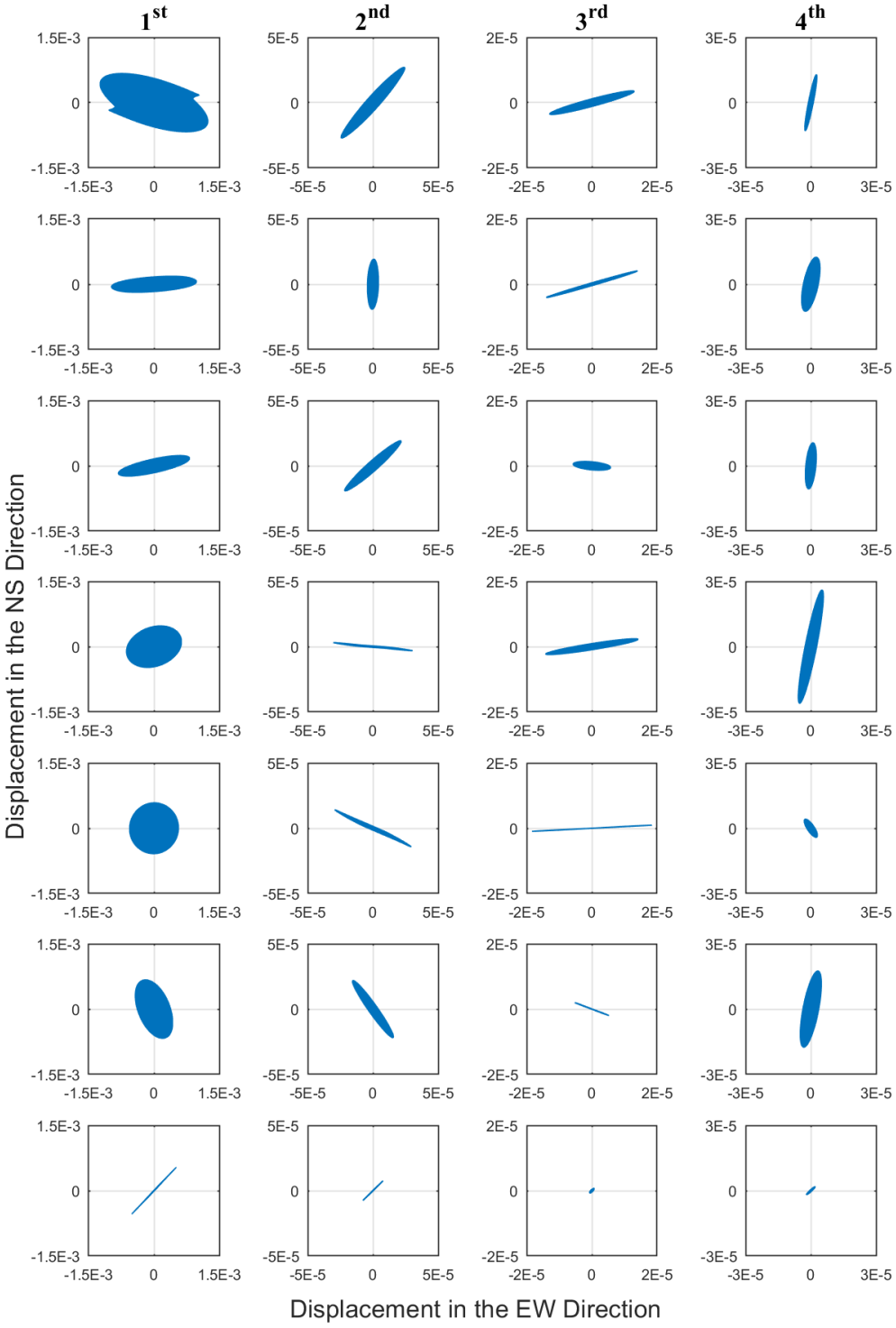

Figure 3.61. Particle motions corresponding to respectively 1st, 2nd, 3rd, 4th mode shapes in the torsional direction at B9, B1, 9th, 14th, 25th, 36th, 52nd floors during M_w = 6.1 Aegean Sea Turkey earthquake of 12 June 2017.

3.2.2.2 Wind Response

Particle motions occurred in the wind of 09 April 2015 are shown Figure 3.64 for the EW direction, Figure 3.65 for the NS direction, and Figure 3.66 for the torsion. There are 4 modes estimated in the EW, NS direction and torsion. In the EW and NS directions 1st, 2nd, 3rd and 4th mode shapes are totally lateral.

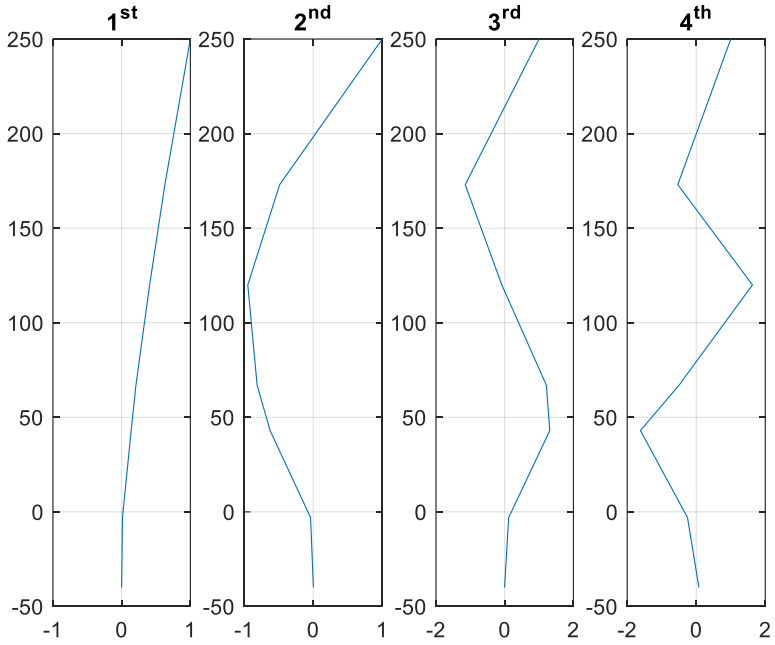

Figure 3.62. First 4 mode shapes in the EW direction, occurred in the wind of 09 April 2015.

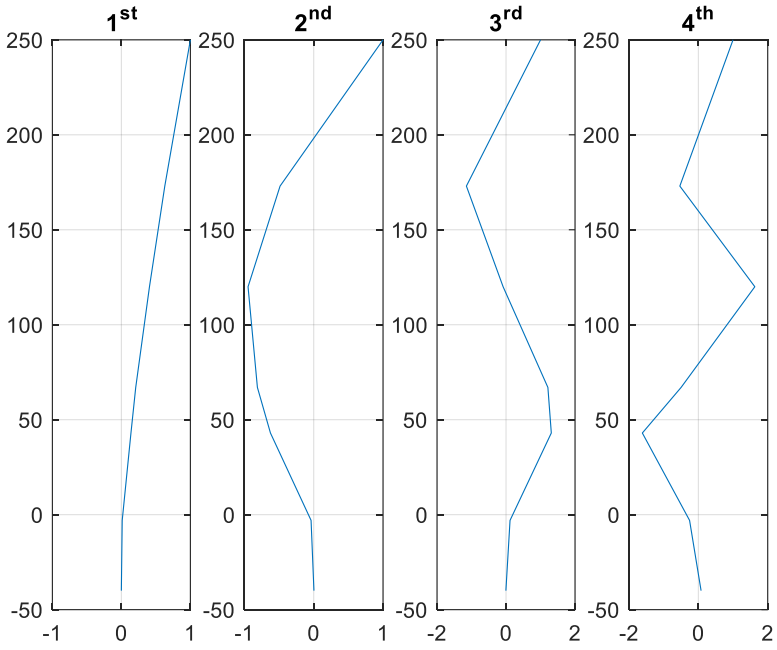

Figure 3.63. First 4 mode shapes in the NS direction, occurred in the wind of 09 April 2015.

Table 3.8. Naturel frequencies and corner frequencies, used in bandpass filter for wind records.

Events	Mode 1			Mode 2			Mode 3			Mode 4		
	Natural Frequency	Corner Frequencies		Natural Frequency	Corner Frequencies		Natural Frequency	Corner Frequencies		Natural Frequency	Corner Frequencies	
Wind of 23 September 2014	0.1638	0.1631	0.1642	0.8423	0.8421	0.8425	1.9760	1.9750	1.9770	3.2380	3.2370	3.2390
Wind of 09 April 2015	0.1625	0.1621	0.1629	0.8347	0.8339	0.8350	1.9490	1.9480	1.9500	3.2290	3.2280	3.2300
Wind of 07 May 2015	0.1625	0.1617	0.1629	0.8362	0.8358	0.8366	1.9580	1.9570	1.9590	3.2140	3.2130	3.2150
Wind of 27 July 2017	0.1617	0.1566	0.1648	0.8354	0.8324	0.8377	1.9490	1.9470	1.9500	2.8120	2.8110	2.8140

Events	Mode 1			Mode 2			Mode 3			Mode 4		
	Natural Frequency	Corner Frequencies		Natural Frequency	Corner Frequencies		Natural Frequency	Corner Frequencies		Natural Frequency	Corner Frequencies	
Wind of 23 September 2014	0.2230	0.2222	0.2235	0.8499	0.8495	0.8503	1.8600	1.8590	1.8610	3.0960	3.0950	3.0970
Wind of 09 April 2015	0.2174	0.2167	0.2178	0.8476	0.8469	0.8480	1.8420	1.8410	1.8430	3.0790	3.0780	3.0800
Wind of 07 May 2015	0.2213	0.2205	0.2220	0.8430	0.8423	0.8438	1.8470	1.8460	1.8480	3.0940	3.0930	3.0950
Wind of 27 July 2017	0.2205	0.2185	0.2228	0.8469	0.8461	0.8476	1.8420	1.8410	1.8450	3.0970	3.0960	0.0980

Events	Mode 1			Mode 2			Mode 3			Mode 4		
	Natural Frequency	Corner Frequencies		Natural Frequency	Corner Frequencies		Natural Frequency	Corner Frequencies		Natural Frequency	Corner Frequencies	
Wind of 23 September 2014	0.4164	0.4160	0.4168	1.4190	1.4180	1.4200	2.8150	2.8140	2.8160	-	-	-
Wind of 09 April 2015	0.4105	0.4089	0.4108	1.3980	1.3970	1.3990	2.8020	2.8010	2.8030	-	-	-
Wind of 07 May 2015	0.4131	0.4124	0.4135	1.4020	1.4010	1.4030	2.8090	2.8080	2.8100	-	-	-
Wind of 27 July 2017	0.4097	0.4074	0.4105	1.4050	1.4030	1.4090	2.8070	2.8090	2.8110	-	-	-

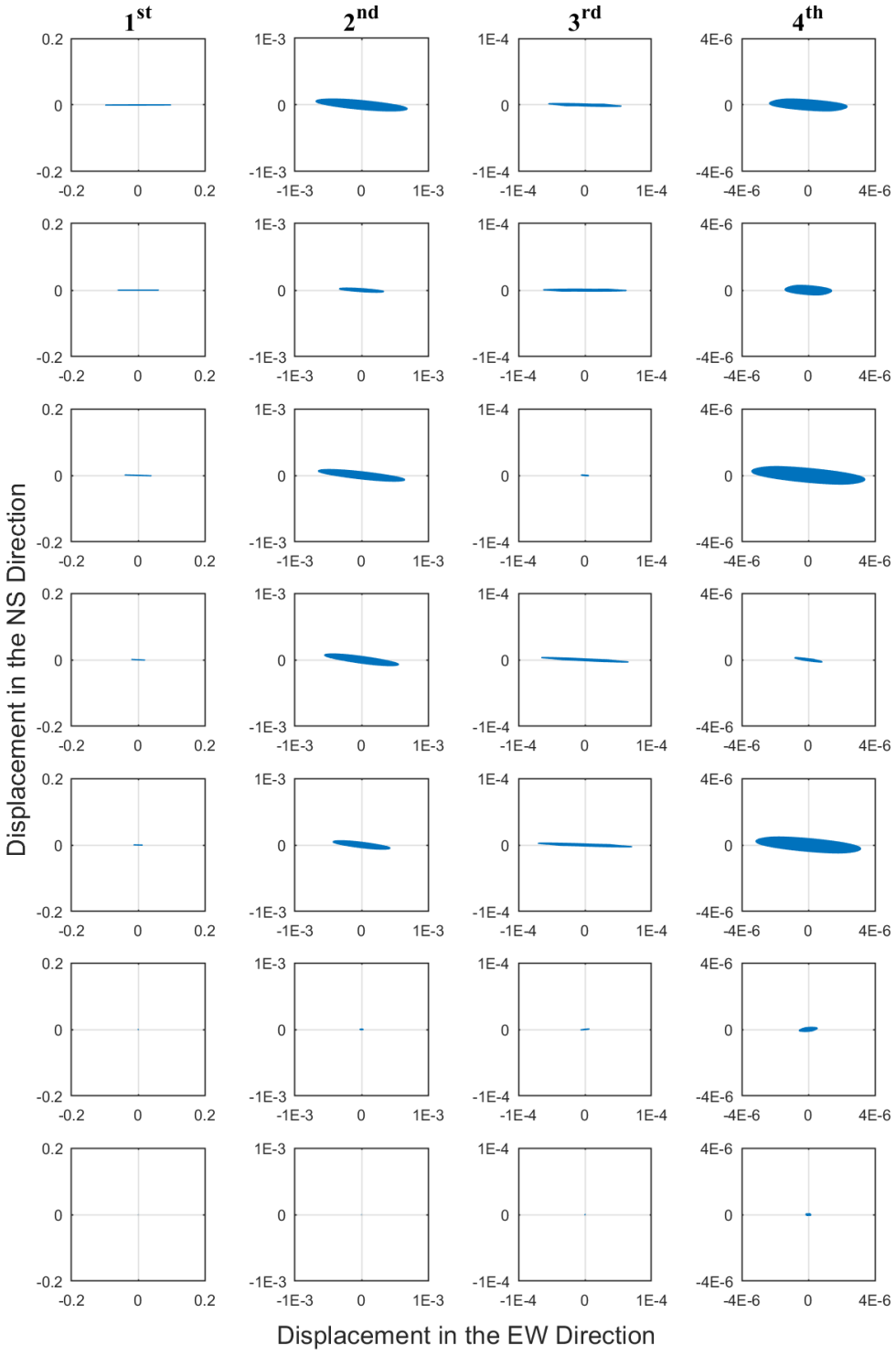

Figure 3.64. Particle motions in the EW direction at B9, B1, 9th, 14th, 25th, 36th, 52nd floors corresponding to respectively 1st, 2nd, 3rd, 4th mode shapes, during the wind of 09 April 2015.

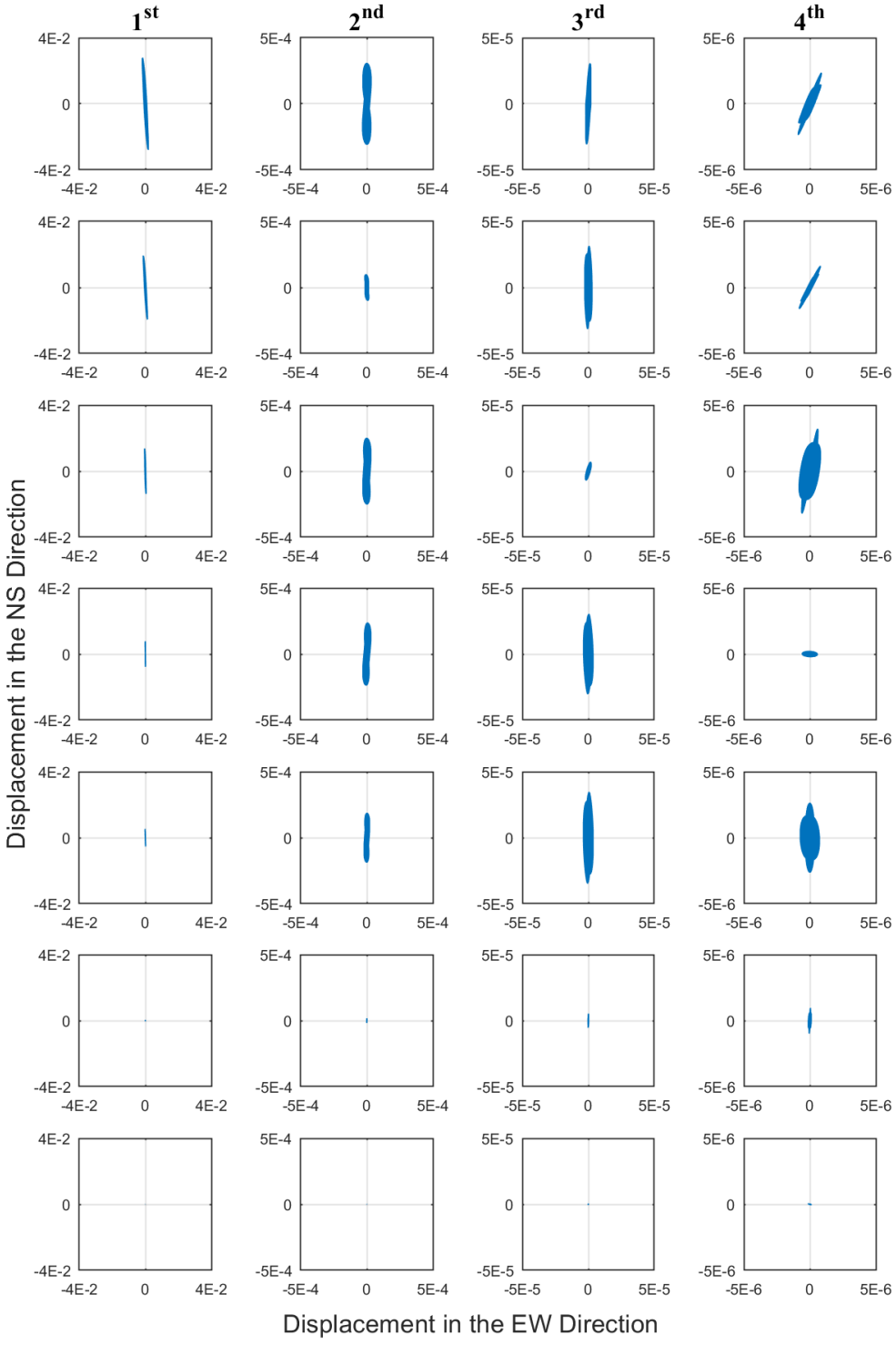

Figure 3.65. Particle motions in the NS direction at B9, B1, 9th, 14th, 25th, 36th, 52nd floors corresponding to respectively 1st, 2nd, 3rd, 4th mode shapes, during the wind of 09 April 2015.

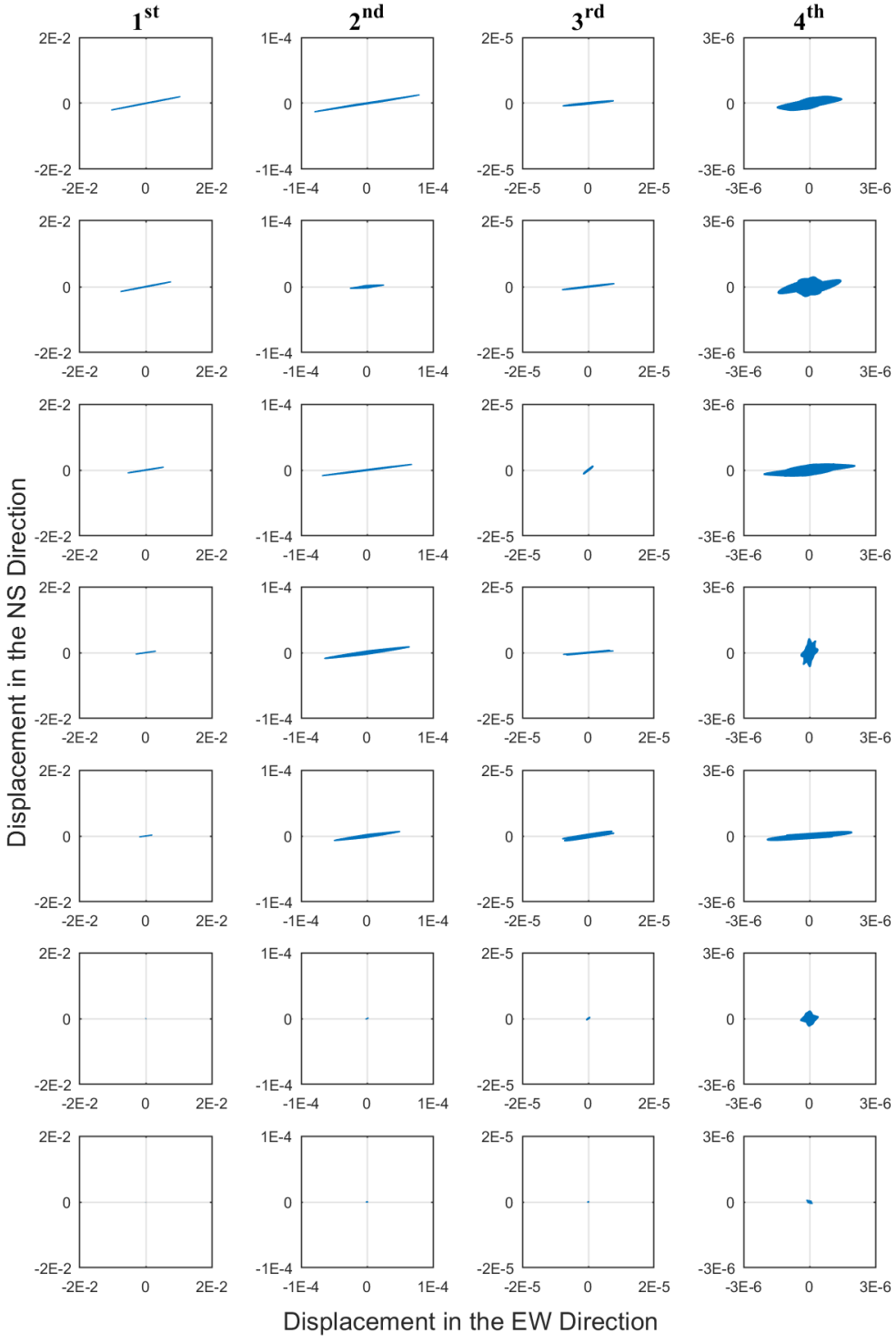

Figure 3.66. Particle motions in the torsional direction at B9, B1, 9th, 14th, 25th, 36th, 52nd floors corresponding to respectively 1st, 2nd, 3rd, 4th mode shapes, during the wind of 09 April 2015.

3.3. Average Drift Ratios

Drift ratio representing damage occurrence of buildings, especially for tall buildings, is one of the main parameters to design of them and hence there is a limitation in all structural codes. In this study, average drift ratios are estimated from displacement time histories between any two floors where accelerations were recorded, since there is no accelerometer in all stories. Average drift ratios derived from computed displacement time histories are calculated between 52nd and 36th, 36th and 25th, 25th and 14th, 14th and 9th, 52nd and 9th, and 36th and 9th floors. After the estimation of maximum average drift ratios, results are compared with drift ratio limits in design codes for different countries.

Table 3.9. Drift ratio limits in design codes in different countries (Çelebi, 2014).

Code	Upper Limit Drift Ratio (%)	Comment	Reference
Chile	0.2	Results in elastic design	Nch433.Of96 (1996) [18]
Japan	1.0	Max for buildings taller than 60 m. For collapse prevention (level 2) motions	Building Center of Japan 2001a, b. [19,20]
USA	2.0	No collapse state	ASCE7-10 (2007) [21]
Turkey	2.0	Can be increased by 50 % in case of some steel frames	DBYYHY: Section 2.10.1.3, Eqn: 2.19 in Turkish Code (2007) [22]
New Zealand	2.5		NZS1170.5(2004) [23]
Eurocode 8	1.0 (max)	For buildings having non-structural elements fixed in a way so as not to interfere with structural deformations, or without non-structural elements	Section 4.4.3.2, Eqn:4.33 Eurocode 8 (2008) [17]

3.3.1 Earthquake Response

Maximum average drift ratios are estimated, during the Aegean Sea earthquake, the Gökova Earthquake, M_w = 6.1 Aegean Sea Turkey earthquake of 12 June 2017 and M_w = 4.5 Taşoluk - Geyve Turkey earthquake of 22 October 2014. Maximum average drift ratios have occurred in the Aegean Sea earthquake. Average drift ratios, shown in Figure 3.67, in the EW direction is about 0.013%, and it in the NS direction is about 0.008%.

A 2% drift ratio is the maximum limit for the design of buildings in Turkey and calculated average drift ratios are far below the limitations.

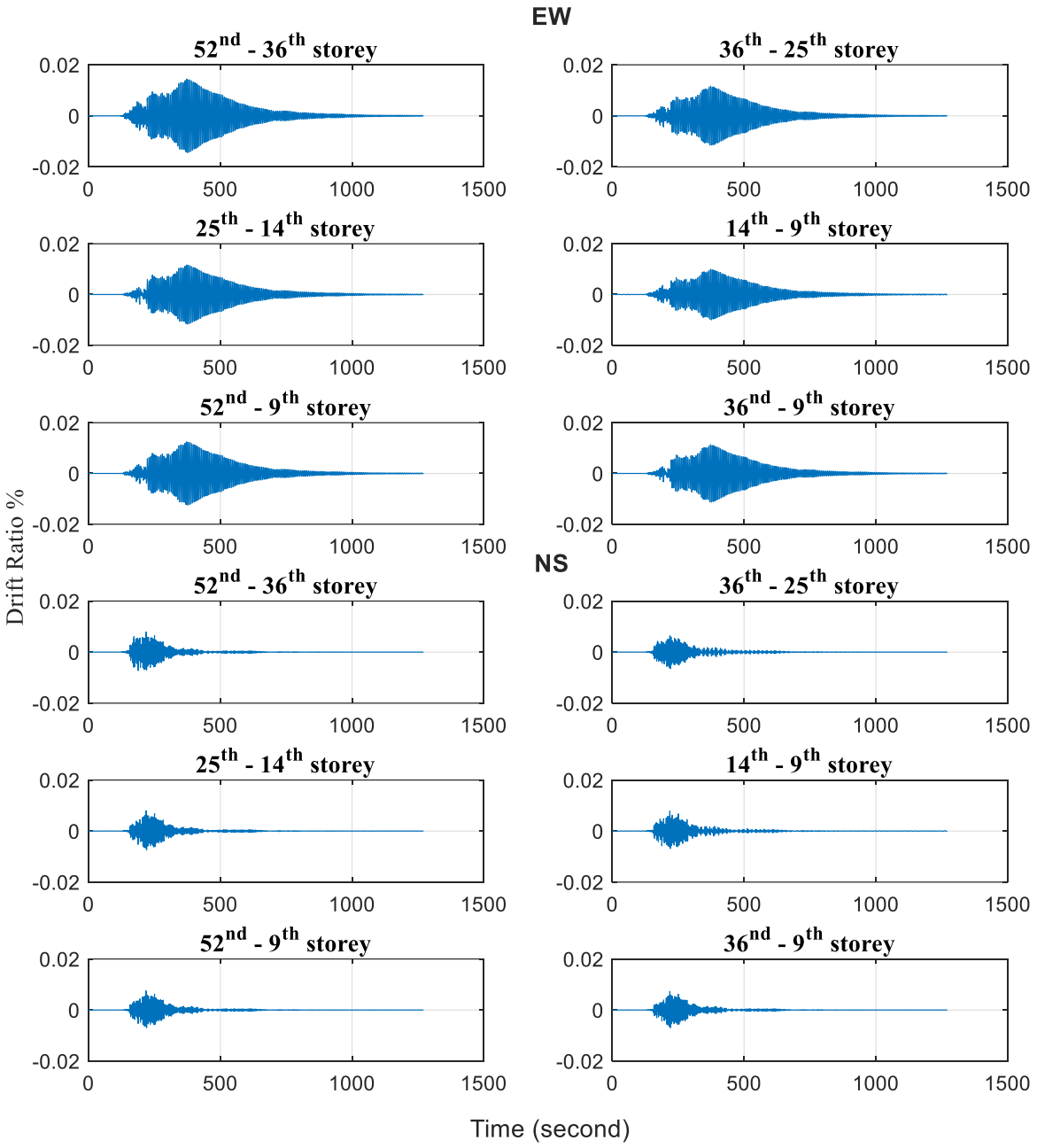

Figure 3.67. Average drift ratios in the EW and NS directions recorded on the southern side of the building between 52nd and 36th, 36th and 25th, 25th and 14th, 14th and 9th, 52nd and 9h and 36th and 9th floor levels, during the Aegean Sea earthquake.

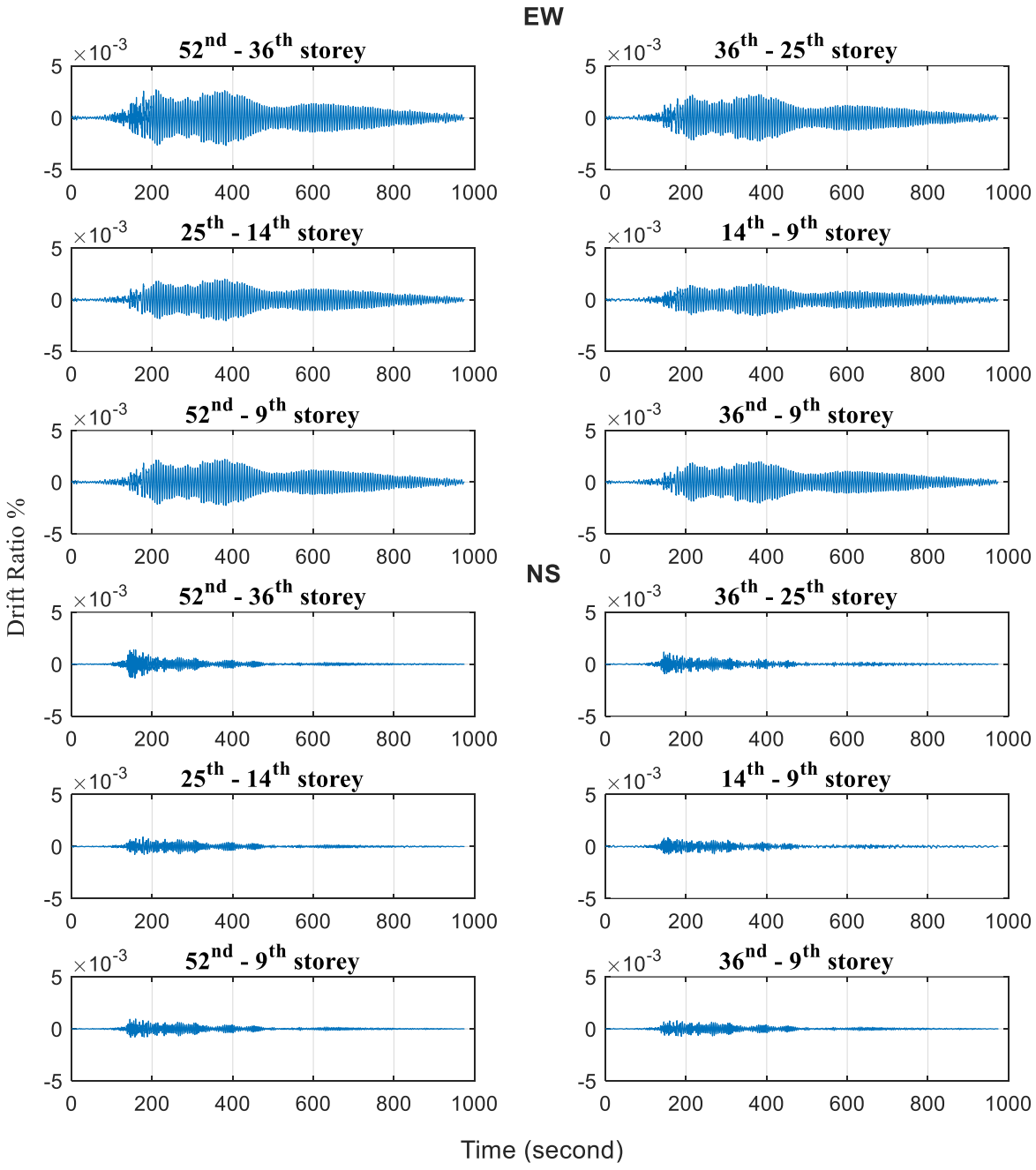

Figure 3.68. Average drift ratios in the EW and NS directions recorded on the southern side of the building between 52nd and 36th, 36th and 25th, 25th and 14th, 14th and 9th, 52nd and 9^{h} and 36th and 9th floor levels, during M_w = 6.1 Aegean Sea Turkey earthquake of 12 June 2017.

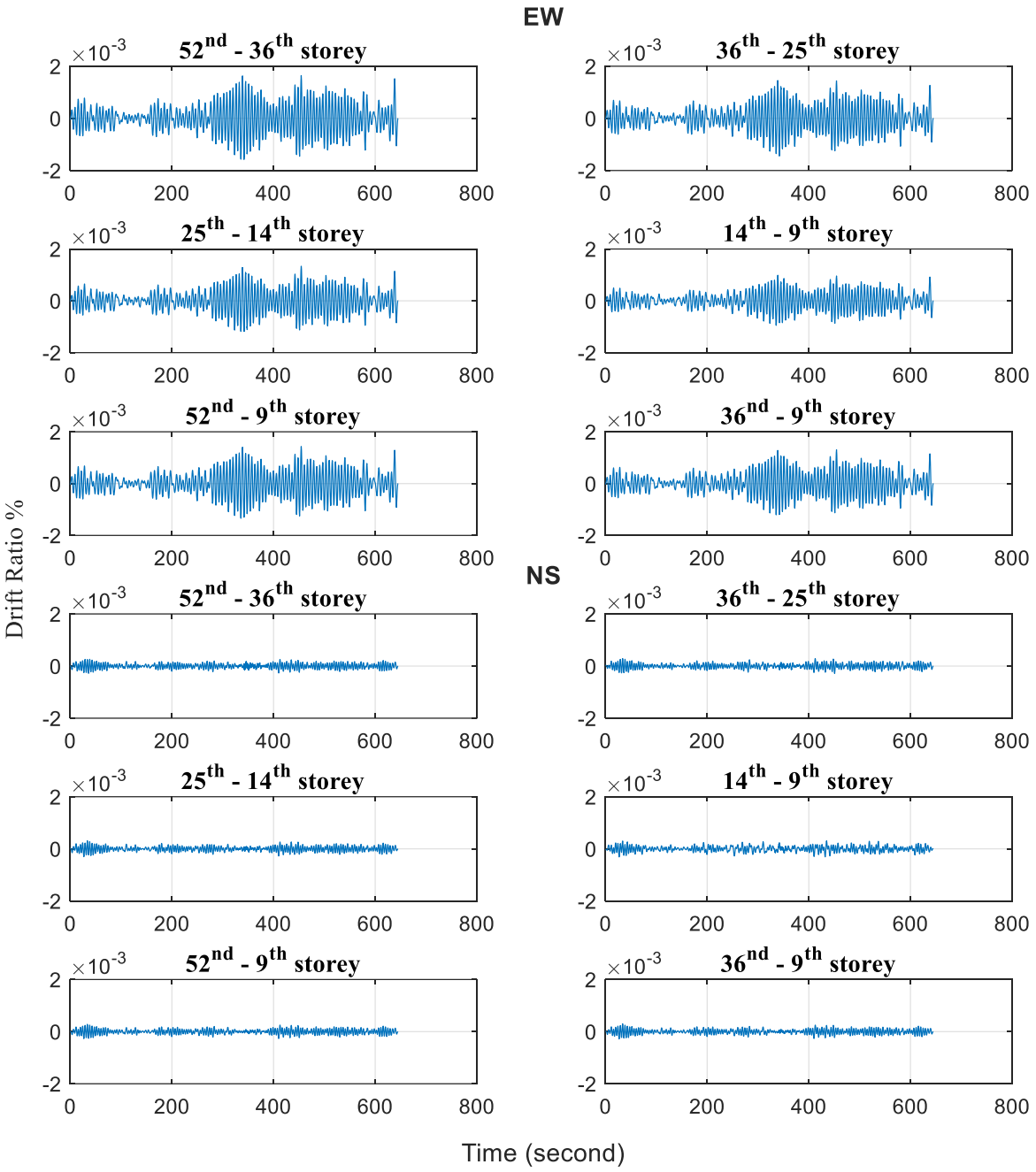

Figure 3.69. Average drift ratios in the EW and NS directions recorded on the southern side of the building between 52nd and 36th, 36th and 25th, 25th and 14th, 14th and 9th, 52nd and 9^{h} and 36th and 9th floor levels, during M_w = 4.5 Taşoluk - Geyve Turkey, earthquake of 22 October 2014.

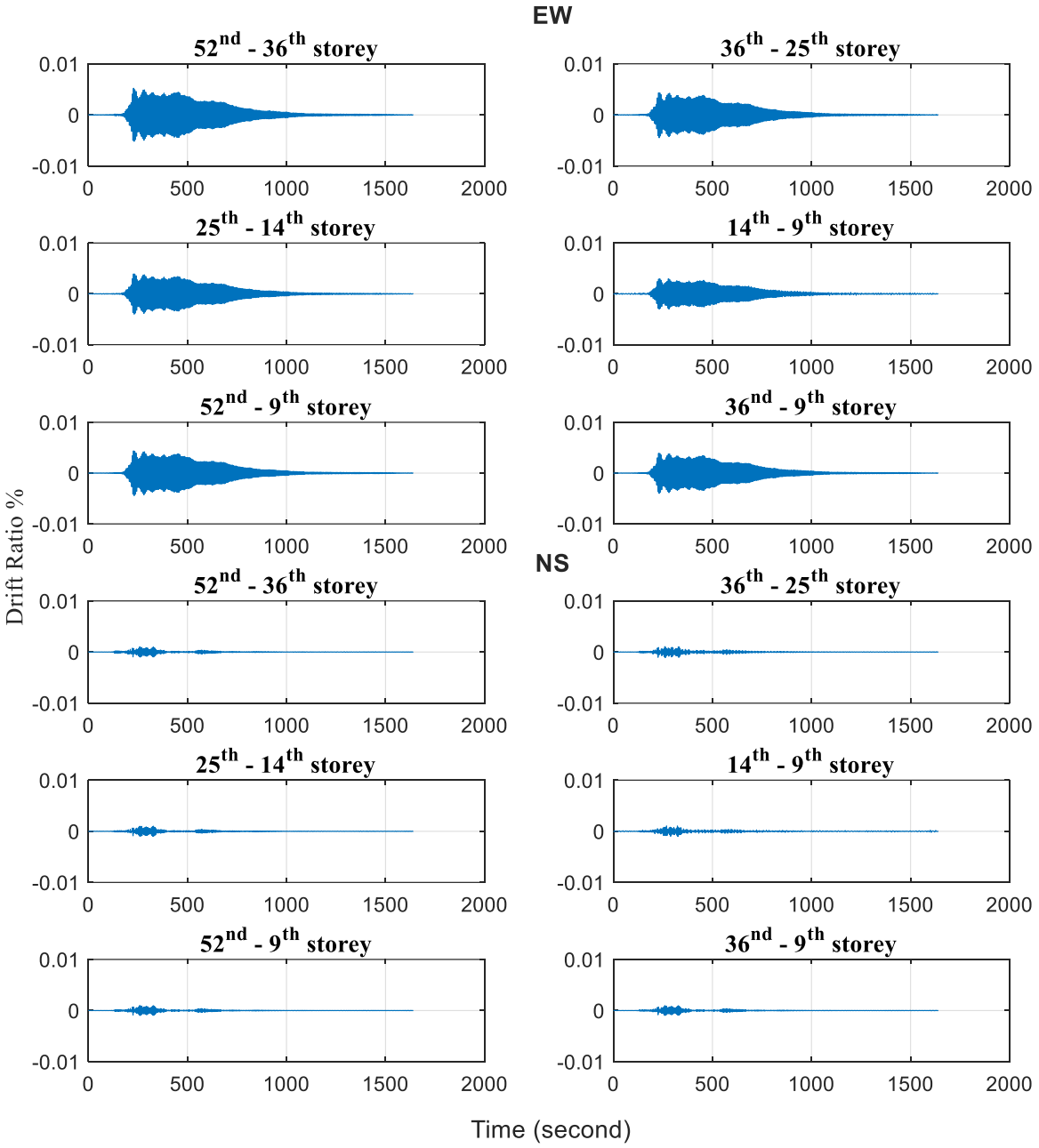

Figure 3.70. Average drift ratios in the EW and NS directions recorded on the southern side of the building between 52nd and 36th, 36th and 25th, 25th and 14th, 14th and 9th, 52nd and 9h and 36th and 9th floor levels, during the Gökova earthquake.

3.3.2 Wind Response

Maximum average drift ratios are estimated, during the wind of 27 July 2017, the wind of 07 May 2015, the wind of 09 April 2015 and the wind of 23 September 2014. Maximum average drift ratios have occurred in wind of 27 July 2017. The average drift ratio, shown in Figure 3.71, in the EW direction, is about 0.015%, whereas it is about 0.005 % in the NS direction.

A 2% drift ratio is the maximum limit for the design of buildings in Turkey and calculated drift ratios are far below the limitations.

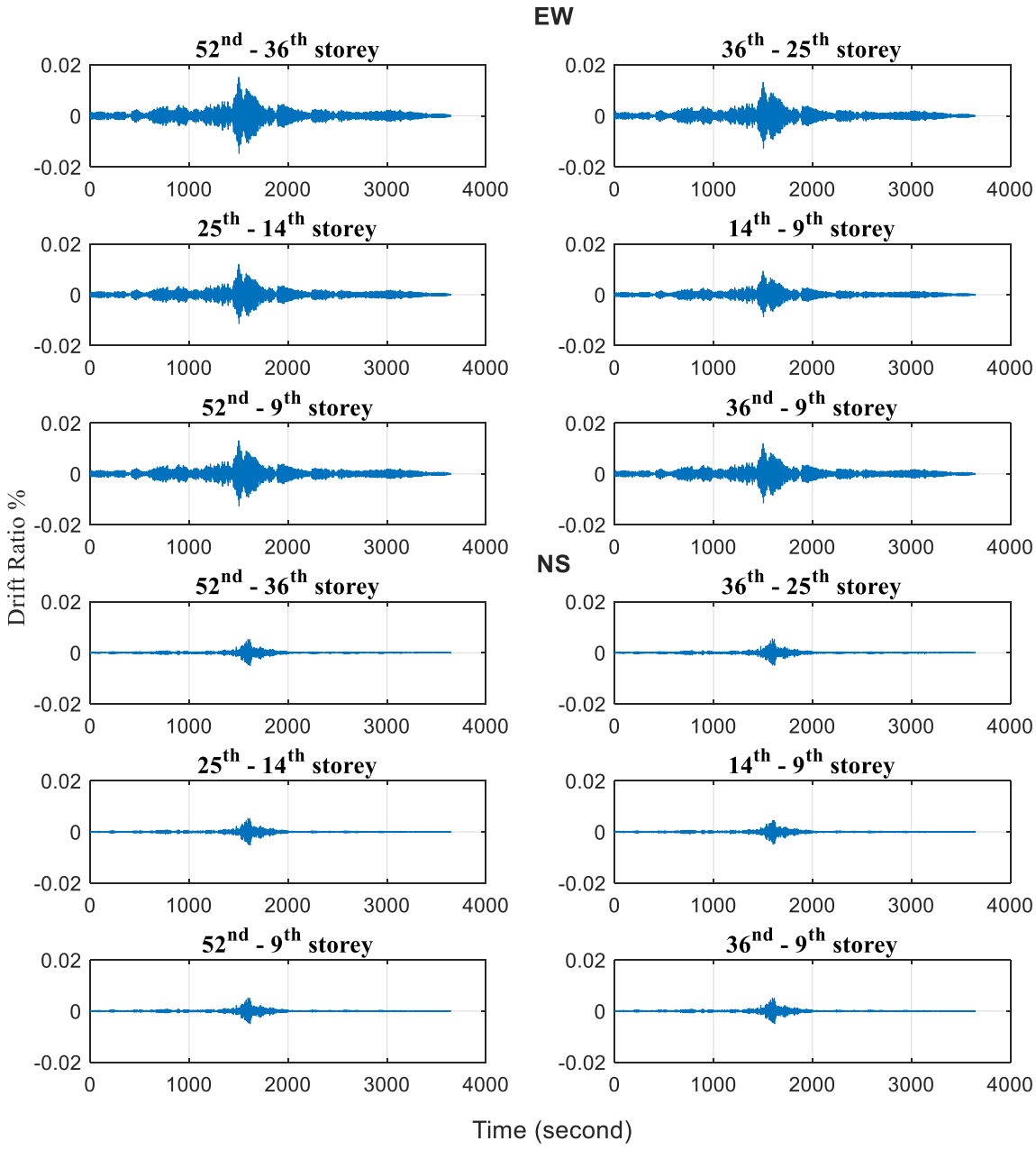

Figure 3.71. Average drift ratios in the EW and NS directions recorded on the southern side of the building between 52nd and 36th, 36th and 25th, 25th and 14th, 14th and 9th, 52nd and 9h and 36th and 9th floor levels, during the wind of 27 July 2017.

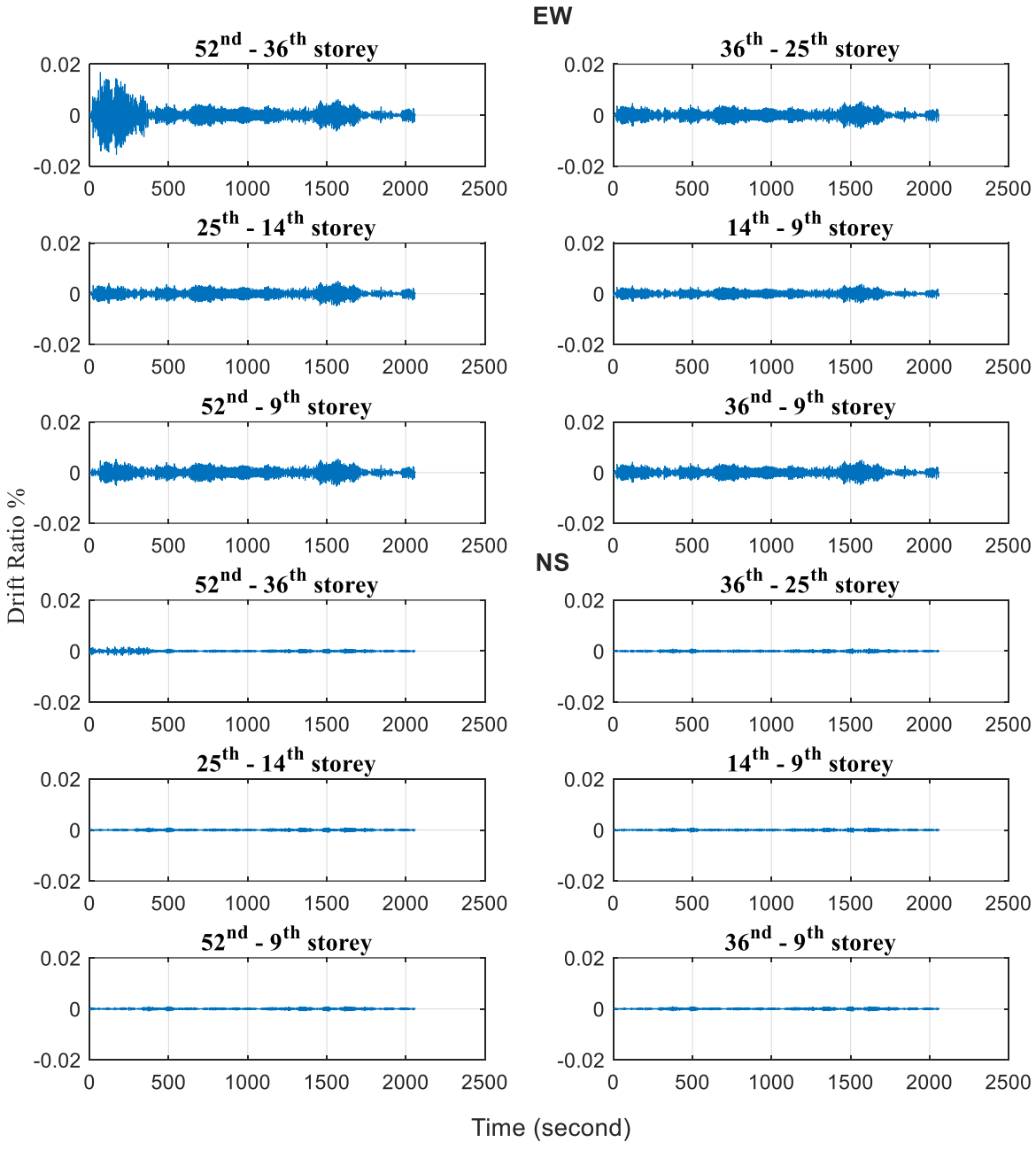

Figure 3.72. Average drift ratios in the EW and NS directions recorded on the southern side of the building between 52nd and 36th, 36th and 25th, 25th and 14th, 14th and 9th, 52nd and 9h and 36th and 9th floor levels, during the wind of 07 May 2015.

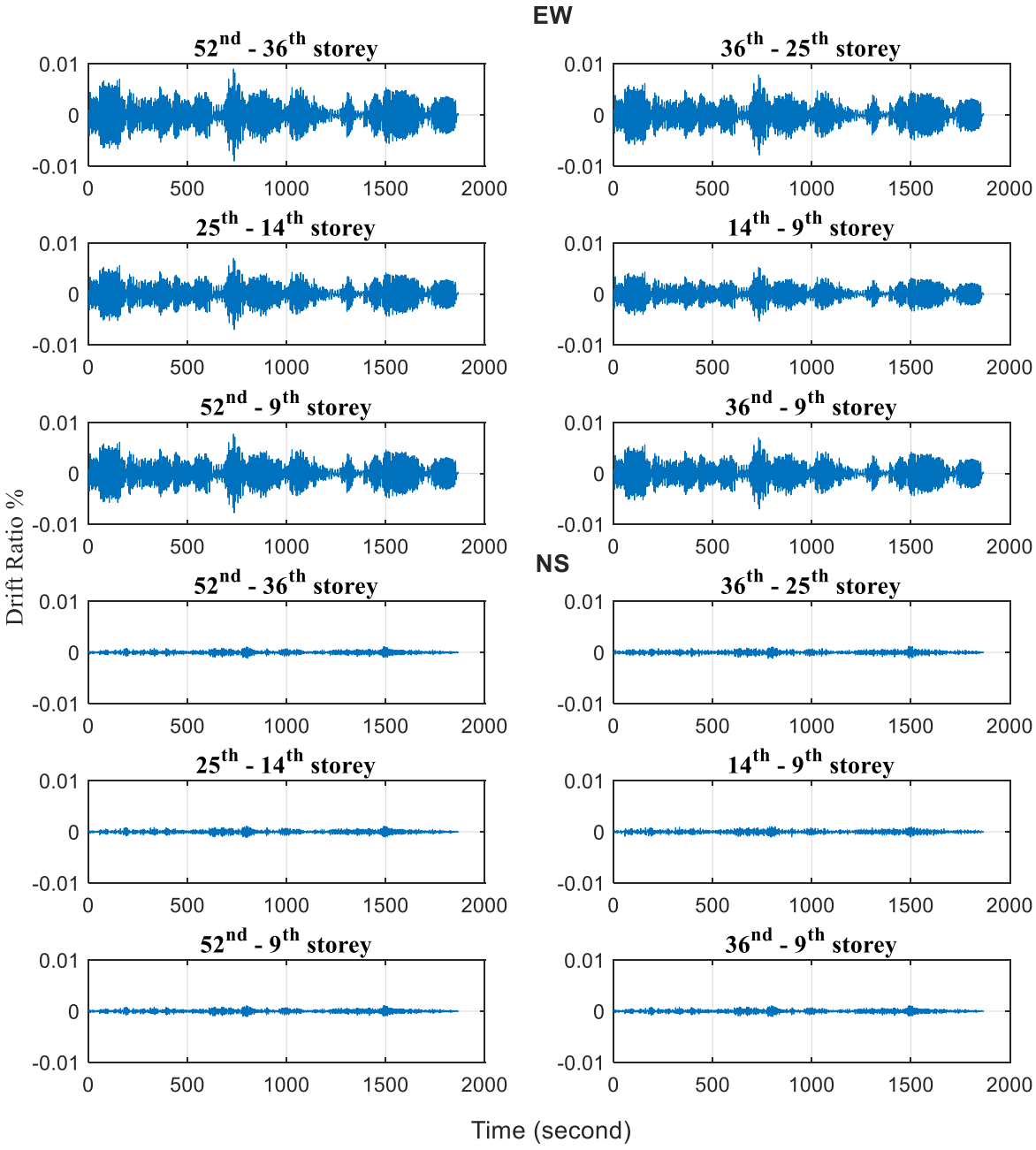

Figure 3.73. Average drift ratios in the EW and NS directions recorded on the southern side of the building between 52nd and 36th, 36th and 25th, 25th and 14th, 14th and 9th, 52nd and 9h and 36th and 9th floor levels, during the wind of 09 April 2015.

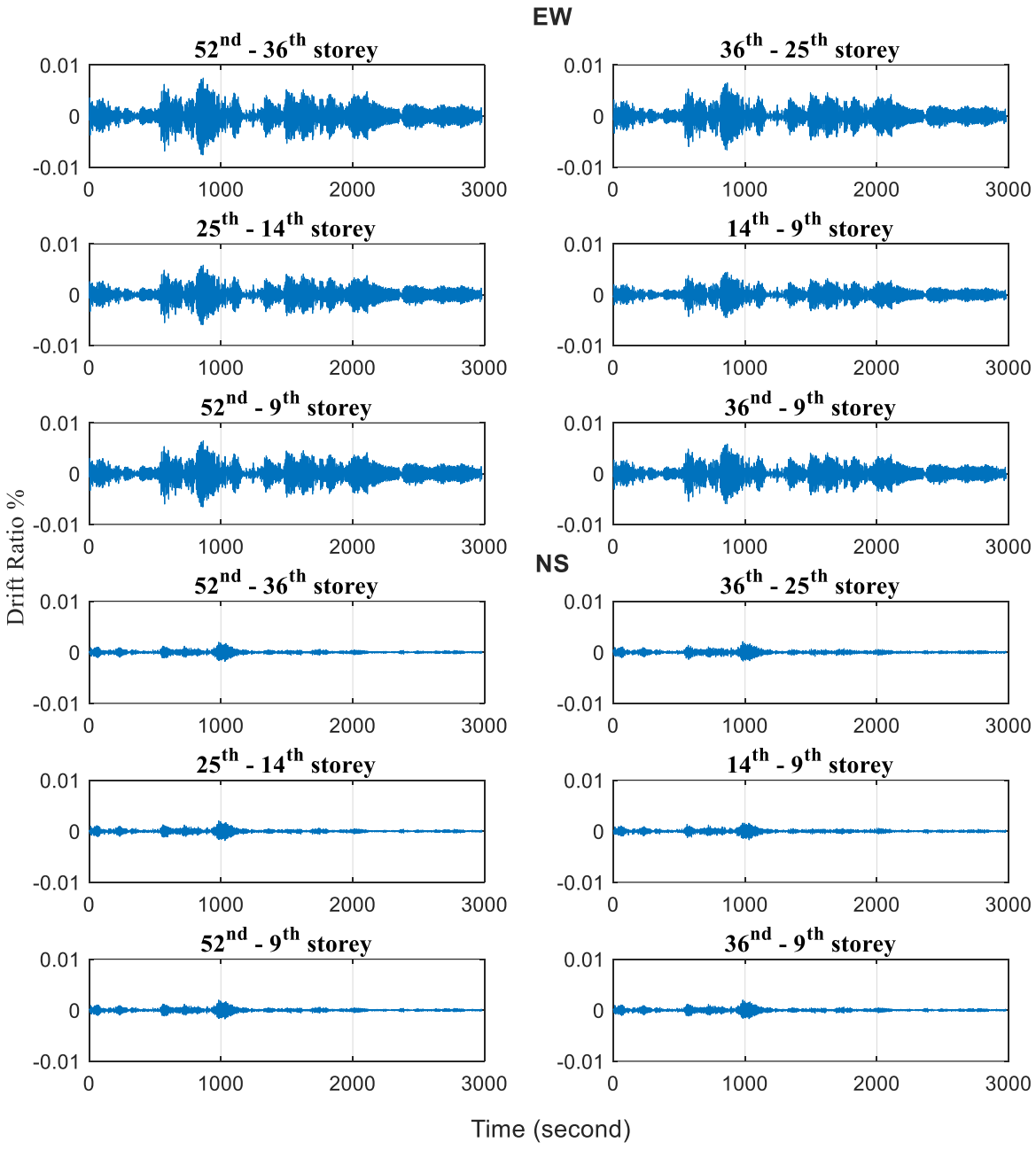

Figure 3.74. Average drift ratios in the EW and NS directions recorded on the southern side of the building between 52nd and 36th, 36th and 25th, 25th and 14th, 14th and 9th, 52nd and 9^{h} and 36th and 9th floor levels, during the wind of 23 September 2014.

3.4. Damping

The damping of the building has a major influence on the dynamic response, and the structural engineer has to make an informed decision as to an appropriate value to assume for design. (Smith & Willford, 2008). There are several methods, which are in the time domain and in the frequency domain to estimate the in-situ damping of the systems. In this study, two methods which are the logarithmic decrement and the half-power bandwidth method, are selected.

Logarithmic decrement, used in the time domain, represents the rate at which the amplitude of a free damped vibration decreases. According to corner frequencies, shown in Table 3.7 for earthquake records and Table 3.8 for wind records, acceleration time histories are filtered for the first and second mode. Finally, damping ratios are estimated from modal displacements.

The other method used in the analysis is the half-power bandwidth method in which the damping ratio is estimated in the frequency domain. After the determination of the peak natural frequencies, these peak values are reduced by 3db and two different frequencies are computed. After that, the damping ratio is derived from these two frequencies. As in the logarithmic decrement method, records are filtered for target mode also in the half-power bandwidth method. The details of the method is shown in standart texts (Chapter 3, Chopra A., 1995).

For buildings taller than 250m, almost all reliable measurements indicate a damping ratio below 1%. Structural designers consider higher values of damping as 5% for the design. (Smith & Willford, 2008). In Turkey, the damping ratio is considered also as %5 in the design of buildings. However, results show that damping ratios, for the Sapphire Building, are below %1 for earthquake excitations and below %0.5 for wind excitations.

3.4.1 Earthquake Response

Damping ratios are estimated for the Aegean Sea earthquake, the Gökova Earthquake, M_w = 6.1 Aegean Sea Turkey earthquake of 12 June 2017 and M_w = 4.5 Taşoluk - Geyve

Turkey earthquake of 22 October 2014. Logarithmic Decrement of the first mode in the EW direction is shown in Figure 3.75 and amplitude spectrum using in half-power bandwidth method is shown in Figure 3.76, occurred in the Aegean Sea Earthquake. Damping ratios computed by means of both logarithmic decrement and half-power bandwidth method are summarized in Table 3.10. Damping ratios computed from both logarithmic decrement and half-power bandwidth method are similar to each other. Whereas damping ratios in the EW direction are below from the 1%, it is above 1% in the NS direction.

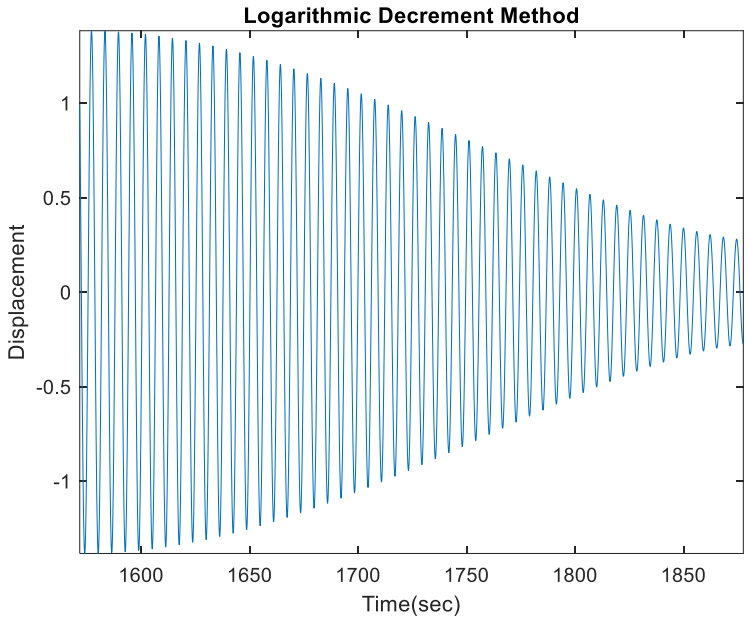

Figure 3.75. Free damped displacement time history, during the Aegean Sea earthquake.

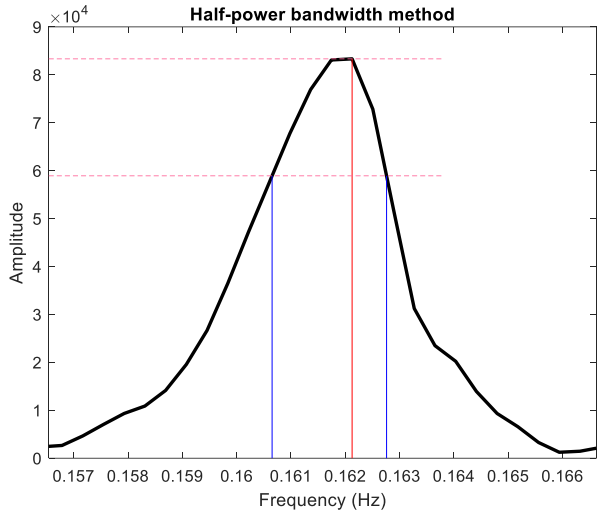

Figure 3.76. Fourier amplitude spectrum of acceleration filtered for the first mode in the EW direction during the Aegean Sea earthquake.

Table 3.10. Damping Ratios for the EW (top) and NS (bottom) directions, during Aegean Sea earthquake, M_w = 6.6 Gökova Körfezi (Akdeniz) Turkey earthquake of 21 July 2017, M_w = 6.1 Aegean Sea Turkey earthquake of 12 June 2017, M_w = 4.5 Taşoluk-Geyve Turkey earthquake of 22 October 2014.

Events	Damping Ratio - EW			
	Logaritmic Decrement		Half Power Bandwidth Method	
	Mode 1	Mode 2	Mode 1	Mode 2
M_w = 6.9 Aegean Sea Turkey, earthquake of 24 May 2014	0.57%	0.49%	0.65%	0.37%
M_w = 6.6 Gökova Körfezi (Akdeniz) Turkey, earthquake of 21 July 2017	0.36%	0.72%	0.43%	0.34%
M_w = 6.1 Aegean Sea Turkey, earthquake of 12 June 2017	0.70%	0.69%	0.41%	0.63%
M_w = 4.5 Taşoluk-Geyve Turkey, earthquake of 22 October 2014	1.27%	0.38%	0.87%	0.16%

	Damping Ratio - NS			
	Logaritmic Decrement		Half Power Bandwidth Method	
	Mode 1	Mode 2	Mode 1	Mode 2
M_w = 6.9 Aegean Sea Turkey, earthquake of 24 May 2014	1.80%	1.40%	1.56%	1.43%
M_w = 6.6 Gökova Körfezi (Akdeniz) Turkey, earthquake of 21 July 2017	1.58%	0.45%	1.22%	0.37%
M_w = 6.1 Aegean Sea Turkey, earthquake of 12 June 2017	0.53%	0.80%	0.56%	0.54%
M_w = 4.5 Taşoluk-Geyve Turkey, earthquake of 22 October 2014	1.47%	0.43%	0.84%	0.14%

3.4.2 Wind Response

Damping ratios are estimated for the wind of 09 April 2015, the wind of 07 May 2015, the wind of 27 July 2017 and summarized in Table 3.11.

Damping ratios computed from both logarithmic decrement and half-power bandwidth method are similar to each other and damping ratios in the both EW and NS directions are below from the 0.5%.

Table 3.11. Damping Ratios for the EW (top) and NS (bottom) direction, occurred in the wind of 23 September 2014, the wind of 09 April 2015, the wind of 07 May 2015, and the wind of 27 July 2017.

Events	Damping Ratio - EW			
	Logaritmic Decrement		Half Power Bandwidth Method	
	Mode 1	Mode 2	Mode 1	Mode 2
Wind of 23 September 2014	0.33%	0.05%	0.20%	0.17%
Wind of 09 April 2015	0.27%	0.05%	0.18%	0.04%
Wind of 07 May 2015	0.24%	0.04%	0.18%	0.06%
Wind of 27 July 2017	0.60%	0.13%	0.76%	0.08%

	Damping Ratio - NS			
	Logaritmic Decrement		Half Power Bandwidth Method	
	Mode 1	Mode 2	Mode 1	Mode 2
Wind of 23 September 2014	0.43%	0.04%	0.15%	0.05%
Wind of 09 April 2015	0.55%	0.04%	1.30%	0.04%
Wind of 07 May 2015	0.24%	0.16%	0.14%	0.08%
Wind of 27 July 2017	0.44%	0.10%	0.36%	0.08%

4. CONCLUSION

One of the significant characteristics of the distant earthquakes is the long-duration strong shaking that affect the tall buildings and long-period structures located at hundreds of kilometers away from the epicenter. Long duration shaking can damage the non-structural content inside the buildings and can panic the occupants causing injuries.

Although the dynamic characteristics profile, comprising acceleration, velocity, and displacement, along the height dramatically change at the level of the 9^{th} of the building in both wind and earthquake excitations, free response of the building begins at 9^{th} floor level, as seen in Figure 3.8 and Figure 3.9 in the earthquake excitations, otherwise there is no free response in wind excitations shown in Figure 3.34, Figure 3.35.

While the biggest response due to earthquake excitation is estimated from the M_w = 6.9 Aegean Sea Turkey earthquake of 24 May 2014 due to wind excitation it is estimated from the wind of 27 July 2017.

PAs, recorded at both B9 and 52^{nd} floor levels, during the Aegean Sea Earthquake are bigger than those during the wind of 27 July 2017. On the other hand, both peak velocities and displacements at 52^{nd} floor levels have similar dynamic responses under wind and earthquake excitations.

Torsional behavior is not dominant both in the wind and earthquake excitations, since shear walls are placed symmetrically.

Average drift ratios estimated from wind record occurred in 27 July 2017 is bigger than occurred in Aegean Sea Earthquake and both of them are not critical for structural safety.

Natural frequencies due to earthquake and wind excitations are similar to each other. However, Fourier amplitude spectra due to wind excitations are clearer when compared with those due to earthquake excitations.

Damping ratios due to both wind and earthquake excitations computed from both logarithmic decrement and half power bandwidth method are similar to each other. Whereas damping ratios due to earthquake excitations in the EW direction are below from the 1%, it is above 1% in the NS direction. However, damping ratios due to wind excitations in the both EW and NS directions are below from the 0.5%. If the damping ratio is considered as 5% in the design process, the result of an overestimation of damping will cause higher lateral accelerations, increased lateral deflections and higher forces in structural members and consequently, structural members will be damaged.

REFERENCES

Boore D.M., Bommer J.J., 2004, “Processing of strong-motion accelerograms: needs, options and consequences”, *Soil Dynamics and Earthquake Engineering* 93–115.

Chopra, A. K., 1995, Dynamics of Structures: Theory and Applications to Earthquake Engineering, Prentice-Hall, New Jersey.

Çaktı, E., Şafak E. 2014, “Structural Health Monitoring Systems in Istanbul”, *2nd European Conference on Earthquake Engineering and Seismology.* 25-29 August, Istanbul

Şafak E., Çaktı E., “Simple Techniques to Analyze Vibration Records from Buildings”, 7th European Workshop on Structural Health Monitoring, Jul 2014, Nantes, France. 2014.

Çelebi M., Okawa I., Kashima T., Koyama S. and Iiba M., "Response of a tall building far from the epicenter of the 11 March 2011 M9.0 Great East Japan earthquake and aftershocks" (2014). *USGS Staff* -- Published Research. 821.

Çelebi M., Şanlı A., 2002, “GPS in pioneering dynamic monitoring of long-period structures”, *Earthquake Spectra*, 18 (1), 47–61.

Los Angeles Tall Buildings Structural Design Council, “An Alternative Procedure for Seismic Analysis and Design of Tall Buildings Located In the Los Angeles Region”, 2017 Edition

Mathworks, 20017a, “System Identification Toolbox for MATLAB”, Mathworks, Inc., Nattick, MA.

Smith, R., & Willford, M., (2008), “Damping in Tall Buildings – Uncertainties and Solutions”, *IABSE 17th Congress*, Paper No: 1290, Chicago.

Turkish Earthquake Design Code, Turkish Standarts Institute, Ankara, 2007

Uchida N., Fukusumi T., Fujitani H., Yoshizawa M., Takahashi D., Takamura M., Iida T., Nakamoto M., Kokunai J., "Dynamic Properties of Building Structure Changed by Strong Earthquake and Its Renewal", *13th World Conference on Earthquake Engineering*, Paper No.2281. 1-6 August 2004, Vancouver, B.C., Canada